SANDIA REPORT SAND81-0984 • Unlimited Release • UC-62a
Printed November 1982

Performance Testing of the Solar Kinetics T-700A Solar Collector

Vernon E. Dudley, Robert M. Workhoven

Prepared by
Sandia National Laboratories
Albuquerque, New Mexico 87185 and Livermore, California 94550
for the United States Department of Energy
under Contract DE-AC04-76DP00789

Issued by Sandia National Laboratories, operated for the United States Department of Energy by Sandia Corporation.

Printed in the United States of America
Available from
National Technical Information Service
U.S. Department of Commerce
5285 Port Royal Road
Springfield, VA 22161

NTIS price codes
Printed copy: A05
Microfiche copy: A01

SAND81–0984
Unlimited Release
Printed November 1982

Distribution
Category UC–62a

Performance Testing of the Solar Kinetics T-700A Solar Collector

Vernon E. Dudley
Energy Measurements Group
EG&G, Inc.
Albuquerque, NM

Robert M. Workhoven
Experimental Facilities Operations Division 9721
Sandia National Laboratories
Albuquerque, NM 87185

Abstract

This report summarizes results of tests conducted by the Collector Module Test Facility on a Solar Kinetics T-700A Solar Collector. The collector was evaluated with a glass mirror and with an acrylic film-reflector surface. Tests were conducted over a temperature range from 20° to 360°C, using three heat-transfer fluids and absorber tubes of two different diameters. Tests were also made with direct normal solar irradiance from 200 to 1050 W/m^2. Collector efficiency and thermal loss were found to change significantly with changes in solar irradiance. Using only a measured efficiency curve, a thermal loss curve, and a measurement of the approximate optical efficiency, a procedure was developed to predict the collector efficiency and thermal loss at any level of solar irradiance and for any temperature within the range of test data.

Contents

Figures

Figures (cont)

Tables

Performance Testing of the Solar Kinetics T-700A Solar Collector

Introduction

A series of concentrating solar collector designs are being tested at the Collector Module Test Facility (CMTF) located at the Sandia National Laboratories (SNL), Albuquerque, New Mexico. The CMTF is a part of the Midtemperature Solar Systems Test Facility (MSSTF). These facilities are operating as part of a Department of Energy program to characterize selected solar collector modules for possible use in commercial energy systems.[1]

This report contains test results obtained during performance testing of a Model T-700A concentrating solar collector, manufactured by Solar Kinetics, Inc.* Initial tests were conducted on a collector module using glass mirrors. Additional tests were run with the collector after replacing the glass mirrors with an acrylic-film reflector. Tests were conducted with three different heat-transfer fluids and with absorber tubes of two different diameters.

Test Objective

The test objective for this test series was to define performance characteristics for the Solar Kinetics T-700A solar collector over a temperature range from 100° to 300°C.

Collector Description

Figure 1 shows the Solar Kinetics T-700A collector installed on the AZTRAK rotating platform at the CMTF. The T-700A is a single-axis, tracking, parabolic trough constructed in modules 6.1 m long and 2.13 m wide. The test array was a single module with a 12.80-m^2 aperture. Figure 2 is a photograph of a T-700A collector module, shown in focus during an efficiency test. Each module was monocoque structure, using full-width aluminum castings as bulkheads and 4-mm-thick, T6-tempered-aluminum sheet front and back surfaces. An aluminum extrusion was used along each edge of the module.

A support pylon was located at each end of the T-700A module. A pylon can support a module on each side, so modules can be joined together to make up a row of any desired length. All the support pylons are identical, except that one special pylon is required in each collector row to contain the collector elevation-tracking drive system.

The collector elevation positioning for sun tracking used a hydraulic cylinder located inside the drive pylon. The drive pylon also contained the hydraulic pump, high-pressure fluid accumulator, associated valves, and sun-tracking electronics. Separate hydraulic valves were used for sun tracking and for collector stow/out-of-stow functions, allowing collector travel speed to be adjusted independently for each.

The sun-sensor and sun-tracking electronics were designed and built by Solar Kinetics. The sun sensor, mounted on one edge of the reflector assembly, operated on a balanced-light principle similar to the shadow-band sensors seen on many other collectors. However, instead of a central shadow bar, the Solar Kinetics design used the shadows from the edges of a deep well. The sun-sensor design had a fairly narrow view angle to prevent sun-tracking errors caused by reflections from other collectors.

A 4.13-cm-dia steel absorber tube was initially used on the T-700A collector. The absorber surface was solar-spectrum-selective, black-chrome plate applied over a nickel plating. A 6.35-cm-dia Pyrex glass tube absorber envelope was used on the receiver. After completion of tests using the 4.13-cm receiver, it was replaced with a smaller 3.18-cm-dia absorber tube. Tests were made with two different glass envelopes on the small receiver: a 5.21-cm-dia quartz glass and a Pyrex glass envelope of the same diameter.

*Solar Kinetics, Inc., 3300 Century Circle, Irving, TX 75060

Figure 1. Solar Kinetics T-700A Installed on the AZTRAK Platform

Performance Testing of the Solar Kinetics T-700A Solar Collector

Introduction

A series of concentrating solar collector designs are being tested at the Collector Module Test Facility (CMTF) located at the Sandia National Laboratories (SNL), Albuquerque, New Mexico. The CMTF is a part of the Midtemperature Solar Systems Test Facility (MSSTF). These facilities are operating as part of a Department of Energy program to characterize selected solar collector modules for possible use in commercial energy systems.[1]

This report contains test results obtained during performance testing of a Model T-700A concentrating solar collector, manufactured by Solar Kinetics, Inc.* Initial tests were conducted on a collector module using glass mirrors. Additional tests were run with the collector after replacing the glass mirrors with an acrylic-film reflector. Tests were conducted with three different heat-transfer fluids and with absorber tubes of two different diameters.

Test Objective

The test objective for this test series was to define performance characteristics for the Solar Kinetics T-700A solar collector over a temperature range from 100° to 300°C.

Collector Description

Figure 1 shows the Solar Kinetics T-700A collector installed on the AZTRAK rotating platform at the CMTF. The T-700A is a single-axis, tracking, parabolic trough constructed in modules 6.1 m long and 2.13 m wide. The test array was a single module with a 12.80-m^2 aperture. Figure 2 is a photograph of a T-700A collector module, shown in focus during an efficiency test. Each module was monocoque structure, using full-width aluminum castings as bulkheads and 4-mm-thick, T6-tempered-aluminum sheet front and back surfaces. An aluminum extrusion was used along each edge of the module.

A support pylon was located at each end of the T-700A module. A pylon can support a module on each side, so modules can be joined together to make up a row of any desired length. All the support pylons are identical, except that one special pylon is required in each collector row to contain the collector elevation-tracking drive system.

The collector elevation positioning for sun tracking used a hydraulic cylinder located inside the drive pylon. The drive pylon also contained the hydraulic pump, high-pressure fluid accumulator, associated valves, and sun-tracking electronics. Separate hydraulic valves were used for sun tracking and for collector stow/out-of-stow functions, allowing collector travel speed to be adjusted independently for each.

The sun-sensor and sun-tracking electronics were designed and built by Solar Kinetics. The sun sensor, mounted on one edge of the reflector assembly, operated on a balanced-light principle similar to the shadow-band sensors seen on many other collectors. However, instead of a central shadow bar, the Solar Kinetics design used the shadows from the edges of a deep well. The sun-sensor design had a fairly narrow view angle to prevent sun-tracking errors caused by reflections from other collectors.

A 4.13-cm-dia steel absorber tube was initially used on the T-700A collector. The absorber surface was solar-spectrum-selective, black-chrome plate applied over a nickel plating. A 6.35-cm-dia Pyrex glass tube absorber envelope was used on the receiver. After completion of tests using the 4.13-cm receiver, it was replaced with a smaller 3.18-cm-dia absorber tube. Tests were made with two different glass envelopes on the small receiver: a 5.21-cm-dia quartz glass and a Pyrex glass envelope of the same diameter.

*Solar Kinetics, Inc., 3300 Century Circle, Irving, TX 75060

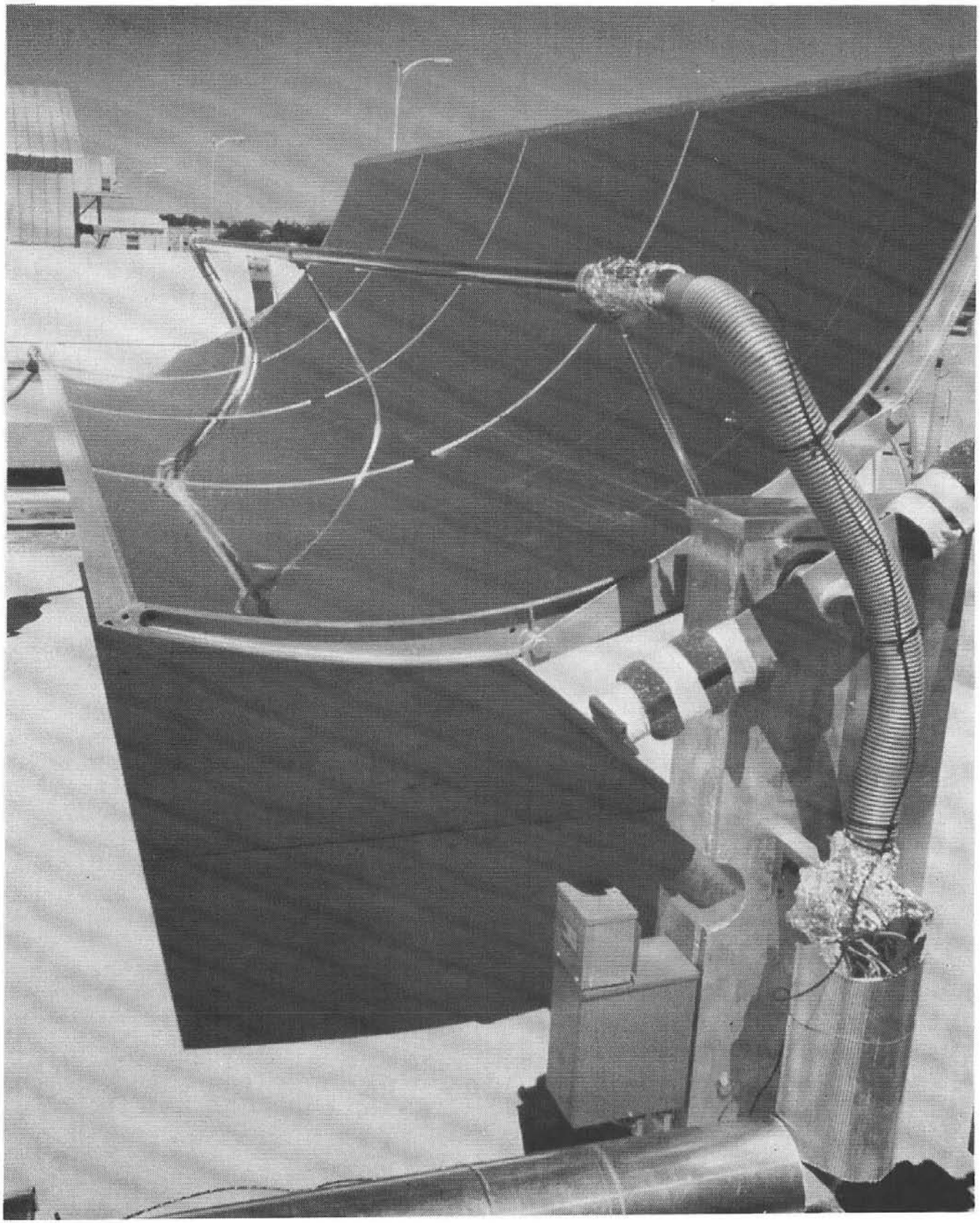

Figure 2. Solar Kinetics T-700A Collector Module

Chemically strengthened 1.27-mm-thick Corning glass mirrors were used on the reflector. The mirrors were epoxy bonded to 2-mm-thick, flat aluminum sheets. The composite mirror sheets were then pressed into position on the collector module, and held in position by retaining strips at the reflector edges. The mirror edge-retaining clips were formed into springs, applying force towards the trough center. The edge springs were necessary to keep the mirror sheets in contact with the module substructure which defined the desired parabolic-reflector shape.

Each glass mirror was 118.8 cm long and 74.6 cm wide; two of these glass mirrors were bonded to a single aluminum sheet. Eight glass/metal composite sheets were used on each collector module for a total of 16 pieces of glass mirror. Each mirror sheet was individually removable for ease of replacement or field repair. Aperture of the collector as tested (one module) was 12.80 m^2.

After finishing the glass-mirror test series, a new T-700A reflector module was installed for further tests with the 3M Company's FEK-244 acrylic-film reflector material. Aperture of the film mirror was approximately the same as the glass mirror. The change from a film-reflector module to a glass-reflector module would be relatively easy. The glass-mirror sheets are installed on top of the existing film, with the edge springs added to hold the mirrors in place. Unfortunately, the glass-mirror module was tested first, and no FEK film had been installed on the structure. Therefore, a new module with a film reflector was obtained to continue the test series.

Test Facility Description

The CMTF's AZTRAK rotating platform was used for the Solar Kinetics test series. AZTRAK is a 4- by 13-m platform rotated hydraulically about a center pivot. The platform is computer-controlled and can be tracked in azimuth so that the collector under test operates at any desired constant solar-radiation incident angle from zero to 90°C. Because the maximum available incident angle depends on the solar elevation, not all incident angles are available at all hours of the day. AZTRAK can also be held stationary in any position to simulate any desired collector axis orientation, such as east-west or north-south. When the AZTRAK is operated to provide a zero incident angle for the collector under test, a single-axis (elevation) tracking collector (such as the Solar Kinetics T-700A) becomes a two-axis tracking collector.

A series of tests were run on the Solar Kinetics collector with three different heat-transfer fluids: (1) Therminol 66, a synthetic, modified terphenyl liquid manufactured by the Monsanto Industrial Chemicals Co.; (2) Q2-1162 (Syltherm 800), a silicone-based, modified dimethyl-siloxane liquid manufactured by the Dow Corning Corp.; and (3) ambient-temperature water from the Albuquerque city water mains.

The CMTF's Fluid Loop 1 is designed to supply Therminol 66 as a heat-transfer fluid at temperatures from about 100° to 300°C. The properties of Therminol 66 were taken from Reference 2. Design flow rates from Fluid Loop 1 range from 4 L/min to about 40 L/min.

Fluid Loop 2 at the CMTF supplies Dow Corning's Q2-1162 liquid as a heat-transfer fluid over the temperature range from 50° to 400°C. Q2-1162 is also known as Syltherm 800. Properties of Syltherm 800 were taken from Reference 3. Design flow rates from Loop 2 range from about 4 to 56 L/min.

Low-temperature water from the Albuquerque city water mains was used in a recent test series to determine an efficiency point near the optical efficiency of the collector. The temperature of the water was quite stable, varying only a degree or so throughout a day's run. Water pressure variations are common, requiring that a pressure regulator be used on the water supply in order to achieve stable flow rates.

A typical test day began by heating the heat-transfer fluid with the fluid loop's electric heaters. The collector was placed in focus as soon as an appropriate fluid flow was established. During a test, both the collector input temperature and the fluid-flow rate were maintained constant, while the output temperature was allowed to vary according to the test conditions.

Fluid-flow rate was measured with dual turbine flow meters. Input and output fluid temperatures were measured with two matched pairs of Type T thermocouples. Direct-solar-radiation measurement was provided by two Eppley pyroheliometers. Total horizontal solar radiation, ambient air temperature, wind speed, and wind direction were also recorded.

The test instrumentation was calibrated by SNL's Primary Standards Labs, using standards traceable to the National Bureau of Standards (NBS). Individual instruments were calibrated to 1% or better; no estimate of the overall accuracy of the total measuring system is currently available. The test instrumentation meets or exceeds the requirements of ASHRAE Standard 93-77 for testing solar collectors.

Analog test data was converted to digital format by several analog-to-digital data systems. An HP1000 minicomputer system processed the input data and provided printed output of critical test data. Real-time plots of insolation and efficiency were made during all test runs; all data was recorded on magnetic tape for future analysis.

Figures 3 and 4 contain reproductions of the printed data output for an efficiency test and for a thermal loss test, respectively. Unless otherwise indicated, the temperatures are in degrees Celsius. The delta temperature column shown in the printouts is not the arithmetic difference of the input and output temperatures, but was calculated from the differential voltage output of the in-out thermocouples.

The speed of the data system was such that all the data channels could be read, calculations performed, and a line in the data table printed in about 15 to 20 s. Fifty measured and calculated data values were generated during each of these data cycles. All were recorded on magnetic tape, but only those shown in Figures 3 and 4 were printed out. Data collection was continuous whenever the system was operating; however, only those data blocks occurring under the best stable conditions are included in this report.

***** SOLAR KINETICS PARABOLIC TROUGH EFFICIENCY EVALUATION *****

TEST DATE: 19 OCTOBER 1981 TIME: 12:32:23 (SOLAR)
12:23:29 (MST)

21.02	(DEG C)	AMBIENT TEMPERATURE
288	(DEGREES)	WIND DIRECTION
2.15	(M/SEC)	WIND SPEED

TEMP IN	TEMP OUT	SOLAR WATTS/M^2	DELTA TEMP	FLOW LITERS/MIN	EFFICIENCY PERCENT
351.43	359.94	963.8	8.48	34.36	53.8
351.47	359.97	962.7	8.53	34.35	54.1
351.43	359.98	959.9	8.53	34.24	54.1
351.44	360	961.9	8.55	34.37	54.3
351.44	360.01	959.9	8.58	34.31	54.6
351.39	359.94	963.6	8.51	34.26	53.8
351.44	359.95	962.4	8.5	34.35	54
351.43	359.94	964.3	8.48	34.35	53.7
351.37	359.92	963.3	8.53	34.38	54.2
351.37	359.79	960.8	8.45	34.35	53.7
		10 POINT AVERAGES			
351.42	359.94	962.26	8.514	34.332	54.03

54.09	AVG EFFICIENCY USING SUB. DELTA T
56.4995	AVG EFFICIENCY CORRECTED FOR OFF-NOON LOSSES
23955.8	AVG HEAT GAIN (KJ/HR)
520	AVG HEAT GAIN (W/M^2)
334.42	AVG RECVR TEMP MINUS AMB TEMP
.347533	(AVG TEMP-AMB T)/I
43108.	REYNOLDS NUMBER

Figure 3. Sample Data Printout for Efficiency Test

***** SOLAR KINETICS PARABOLIC TROUGH THERMAL LOSS TEST *****

TEST DATE: 19 OCTOBER 1981 TIME: 17:45:33 (SOLAR)
17:36:39 (MST)

15.54	(DEG C)	AMBIENT TEMPERATURE
200	(DEGREES)	WIND DIRECTION
.87	(M/SEC)	WIND SPEED

TEMP IN	TEMP OUT	DELTA TEMP	FLOW LITERS/MIN	WATTS GAIN/LOSS
351.14	349.77	-1.34	34.84	-1059.5
351.22	349.82	-1.37	34.82	-1082.6
351.2	349.83	-1.35	34.82	-1066.8
351.17	349.81	-1.34	34.84	-1059.5
351.2	349.81	-1.35	34.84	-1067.4
351.23	349.84	-1.37	34.82	-1082.6
351.24	349.85	-1.35	34.83	-1067
351.25	349.87	-1.35	34.82	-1066.7
351.23	349.89	-1.29	34.81	-1019.1
351.2	349.85	-1.34	34.81	-1058.6
		10 POINT AVERAGES		
351.208	349.834	-1.345	34.825	-1063.07

-.94	(W/M^2)	AVERAGE DIRECT INSOLATION
-1078.09	(WATTS)	AVERAGE LOSS (SUB DELTA T)
-3826.76	(KJ/HR)	AVG LOSSES (W/M^2)= -83.0663
-153.712	(W/M)	AVG LOSS
335.029	AVG RECVR TEMP MINUS AMB TEMP	
44913.1	AVG REYNOLDS NUMBER	

Figure 4. Sample Data Printout for Thermal Loss Test

Heat Gain/Loss Performance Test Definition

During a test run, both the specific heat and density of the heat-transfer fluid were calculated for each data set, using the average temperature of the fluid in the absorber tube. Heat gain (or loss) was then calculated from

$$Q = \dot{m}\, c_P\, \Delta T \qquad (1)$$

in which

Q = heat gain, kJ/h
$\dot{m}$ = mass flow rate of fluid, kg/h
c_P = specific heat of fluid, kJ/kg°C
ΔT = in-out temperature differential, °C.

For the large (4.13-cm) diameter receiver, thermal-loss tests were conducted in four different ways. Two sets of loss measurements were made with the collector rotated far enough from focus that the reflector assembly shaded the receiver from direct sunlight. One of the "shaded" loss tests was made with the reflector aimed at the north sky; the other was made with the reflector facing south and pointed at the ground.

The second set of thermal-loss measurements was made with the collector defocused as far as possible, so that no light from the mirrors would fall on the receiver assembly, but positioned so that the receiver remained exposed to direct sunlight. As described above for the shaded receiver loss test, one measurement was made with the reflector aimed at the north sky; the second measurement was made with the reflector facing down and to the south. During all the thermal-loss tests, the AZTRAK platform was operating in the solar azimuth tracking mode so that no changes in direct solar-radiation incident angle would occur during the test.

Only two types of thermal-loss tests were made on the small (3.18-cm) diameter receiver. Some of the tests were made in the same way as the "shaded, north" tests described above. The remaining thermal-loss tests on the small receiver were conducted at night, with the reflector aimed at the zenith. Both thermal-loss measurements produced equivalent results.

A successful loss measurement is defined as at least one ten-point data block (preferably preceeded by a number of others of equal stability) during which the values for input and output temperatures remained constant to within 0.1°C or less, the flow rate varied by 0.1 L/min or less, and the receiver delta temperature changed by 0.1°C or less. These values do not imply that the absolute accuracy of the measurements are that good; the objective is to achieve the best stability possible.

Efficiency Test Definition

The stability requirements for an efficiency test point are the same as for a loss test, except that the direct solar-radiation input must remain constant to about 1% during the measurement period and have an absolute value $\gtrsim$900 W/m^2. Measured efficiency of concentrating solar collectors has been found to change significantly with changes in insolation, therefore, the CMTF attempts to make all the peak efficiency characterization test runs within a narrow range of insolation between 900 and 1050 W/m^2. Other tests are scheduled as required to define the performance of the collector under less than ideal solar-radiation input.

Heat-gain (efficiency) tests were conducted with the collector focal point adjusted for maximum efficiency at zero angle of incidence of direct solar irradiance. If required, mirror surfaces and absorber glass were cleaned daily with a detergent and deionized water.

Given the required stability, efficiency was then calculated from

$$\eta = \frac{Q/A}{I} \tag{2}$$

in which

η = solar collector efficiency
Q = heat gain (W)
A = collector aperture area (m^2)
I = direct solar radiation (W/m^2)

Several solar-collector test standards require the use of a collector time-constant during efficiency testing. Collector time-constant measurements were not made or used during the test series at Sandia. Collector time constant can be used to determine the minimum time required for thermal stability to exist before recording an efficiency measurement. Our test procedure required continuous measurement, and thermal stability times were always much greater than required by use of a collector time constant.

Measured efficiency data is shown in this report in several different formats. Each graphical format has advantages and some disadvantages. Laymen like to see efficiency data shown as a function of collector output temperature because it is easy to understand. However, such a curve is actually correct only when the ambient air temperature matches that existing when the data was measured and only at the same solar irradiance existing during the test measurements.

Two other data curve formats eliminate the problem with changes in ambient air temperature, but do nothing to show how the efficiency varies with changes in solar irradiance level. These data plots show measured efficiency as a function of average receiver fluid temperature above ambient air temperature, or as average temperature above ambient, quantity divided by solar irradiance (delta-T/I). The delta-T/I presentation is popular in the solar community, because it is a long-established standard for flat-plate collector testing. Of the two, the delta-T/I presentation is the most deceiving and the most easily misused, because even though the solar irradiance (I) appears in the efficiency equation, I is not usually treated as a variable in deriving the efficiency equation, but is actually a constant value equal to the irradiance existing during the test measurements, just as it is for all the other efficiency plots. This causes no problems for nonconcentrating, low temperature solar collectors, but can be a source of error for a high-concentration-ratio collector operating at high temperature.

The only truly correct way to show the operating efficiency of a concentrating solar collector is with a three-variable equation, containing efficiency as a function of both delta T and solar irradiance. For a parabolic-trough concentrating-solar collector, such an equation in graphical form appears as a three-dimensional surface, with a parabolic curvature along the temperature axis and a hyperbolic curvature along the solar irradiance axis. There are no less-complex curves that will correctly show the collector performance under all operating conditions. The problem of solar irradiance and its effect on collector efficiency will be discussed in detail during presentation of the test data (later in this report).

Thermal Stability Requirement

The temperature, flow rate, and solar radiation stability criteria outlined above are necessary because the heat-gain formula used assumes steady-state conditions. If near steady-state conditions can be achieved during a collector test, the computed values for heat gain (or loss) and efficiency will be nearly constant also, with some scatter in the data caused by noise. Because of the thermal mass of the collector and fluid-loop system, any change in temperature, flow rate, or insolation will result in transient measurements that do not correctly represent the performance of the collector.

Even on a clear sunny day that appears ideal for testing a solar collector, there are still variations in solar radiation. However, these variations can be relatively small, as can be seen in several of the test data plots later in this report. Small, rapid variations of this kind produce scatter in the efficiency data, but no long-term systematic errors.

As operated at the CMTF, the heat-transfer fluid supply loop tends to produce fluid flow rate variations similar to those seen in the solar-radiation input—small, rapid fluctuations with no long-term trend towards a higher or lower flow rate. These flow variations also produce scatter in the measured data.

Small, rapid temperature fluctuations also appear in the measured data, again producing data scatter. However, the temperature measurements are subject to fairly long-term, slow changes that can result in fairly large, systematic errors in heat gain/loss and efficiency calculations. One typical source of this kind of temperature drift is the constantly increasing temperature that occurs each test day as the fluid system is heated towards the intended operating temperature. Even after the fluid coming out of the heater is at a constant temperature, the fluid at the collector inlet may not be—the fluid must still transfer enough energy to the large mass of fluid pipe and pipe insulation to reach an equilibrium with heat losses. The same problem in reverse occurs with the temperature decay that continues for very long times after the collector system is defocused to begin a thermal-loss test.

Another source of thermal instability became apparent during the T-700A test series: changes in the intensity of solar irradiance. When efficiency testing was continuous through the time of sunrise or sunset, the changes in solar irradiance were often rapid enough to cause errors in the measured efficiency because of the resulting rapidly changing collector-output temperatures.

At the CMTF, collector input and output temperatures are usually measured less than one second apart in time. However, the fluid whose temperature is being measured at the collector input may not arrive at the collector output for a relatively long time—from several seconds to several minutes. Thus, an efficiency or heat gain/loss measurement will not be valid unless the input and output temperatures are unchanging for at least as long as the transit time of the heat-transfer fluid through the system.

Because of the thermal mass of both the fluid-supply system and the collector, stable temperatures must be held for relatively long periods of time before the complete system is in thermal equilibrium and valid measurements can be made. A small, constant drift in temperature can produce test data that looks quite acceptable; however, it contains a systematic error because of the thermal mass shift of in/out delta temperature. During the T-700A test series, a constant temperature increase of 0.7°C/min produced an efficiency measurement that had a very small data scatter, a constant efficiency value, and a constant in-out delta temperature. This measured efficiency value turned out to be 5 percentage points lower than the efficiency measured later with more stable temperatures; this corresponds to an efficiency error of about 10%.

In another case, with a collector system of greater thermal mass, a similar slow drift in temperature produced an efficiency measurement 15 percentage points lower than the true value.

If the input temperature drift is towards lower temperatures, errors of similar magnitude result, but the measured efficiency will be greater than the value obtained under stable conditions.

The same problem as outlined above for an efficiency measurement also occurs during thermal-loss measurements. The error in thermal loss from unstable temperatures is larger than the efficiency error because the receiver delta temperature during a loss test is usually much less than during an efficiency measurement.

The requirement for 0.1°C stability in measured temperatures for a usable data point is empirically based. It appears to produce valid data and is about as good as the fluid loop and collector system can attain in the outdoor test environment.

Calculations of Incident Angle Modifier

The efficiency of a concentrating solar collector is at its maximum value only when the incoming solar radiation is perpendicular to the reflector aperture. At other times of the day, efficiency is less than the noon value and is approximately proportional to the cosine of the incident angle. Incident angle is defined as the angle between direct-solar radiation from the sun and a perpendicular to the plane of the collector's aperture. Thus, the incident angle on an east-west axis, solar elevation tracking collector is zero only at noon. Incident angle for a two-axis tracking collector is always zero.

ASHRAE Standard 93.77 defines a test method for determining the quantity K, called the incident angle modifier. (ASHRAE 93-77 defines testing standards for flat-plate solar collectors, but many of the procedures also apply to concentrating collectors.) The incident-angle modifier, K, defines the change in collector efficiency as the incident angle increases. The incident-angle modifier experimentally combines the cosine effect with several other factors such as mirror-slope errors, reflections from the receiver cover glass at large angles, etc.

Incident-angle modifier can be defined as the ratio of optical efficiency at a given incident angle to the optical efficiency at a zero-incident angle, both quantities measured on an infinitely long collector row.

Measured efficiency from a short collector module cannot be used directly to calculate the incident-angle modifier; corrections for end loss first must be applied. For parabolic troughs with a receiver length equal to the aperture length and negligible thermal losses from the unilluminated portion of the receiver, measured efficiency can be converted to an equivalent efficiency for a long collector row by use of the relationship:

$$\eta = \eta_s \left(1 + \frac{\tan\theta\,(fw + w^3/48f)}{wL - \tan\theta\,(fw + w^3/48f)}\right) \qquad (3)$$

where

η_s = efficiency measured on a short row
η = efficiency corrected for end loss
θ = solar radiation incident angle
f = collector focal length
w = width of collector aperture
L = length of collector aperture

The efficiency test used for determining incident angle modifier must be done with the collector receiver operating at ambient air temperature. If this cannot be done, corrections for thermal loss must also be made. As will be seen later in this report, thermal loss from a concentrating solar collector is not at all a simple function. The uncertainty of a thermal loss correction can be avoided if the incident angle data is taken at ambient air temperature, where the thermal loss, though still not zero, is small enough not to cause serious errors.

Test Results With Corning Glass Reflector

Cold Water as Heat-Transfer Fluid

Solar Kinetics' T-700A was the first (and only) collector module tested with the CMTF's new Fluid Loop 2 and the AZTRAK rotating platform. The collector was installed on the platform by Solar Kinetics; preliminary testing began on 24 July 1980. Initial tests on the T-700A were run with cold water as the heat-transfer fluid.

Figure 5 shows a data plot made on 24 July, the first full test day. The AZTRAK tracked the sun in azimuth, with the T-700A providing solar-elevation tracking. Figure 5 shows the flat efficiency curve that normally results from two-axis sun tracking. The efficiency data was somewhat scattered because of water pressure variations causing slight fluctuations in water flow rate. Efficiency increased slightly through the day as the elevation tracking was adjusted for optimum results. Measured efficiency was very high, averaging 78.6% at an average receiver fluid temperature 1.1°C above the ambient air temperature.

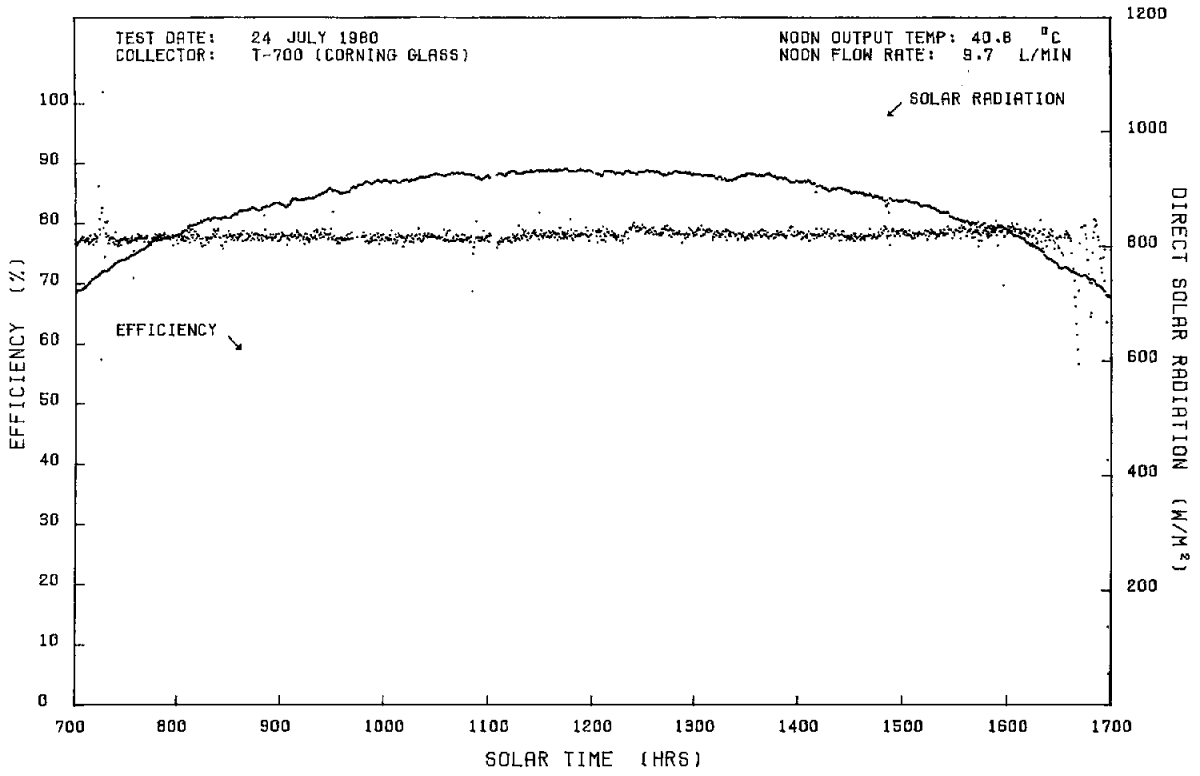

Figure 5. Solar Kinetics Parabolic Trough Efficiency Evaluation at 26.9°C

Data plots such as that shown in Figure 5 were made in real-time during each test day. The plots have proven invaluable in detecting data trends and oscillations that are not obvious in tabular printed data output. Each 15- to 20-s data-measurement cycle produces a solar-irradiance measurement and an efficiency point (plus many other data values that are recorded on magnetic tape); these two data values are plotted on the data curves as single dots. With stable measurements, the dots blend into continuous curves; with less stable conditions, the data rate is high enough to trace transients. More than 3000 data sets are found on some of the all-day efficiency curves.

Figure 6 was obtained a few days later, on 29 July. For this test, the AZTRAK platform was stationary; it was parked with the collector axis oriented east-west. The large dip in the efficiency curve just after 0700 was caused by the shadow of a large water-storage tower passing across the collector. Peak measured efficiency at noon was the same as observed during the 24 July test shown earlier in Figure 5. Cause of the dips in the efficiency curve near 1330 and at 1600 was not immediately identified, but will be seen again on successive test days at the same times.

Figure 7 shows a data plot obtained on 4 August. This test was more a test of the AZTRAK than of the collector; the platform was programmed to track the sun in such a way as to produce constant solar-radiation incident angles. The programmed incident angles (shown on Figure 7) were decreased in 10° increments at about 30-min intervals. The test was a success; if Figures 6 and 7 are overlaid, the efficiency at each of the several incident angles can be seen as the same on both curves.

"All-day" tests such as shown in Figure 6 have been made at the CMTF for several years; we have always assumed that the rate-of-change of solar azimuth was slow enough that the efficiency measurements taken were representative of constant, stable conditions. The test shown in Figure 7, and later tests at higher temperatures, confirmed the validity of the all-day test curves; the efficiency measurements were not changed when the incident angle was held constant for longer periods.

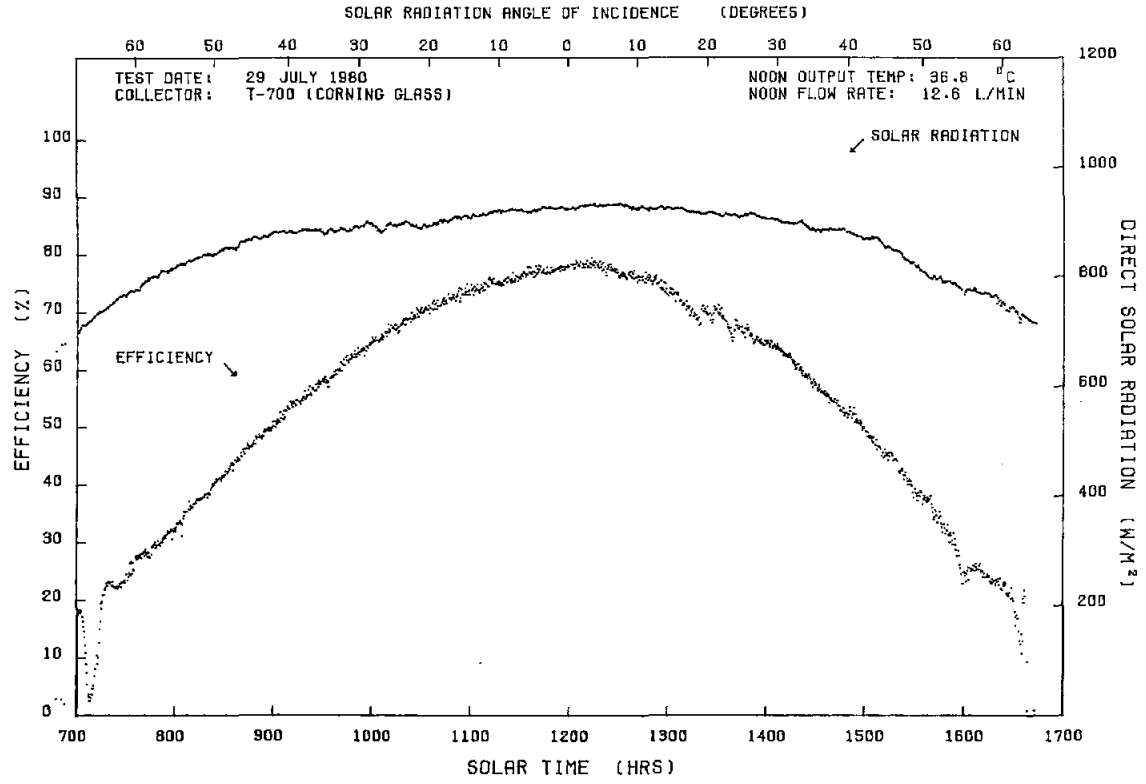

Figure 6. Solar Kinetics Parabolic Trough Efficiency Evaluation at 26.3°C

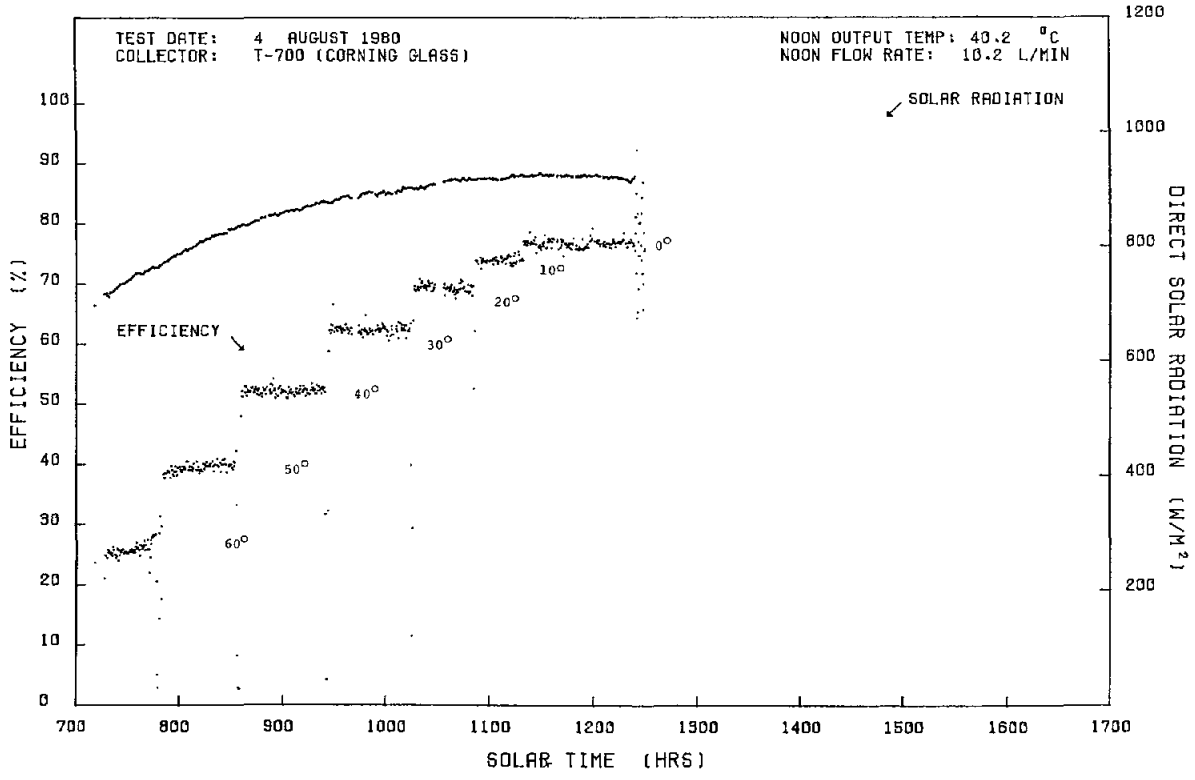

Figure 7. Solar Kinetics Parabolic Trough Efficiency Evaluation at 27.3°C

Syltherm 800 as Heat-Transfer Fluid

After completion of the collector tests with water, the plumbing was changed to furnish Dow Corning's Syltherm 800 from Fluid Loop 2 as the heat-transfer fluid. The lowest Syltherm 800 input temperature used was 52.1°C, the highest output temperature was 320°C. Figure 8 is a data plot from a test at 76°C input temperature; the collector axis was fixed and oriented east-west. Peak efficiency at noon was 77%. The irregularities in the afternoon efficiency curve, as seen earlier in Figure 6, were again present; these were eventually traced to several small irregularities along the shadow-forming edges of the sun-tracking sensor. After Solar Kinetics replaced the sun sensors, smooth tracking was achieved throughout the day.

Tests were continued, increasing the temperatures in about 50°C increments. Test data plots from most of these tests are not shown in this report since most of them are rather uninteresting straight lines. The next three figures were made at temperatures near 300°C, and again illustrate the varied test procedures and data available with a test platform such as the AZTRAK. Figure 9 was obtained from a test on 17 September, with the AZTRAK programmed to track the sun for a zero solar-radiation incident angle on the collector. Figure 10 shows the results of a test in which the incident angle was held constant for about 20 to 25 min each, beginning at 65° and decreasing the angle to zero in 5° increments. Finally, Figure 11 shows the test results with a fixed east-west collector axis. In all three cases, the measured average peak efficiency was about 57%.

Test data accumulated to this point is shown in Table 1. The same data in graphical form is shown in Figures 12, 13, and 14.

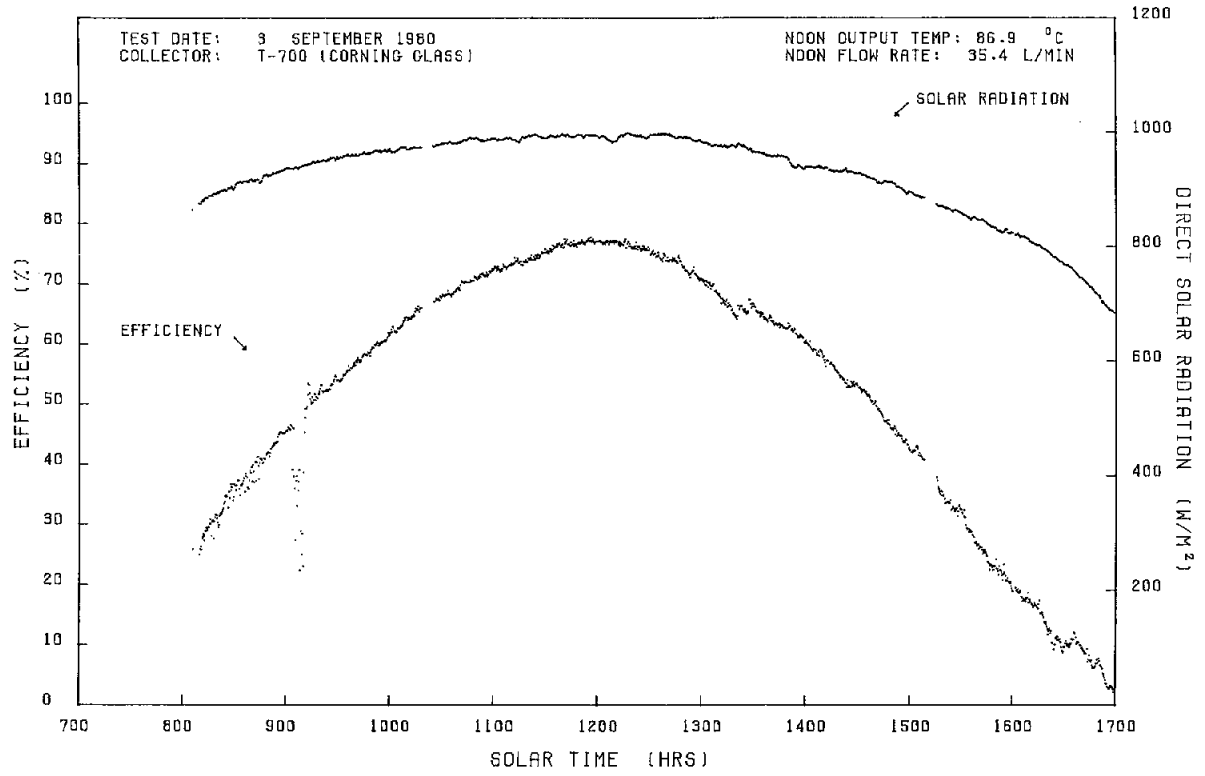

Figure 8. Solar Kinetics Parabolic Trough Efficiency Evaluation at 76.2°C

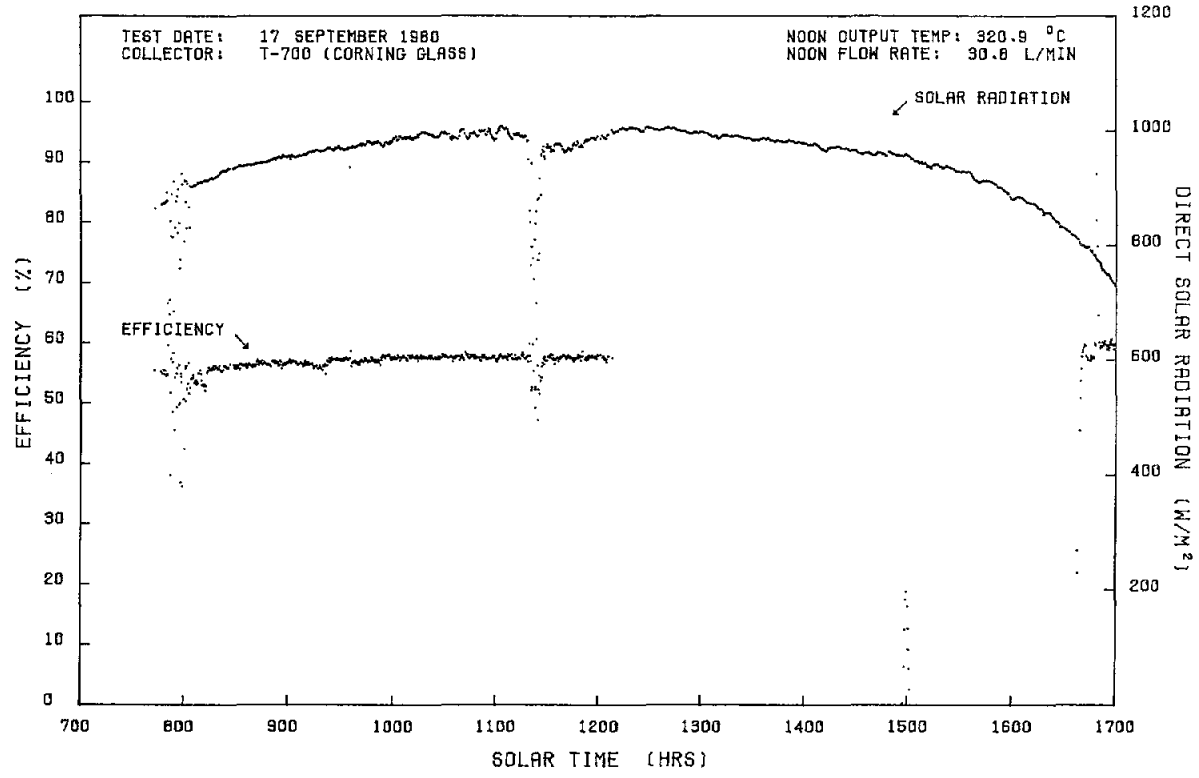

Figure 9. Solar Kinetics Parabolic Trough Efficiency Evaluation at 310.7°C

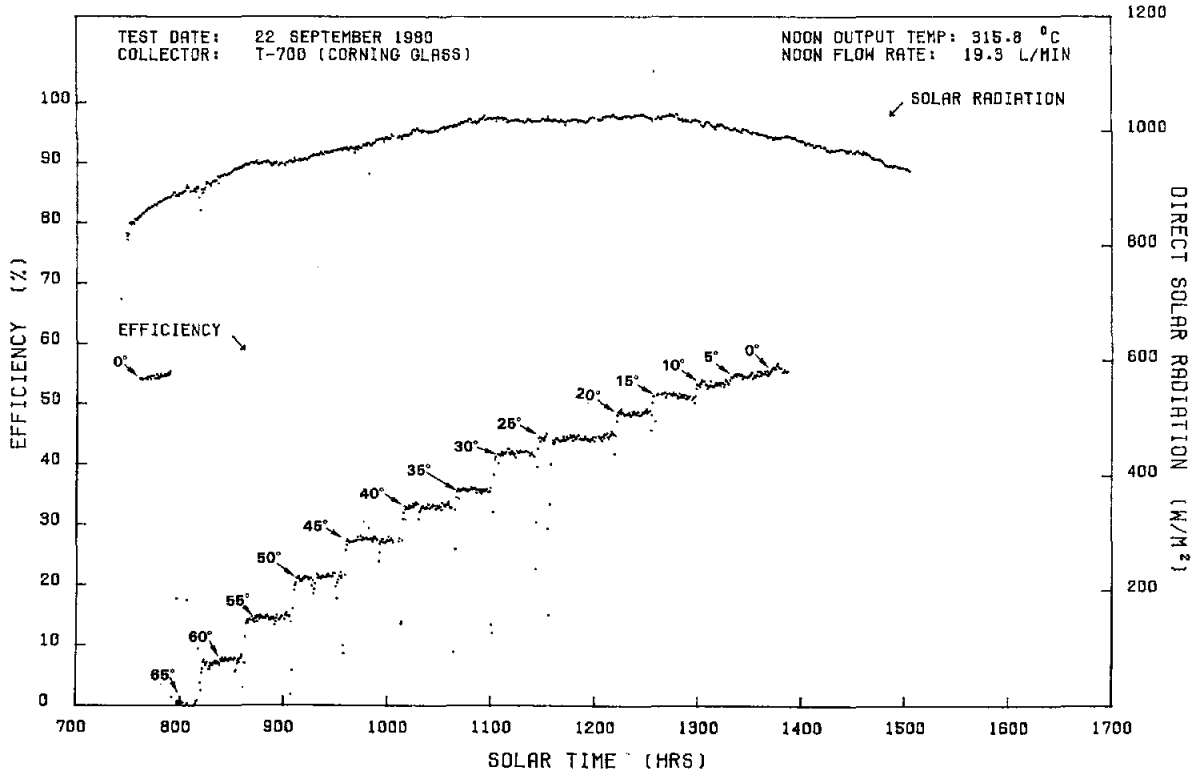

Figure 10. Solar Kinetics Parabolic Trough Efficiency Evaluation at 302.9°C

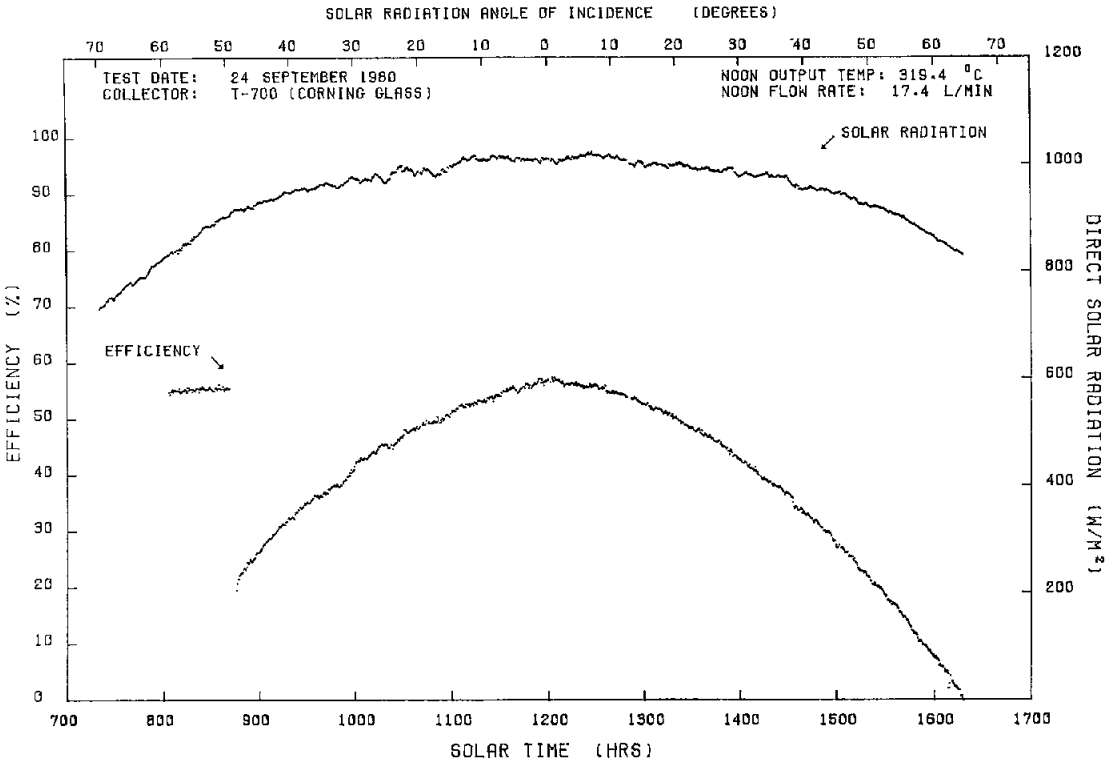

Figure 11. Solar Kinetics Parabolic Trough Efficiency Evaluation at 301.6°C Input

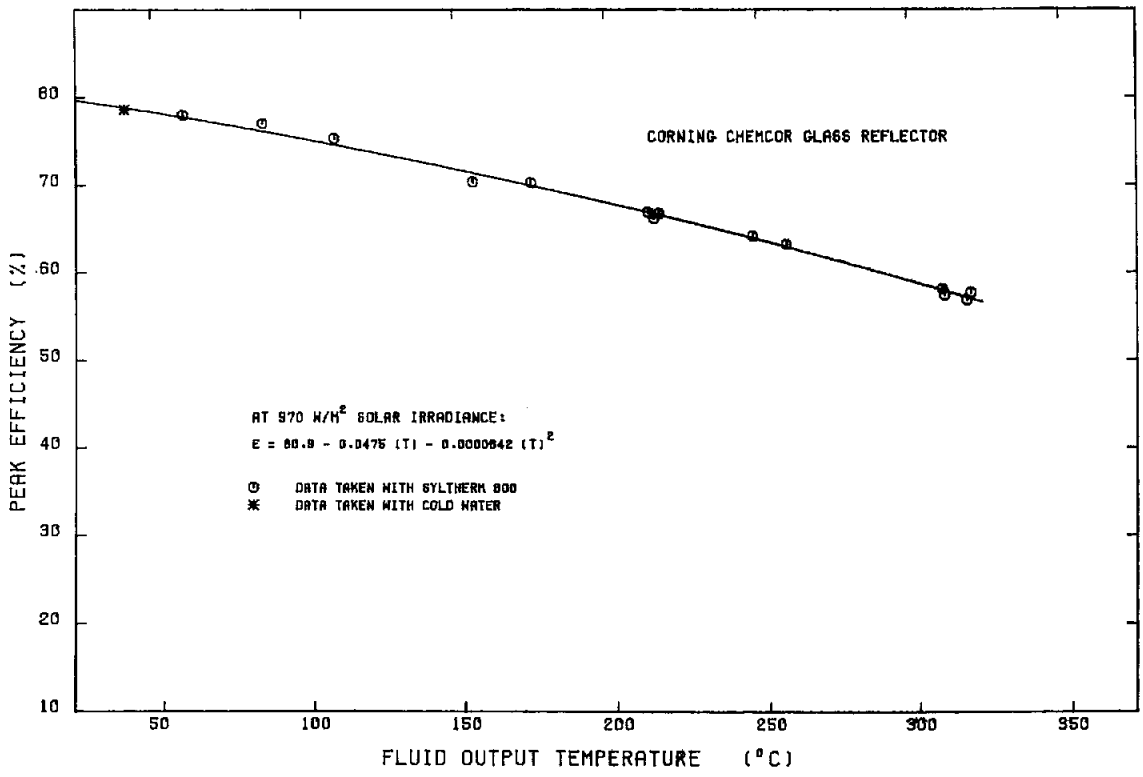

Figure 12. Solar Kinetics T-700A Efficiency vs Output Temperature

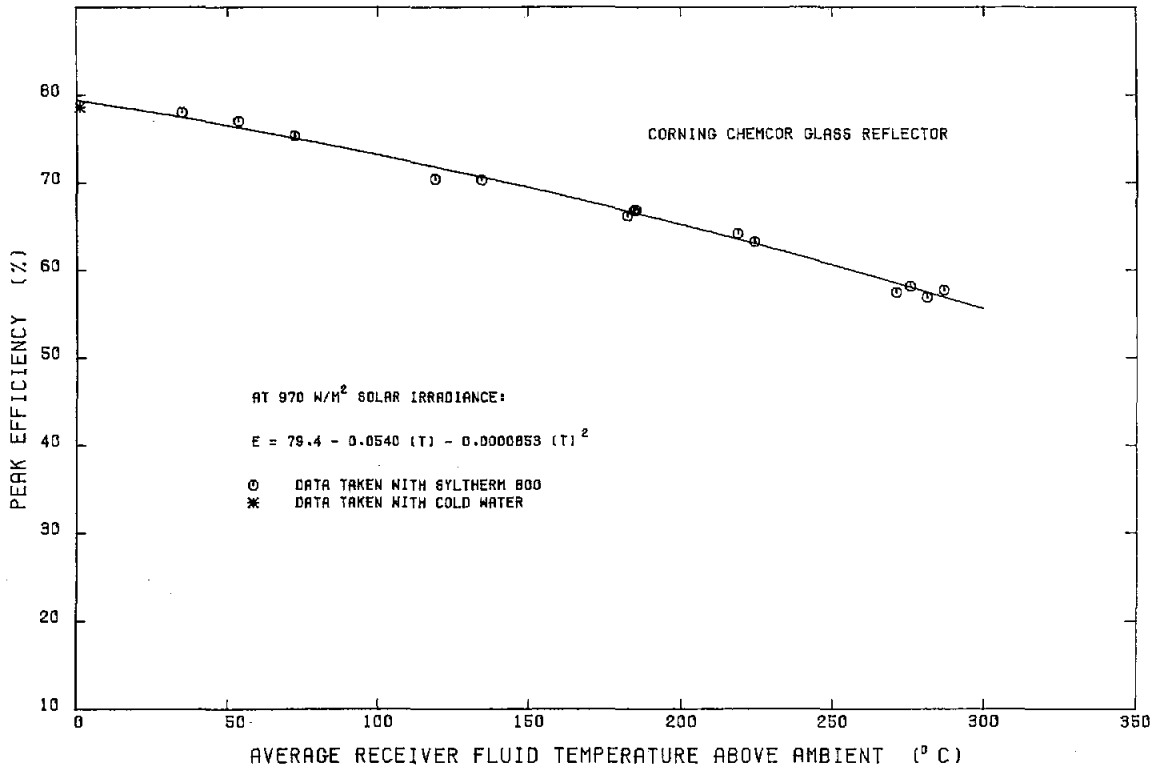

Figure 13. Solar Kinetics T-700A Efficiency vs Temperature Above Ambient

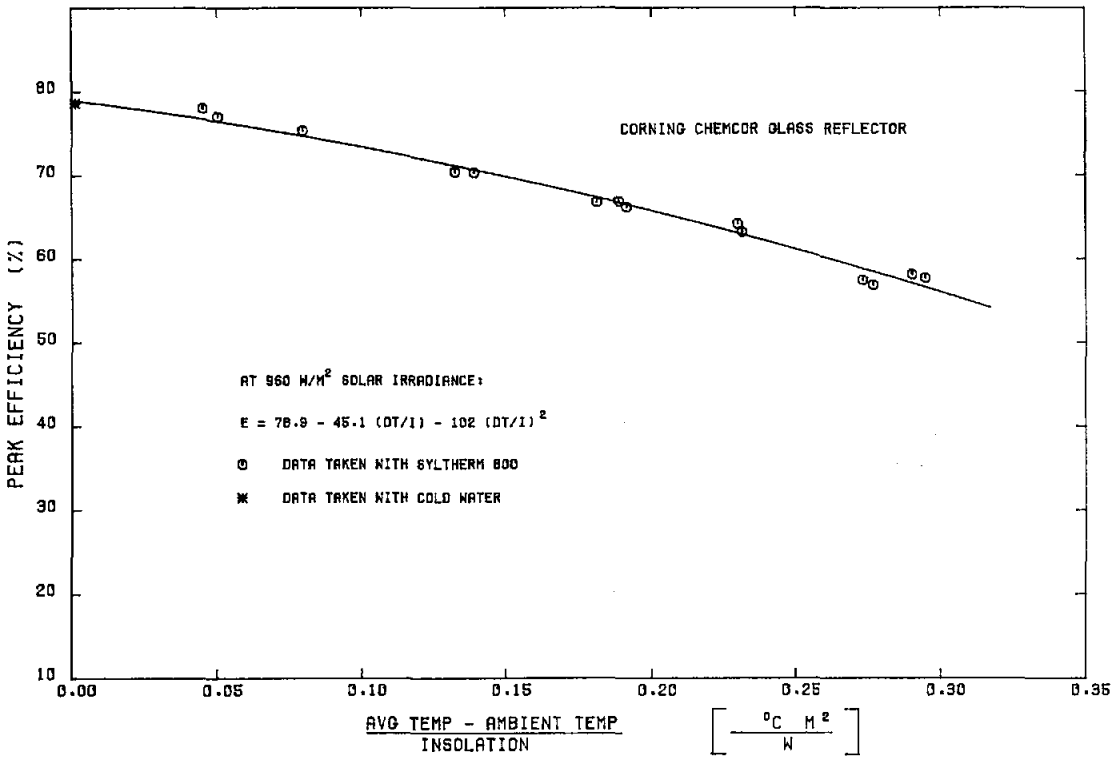

Figure 14. Solar Kinetics T-700A Efficiency vs Delta-T/I

Therminol 66 as Heat-Transfer Fluid

All the collectors tested previously at the CMTF had been evaluated using either Therminol 66 or water as the heat-transfer fluid. Very few had been checked with both fluids; none had been tested using the new Syltherm 800 heat-transfer fluid. For a comparison of collector performance using the different fluids, the Solar Kinetics T-700A collector was replumbed to use Monsanto's Therminol 66 from CMTF Fluid Loop 1. Testing with Therminol began on 30 September; efficiency measurements were made at output temperatures from 80° to 317°C. Data plots from these tests look much like those already presented, and are not included in this report. Efficiency test data is summarized in Table 2. Effficiency curves derived from least-squares fits to the test data are shown in Figures 15, 16, and 17. A comparison of the test results for Syltherm 800 and Therminol 66 is shown in Figures 18, 19, and 20.

Table 1. Solar Kinetics T-700A Efficiency Test Data, Syltherm 800 Heat-Transfer Fluid, Glass Reflector

Test Date	Direct Irradiance (W/m^2)	Temp Out (°C)	Receiver Delta T (°C)	Flow Rate (L/min)	$\frac{\text{Delta-T}}{I}$ ($°C \cdot m^2/W$)	Efficiency (%)
7/24/80	925.5	41.2	14.3	9.4	0.0012	78.6*
8/07/80	891.4	156.5	10.11	31.4	0.1335	70.4
8/28/80	962.0	259.5	8.11	39.6	0.2330	63.2
8/29/80	943.3	311.3	8.18	36.5	0.2923	58.1
9/03/80	983.8	86.8	10.62	35.4	0.0504	77.0
9/04/80	902.2	110.7	9.77	34.9	0.0801	75.3
9/12/80	973.1	214.0	9.37	35.9	0.1902	66.9
9/15/80	766.2	60.3	8.13	36.3	0.0453	78.0
9/15/80	943.7	248.3	7.01	45.4	0.2315	64.2
9/16/80	957.6	175.8	20.89	16.4	0.1402	70.3
9/17/80	965.9	320.7	9.88	30.8	0.2969	57.7
9/18/80	946.2	215.9	14.86	21.7	0.1928	66.2
9/18/80	1009.6	217.6	16.00	21.7	0.1827	66.8
9/19/80	985.5	311.9	17.90	17.1	0.2752	57.5
9/24/80	1008.6	319.4	17.80	17.4	0.2788	56.9

*Data taken with cold water.

Table 2. Solar Kinetics T-700A Efficiency Test Data, Therminol 66 Heat-Transfer Fluid, Glass Reflector

Test Date	Direct Irradiance (W/m^2)	Temp Out (°C)	Receiver Delta T (°C)	Flow Rate (L/min)	$\frac{\text{Delta-T}}{I}$ ($°C \cdot m^2/W$)	Efficiency (%)
9/01/80	1023.2	255.2	9.2	27.3	0.2195	65.1
9/01/80	1001.2	307.5	11.02	20.2	0.2670	61.1
9/01/80	945.1	213.2	12.30	20.3	0.1807	68.3
9/02/80	942.1	86.8	8.02	39.0	0.0659	75.6
9/02/80	957.9	107.5	7.70	39.5	0.0854	74.1
9/02/80	947.6	160.3	11.40	23.9	0.1322	71.2
9/03/80	988.0	317.0	9.30	23.1	0.2852	60.1

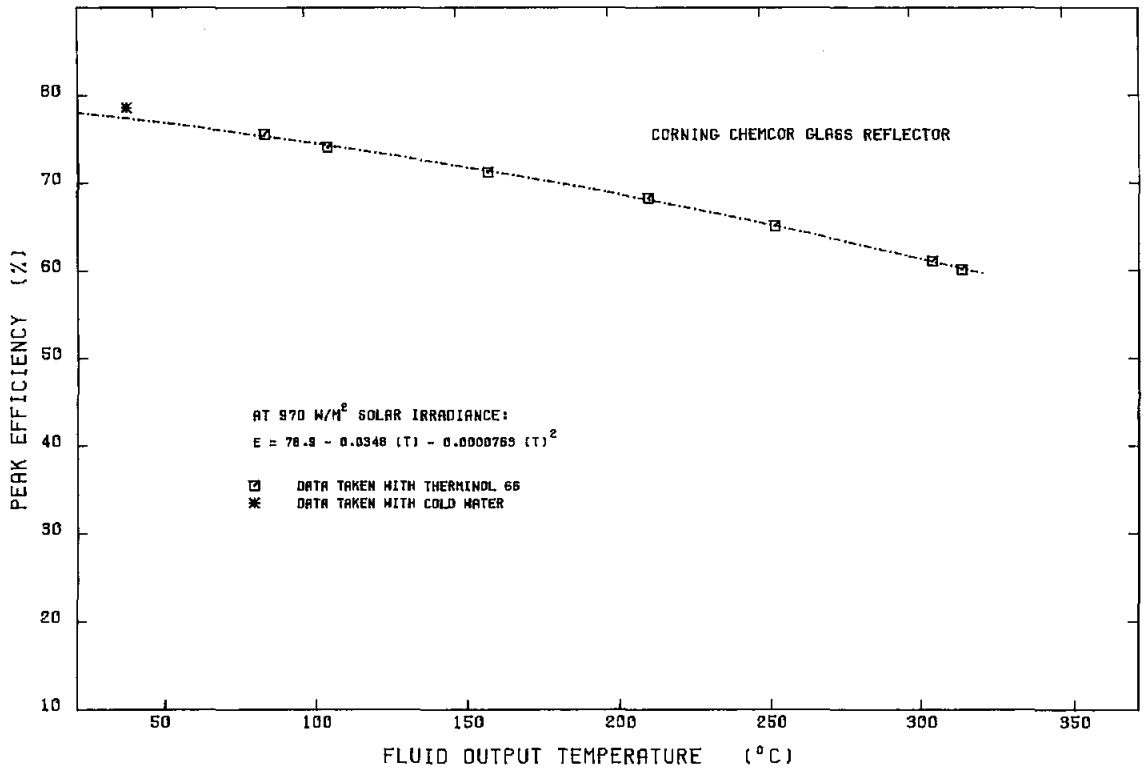

Figure 15. Solar Kinetics T-700A Efficiency vs Output Temperature

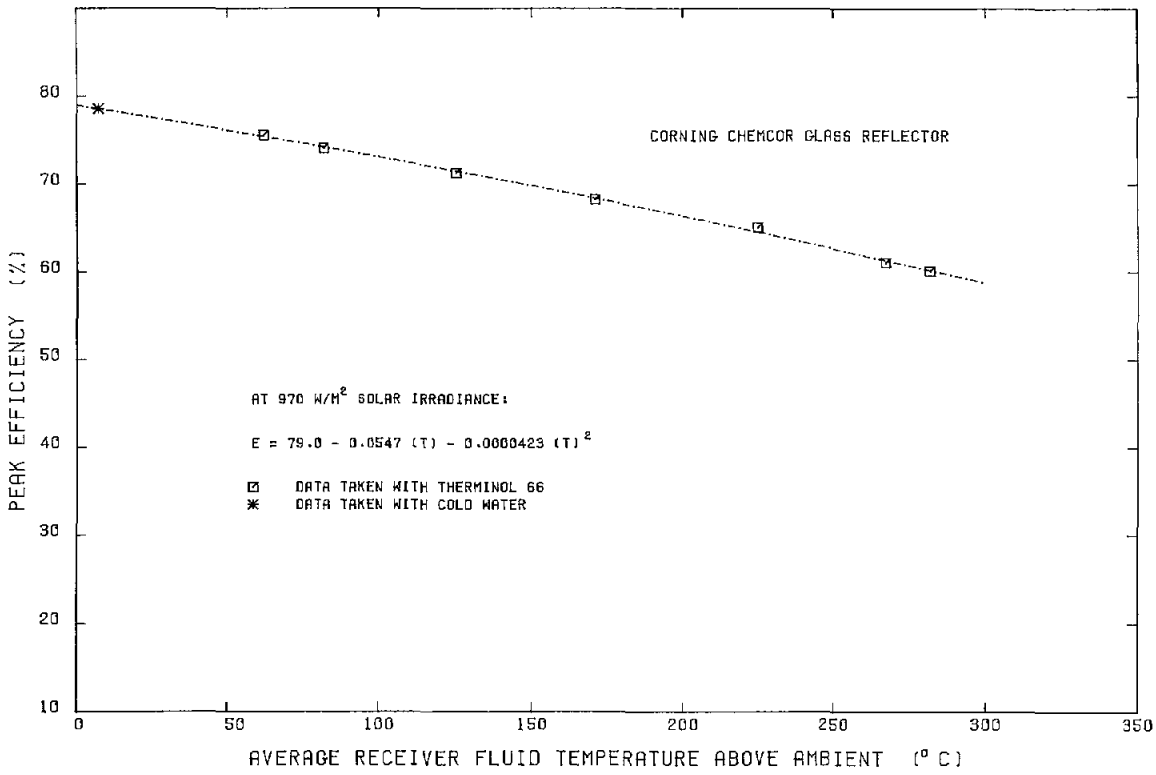

Figure 16. Solar Kinetics T-700A Efficiency vs Temperature Above Ambient

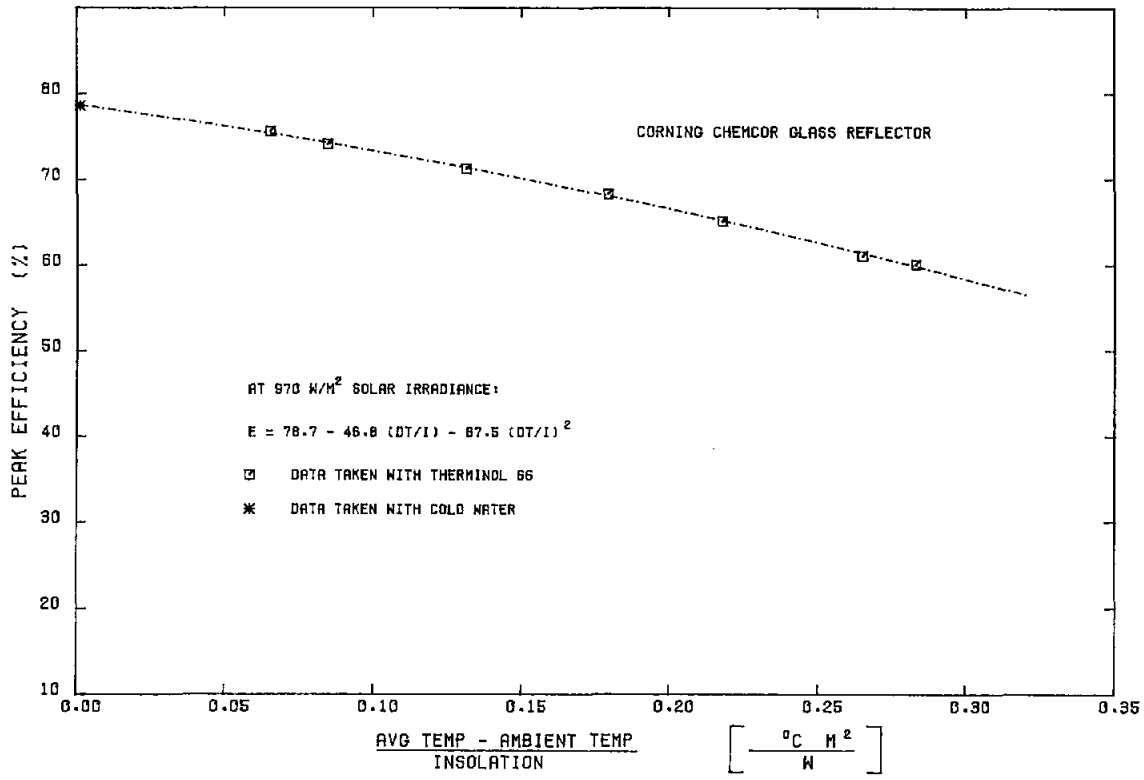

Figure 17. Solar Kinetics T-700A Efficiency vs Delta-T/I

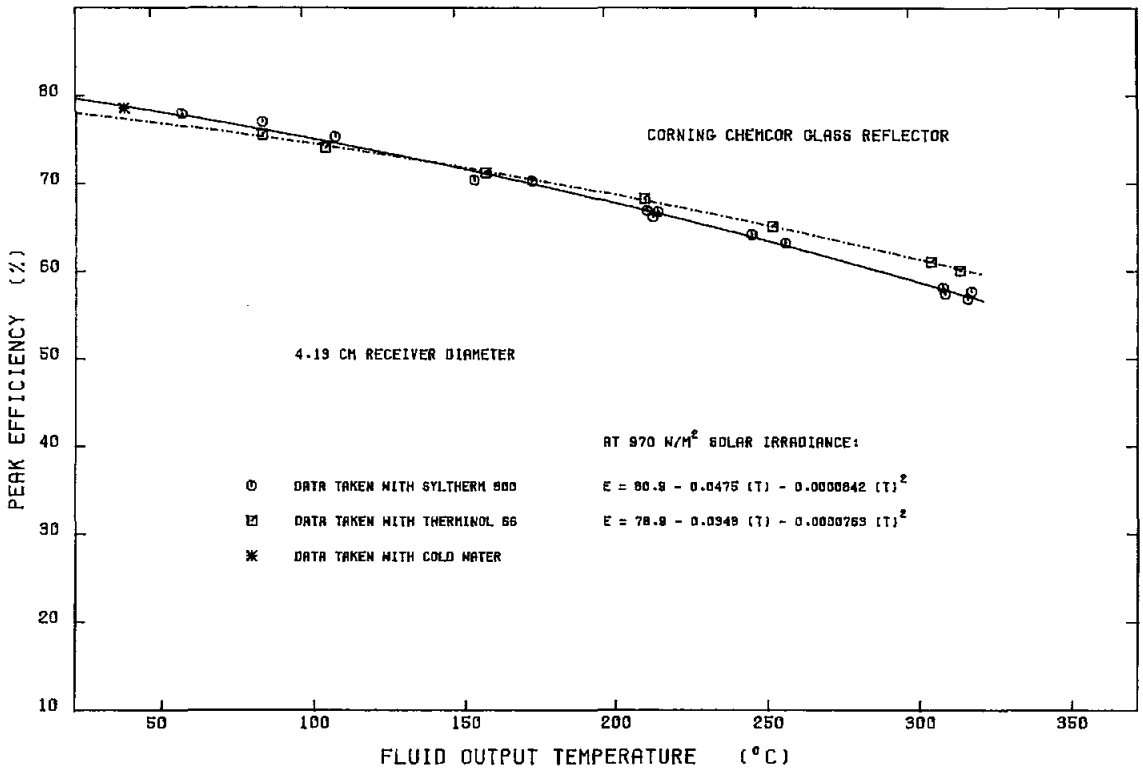

Figure 18. Performance Comparison—Syltherm 800 vs Therminol 66 (Efficiency vs Fluid Output Temperature)

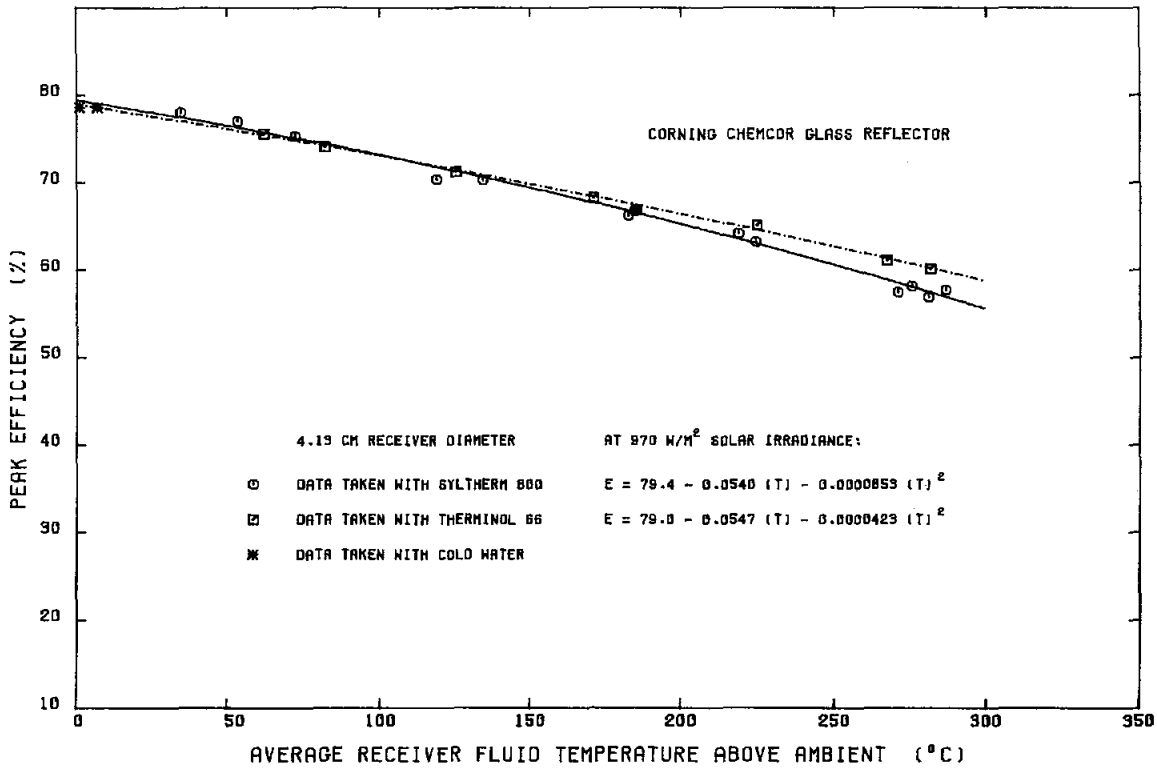

Figure 19. Performance Comparison—Syltherm 800 vs Therminol 66 (Efficiency vs Average Fluid Temperature Above Ambient)

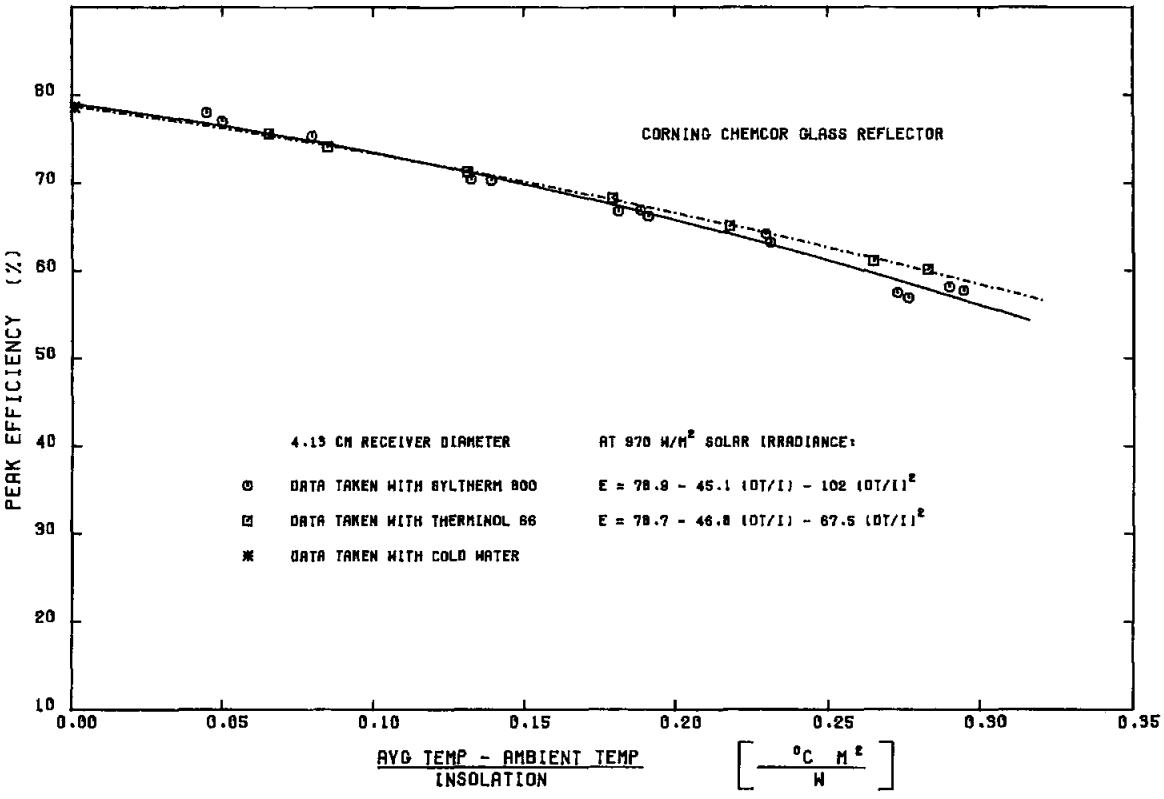

Figure 20. Performance Comparison—Syltherm 800 vs Therminol 66 (Efficiency vs Delta T/I)

Solar Kinetics T-700A Test Results With FEK-244 Acrylic-Film Reflector

4.13-cm-dia Absorber, Pyrex Glass Envelope

In April 1981, the Corning glass reflector assembly was replaced by a new assembly using the 3M Company's FEK-244 acrylic-film reflector material. A complete test series was again performed, beginning with ambient temperature tests using cool water as the heat-transfer fluid. Syltherm 800 was used for all the elevated temperature measurements that covered the range from 70° to 317°C.

As expected, measured efficiencies with the acrylic-film reflectors were somewhat lower than those produced by the glass mirrors. Most of the difference was caused by the lower reflectance of the second-surface acrylic film (about 0.84 for FEK-244 vs ~ 0.94 for glass). The focus accuracy of the two reflector assemblies was not identical, so the exact difference in measured efficiency because of reflectance alone is uncertain. There were no surprises during the test series; the data plots made during each test day do not look very interesting, and have been omitted from this report. Table 3 contains the data accumulated during the efficiency test series. Thermal loss was not measured again because the receiver configuration was identical to that used during the glass-mirror test series. The efficiency test data from Table 3 is also shown in Figures 21, 22, and 23. For comparison, the data from the glass-reflector test is also shown in the figures.

Beginning in late April 1981, a very interesting set of efficiency measurements was made to determine changes in collector performance with lower than usual levels of input solar radiation. These tests were made with the FEK-244 reflector and 4.13-cm-dia absorber; the test results are covered in a separate section of this report.

Table 3. Efficiency Test Data, Syltherm 800 Heat-Transfer Fluid, FEK-244 Acrylic-Film Reflector, 4.13-cm-dia Absorber

Test Date	Direct Irradiance (W/m^2)	Temp Out (°C)	Receiver Delta-T (°C)	Flow Rate (L/min)	$\frac{\text{Delta-T}}{I}$ ($°C \cdot m^2/W$)	Efficiency (%)
4/07/81	1022.5	29.9	9.60	14.3	0.00212	73.12*
4/07/81	1023.9	29.8	9.54	14.4	0.00224	72.74*
4/09/81	1056.6	116.9	9.40	36.9	0.0822	65.69
4/09/81	1044.9	163.0	10.27	33.4	0.1263	64.88
4/09/81	1005.9	209.4	9.48	33.7	0.1758	61.55
4/09/81	953.8	256.9	8.32	34.3	0.2354	56.8
4/10/81	999.9	71.8	9.84	36.1	0.0422	71.84
4/10/81	1018.1	113.7	9.87	35.3	0.0828	68.63
4/10/81	1029.4	162.3	9.11	37.6	0.1274	65.76
4/10/81	1031.2	207.6	8.44	39.2	0.1732	62.13
4/10/81	1030.5	256.0	7.75	40.2	0.2196	57.25
4/10/81	1019.3	259.1	11.60	26.0	0.2213	56.25
4/13/81	958.1	307.5	7.77	34.7	0.2892	51.77
4/17/81	981.7	170.9	10.29	31.6	0.1419	65.29
4/17/81	995.5	317.7	8.56	32.9	0.2883	51.88
4/20/81	928.9	166.3	10.36	29.6	0.1516	65.20

*Data taken with cool water.

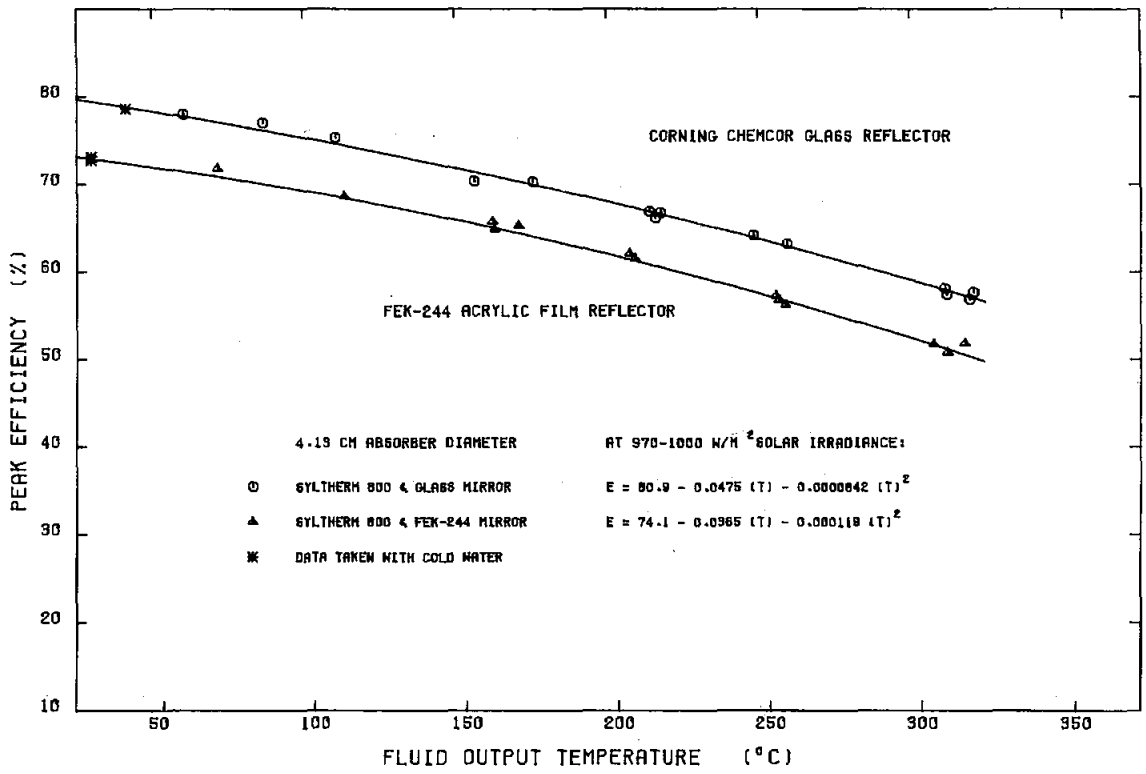

Figure 21. Performance Comparison—Glass Mirror vs FEK-244 Film Mirror (Efficiency vs Fluid Output Temperature)

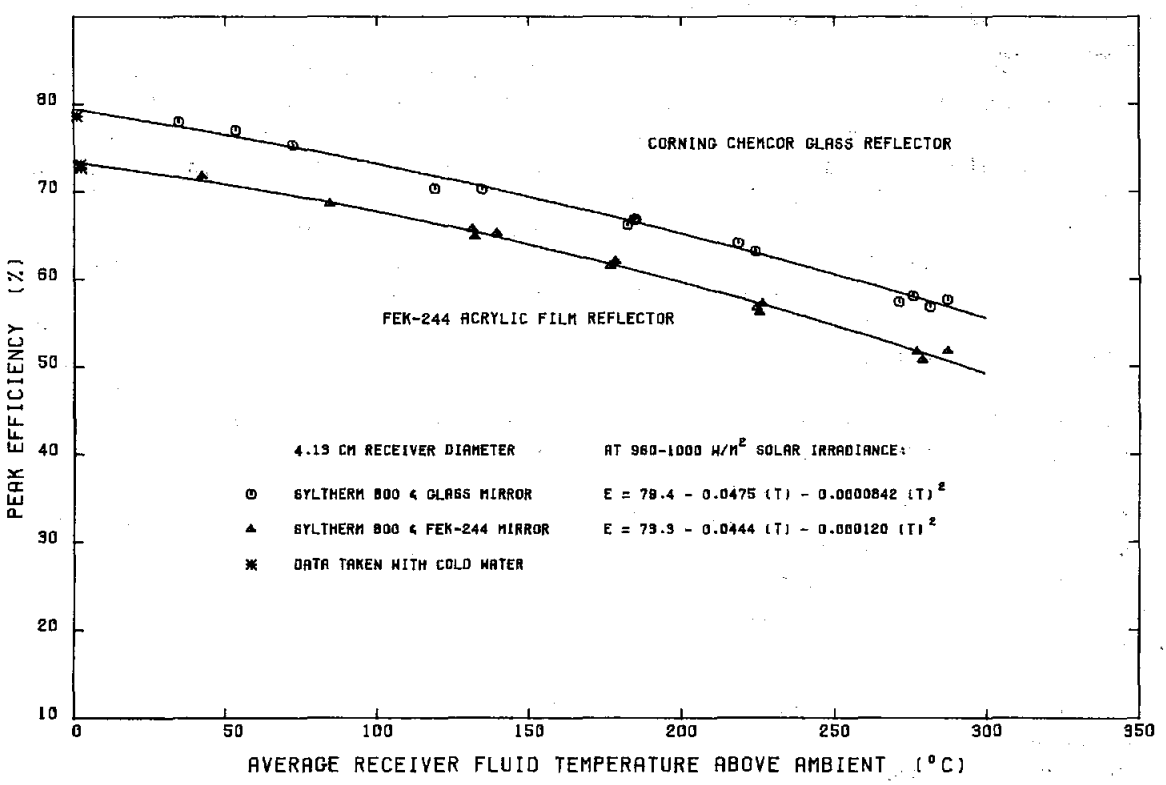

Figure 22. Performance Comparison—Glass Mirror vs FEK-244 Film Mirror (Efficiency vs Average Fluid Temperature Above Ambient)

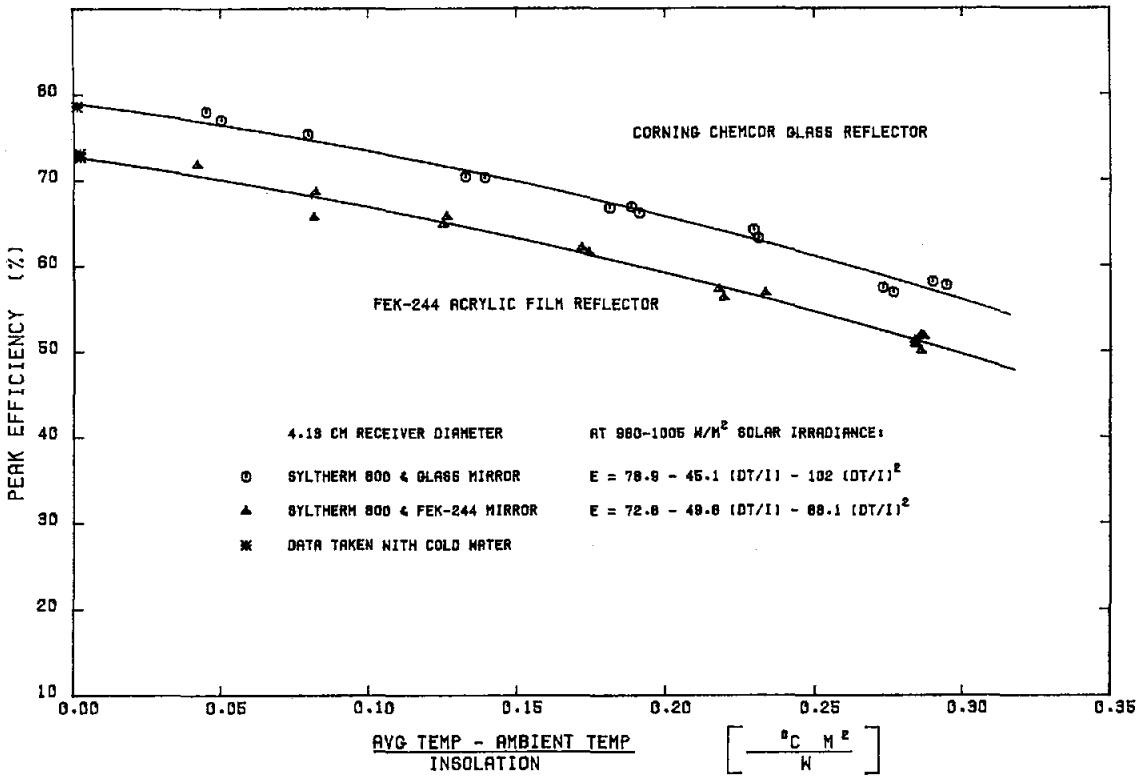

Figure 23. Performance Comparison—Glass Mirror vs FEK-244 Film Mirror (Efficiency vs Delta T/I)

3.18-cm-dia Absorber, Quartz Glass Envelope

After completion of the test series with the 4.13-cm-OD absorber, a new receiver assembly was installed. The new absorber was smaller, 3.18-cm OD (1.25 in.) vs 4.13-cm OD (1.625 in). The receiver envelope was also smaller (5.21 cm O.D. vs 6.35 cm O.D.) and was made of a quartz glass. The smaller absorber had 23% less surface area; it was hoped that the smaller absorber and the quartz glass would result in less thermal loss and higher operating efficiency at high temperatures.

The tests conducted on the T-700A collector to this point had been very stable and repeatable from day to day. Initial tests with the small-diameter absorber were confusing—efficiency was varying from day to day and at different times of the day. Eventually the problem was traced to two different factors: a slightly malfunctioning sun sensor in the tracking system and movement of the absorber in the focal pattern.

A new sun-sensing head was installed, which improved things slightly. The problem did not go away until an additional support was added at the end of the receiver to prevent flex-hose loads from bending the absorber. The smaller receiver was significantly more flexible than the original design. As the collector moved in elevation during the day, the rather stiff flex hoses produced enough force to move portions of the absorber tube far enough out of focus to change the measured efficiencies. In addition to changes in the amount of focused light striking the absorber surface as the tube moved, we also found that the thermal loss varied by 25% or more as the absorber-to-glass spacing changed; this variation in thermal loss significantly affected the efficiency measurements.

Because of the problems mentioned above, the data scatter at each temperature was larger than in any of the other tests performed. Finally, the whole data set was thrown out, and a new test series was made after stiffening the receiver assembly enough to obtain repeatable measurements. The test data is shown in Table 4, and in Figures 24, 25, and 26.

With the smaller absorber diameter, more of the focused light was missing the receiver. This visual observation was confirmed by the low-temperature efficiency measurements—~66% with the 3.18-cm absorber vs nearly 73% with the 4.13-cm absorber. However, the lower thermal loss of the smaller absorber surface area gave the desired result at high temperatures. At 300°C, the smaller absorber was better, with observed efficiencies near 56% vs ~52% for the larger absorber. The improvement was even more pronounced at 350°C.

Table 4. Efficiency Test Data, Syltherm 800 Heat-Transfer Fluid, FEK-244 Acrylic-Film Reflector, 3.18-cm Absorber, Quartz Glass Envelope

Test Date	Direct Irradiance (W/m^2)	Temp Out (°C)	Receiver Delta T (°C)	Flow Rate (L/min)	$\frac{\text{Delta-T}}{I}$ ($°C \cdot m^2/W$)	Efficiency (%)
10/22/81	878.4	107.1	7.94	35.3	0.0950	63.89
10/26/81	930.6	171.4	8.14	36.3	0.1610	62.41
10/26/81	1022.1	208.0	8.96	36.0	0.1830	61.11
10/26/81	986.2	259.7	8.22	37.1	0.2347	58.53
10/26/81	941.1	304.4	7.58	37.7	0.2948	55.95
10/29/81	962.3	105.7	8.34	37.0	0.0843	64.24
10/29/81	997.5	206.0	7.57	41.2	0.1812	60.60
10/29/81	991.1	309.2	6.98	42.9	0.2858	55.48
10/29/81	914.5	357.9	7.04	37.1	0.3605	50.86
11/02/81	971.4	70.2	10.03	31.3	0.0577	65.36
11/10/81	982.5	23.4	3.98	30.1	0.0046	66.19*

*Data taken with cool water.

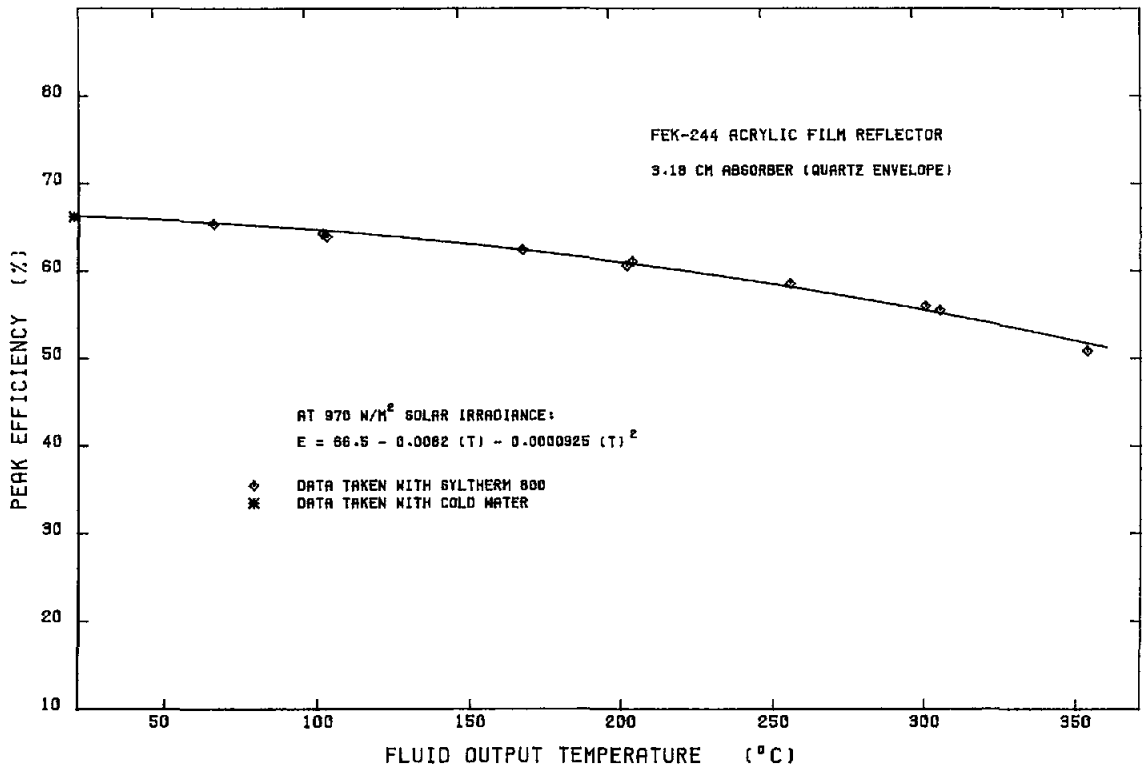

Figure 24. Solar Kinetics T-700A Efficiency vs Output Temperature

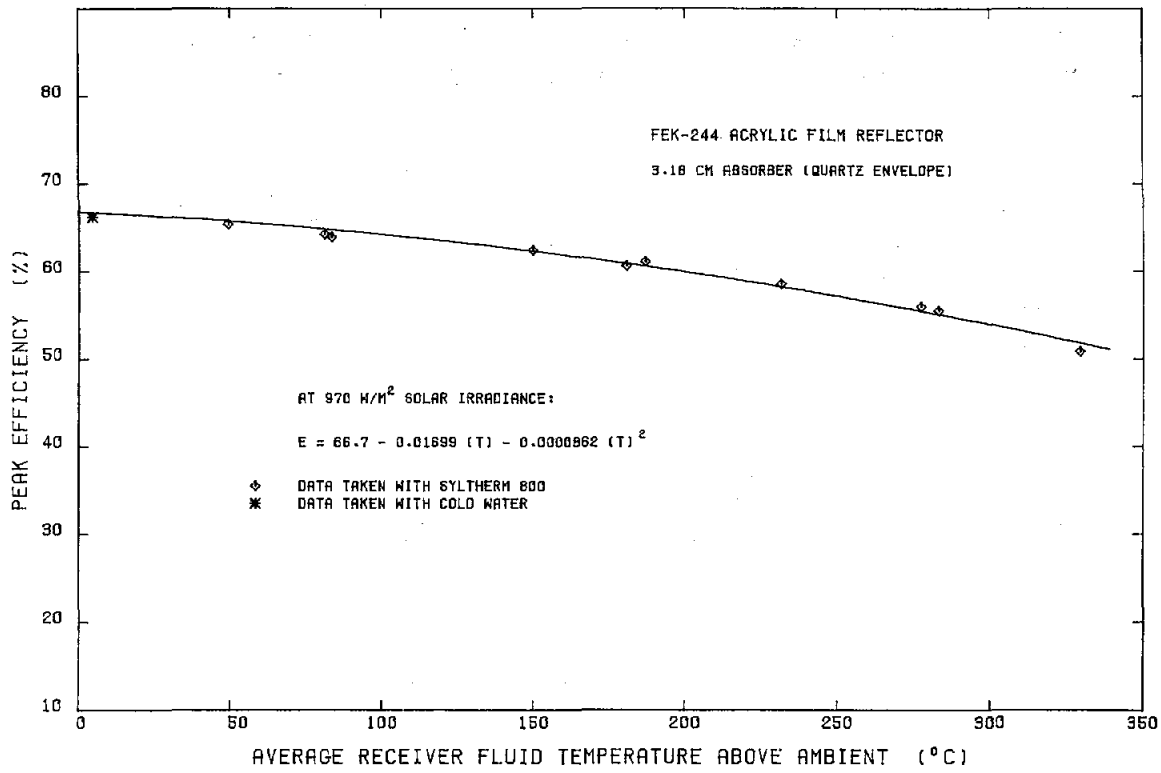

Figure 25. Solar Kinetics T-700A Efficiency vs Temperature Above Ambient

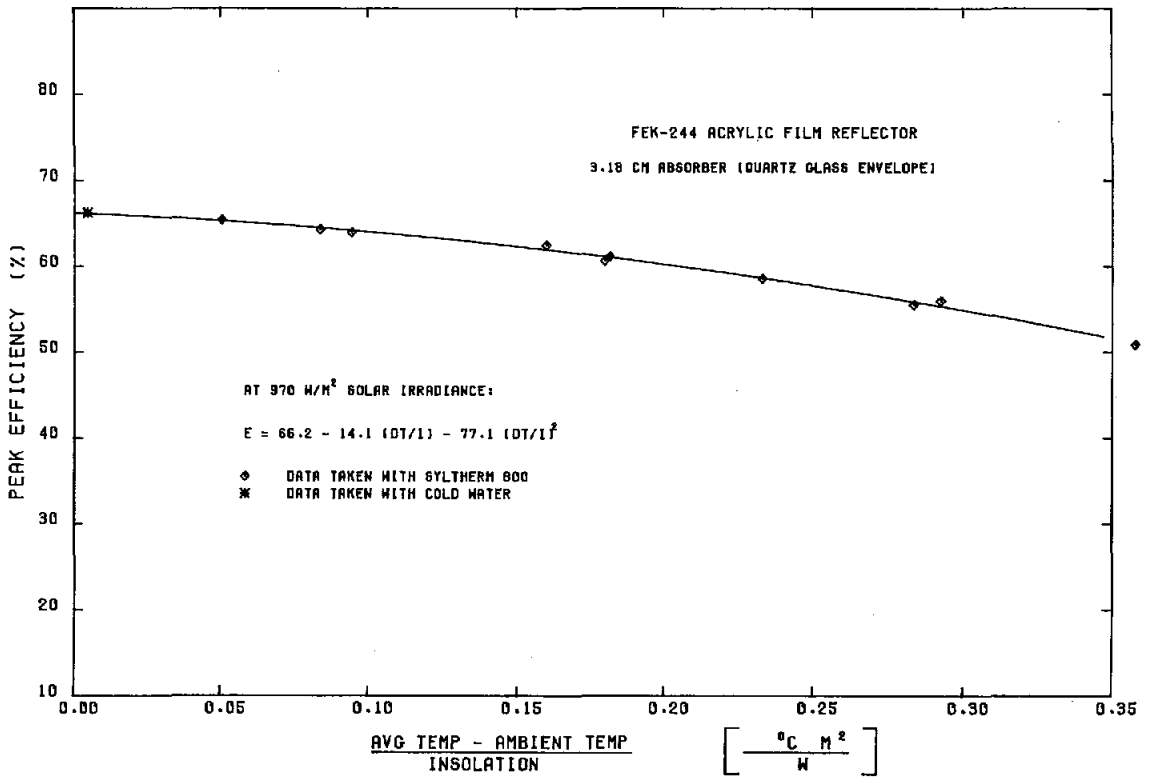

Figure 26. Solar Kinetics T-700A Efficiency vs Delta T/I

3.18-cm-dia Absorber, Pyrex Glass Envelope

For the test just discussed above, two changes had been made: a smaller diameter absorber tube, and the use of a quartz-glass envelope instead of the Pyrex-glass envelope usually found on most parabolic trough collectors. It was not clear how much of the performance change was caused by each of the two factors. A new Pyrex-glass envelope, identical in diameter to the quartz glass, was installed on the receiver assembly for another test series. Test data obtained is shown in Table 5, and in Figures 27, 28, and 29. For comparison, Figure 30 shows the efficiency curves obtained during the FEK-244 reflector tests with all three receiver design variations.

The transmissivity of the Pyrex glass appears to be lower than that of the quartz glass, resulting in a slightly lower efficiency at low temperatures. However, the efficiency at 300°C was even better than that obtained with the quartz glass, probably because the quartz is more transparent to infrared radiation, resulting in increased thermal loss at high temperatures.

Incident Angle Modifier Test Results

In combination with the AZTRAK platform, the Solar Kinetics T-700A collector performed as a two-axis sun-tracking device. However, in an actual field installation, the collector would have only elevation tracking available. The peak efficiency curves determined for the collector (such as Figures 12 through 30) apply only when the solar radiation incident angle is zero. For a fixed collector axis, oriented east-west, zero incident angle occurs only at solar noon. At other times of the day, collector efficiency decreases with increasing incident angle, as shown in several of the all-day efficiency plots in this report.

Table 5. Efficiency Test Data, Syltherm 800 Heat-Transfer Fluid, FEK-244 Acrylic-Film Reflector, 3.18-cm-dia Absorber, Pyrex Glass Envelope

Test Date	Direct Irradiance (W/m^2)	Temp Out (°C)	Receiver Delta-T (°C)	Flow Rate (L/min)	$\frac{\text{Delta-T}}{I}$ ($°C \cdot m^2/W$)	Efficiency (%)
7/08/81	893.7	34.1	6.17	17.5	0.0012	65.79*
9/21/81	920.6	105.7	7.74	38.1	0.0785	64.26
9/21/81	938.3	105.9	7.86	38.1	0.0775	64.07
10/09/81	946.0	210.2	8.23	37.4	0.1945	63.03
10/09/81	957.0	210.3	8.33	37.3	0.1922	62.84
10/09/81	995.4	258.3	7.77	41.0	0.2334	60.68
10/09/81	922.8	307.2	6.93	41.7	0.2983	57.59
10/13/81	897.5	73.4	8.88	33.1	0.0547	66.17
10/13/81	954.8	108.5	8.58	36.2	0.0871	65.23
10/13/81	992.4	160.6	8.32	38.3	0.1359	63.40
10/13/81	972.7	210.2	7.97	39.3	0.1862	62.44
10/16/81	988.3	209.2	8.24	38.1	0.1905	61.62
10/16/81	963.4	359.3	8.37	34.7	0.3443	53.70
10/19/81	952.8	301.0	8.70	33.9	0.2845	57.40
10/19/81	972.8	360.2	8.66	34.5	0.3470	54.60
10/20/81	966.3	23.4	3.54	33.3	-0.0052	66.51*
10/20/81	987.6	23.7	3.60	33.5	-0.0004	66.32*
10/20/81	1003.1	26.1	5.91	20.7	-0.0002	66.39*

*Data taken with cool water.

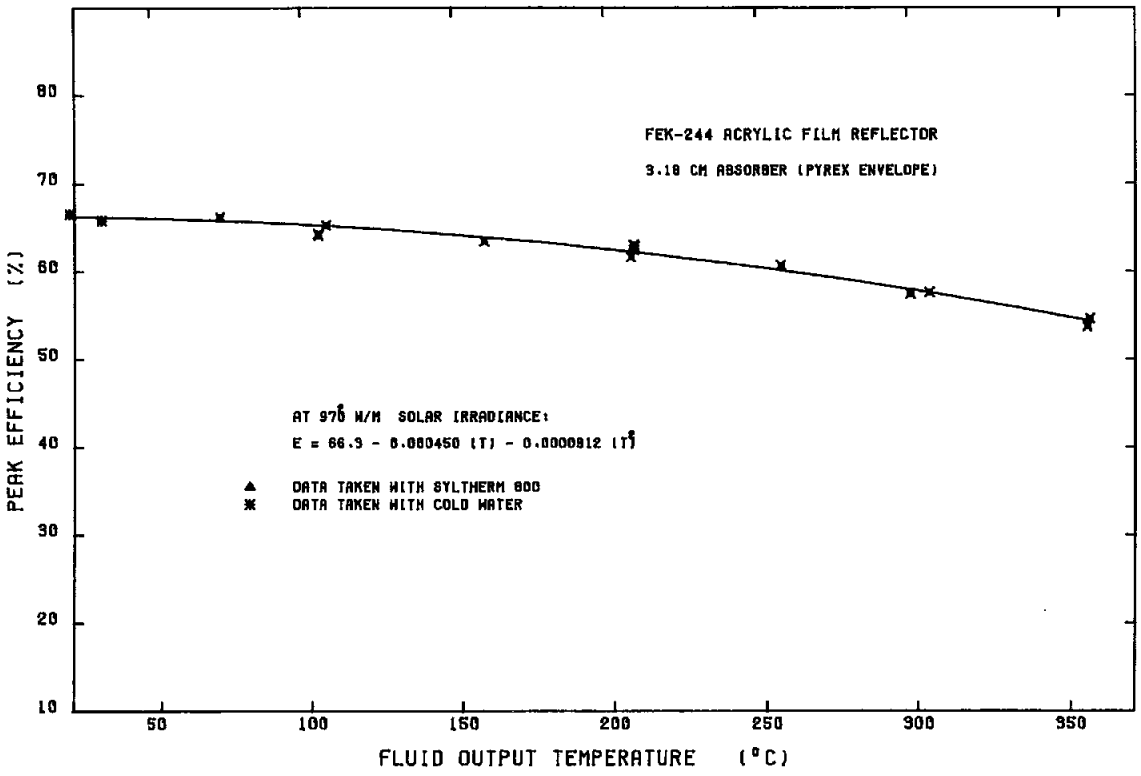

Figure 27. Solar Kinetics T-700A Efficiency vs Output Temperature

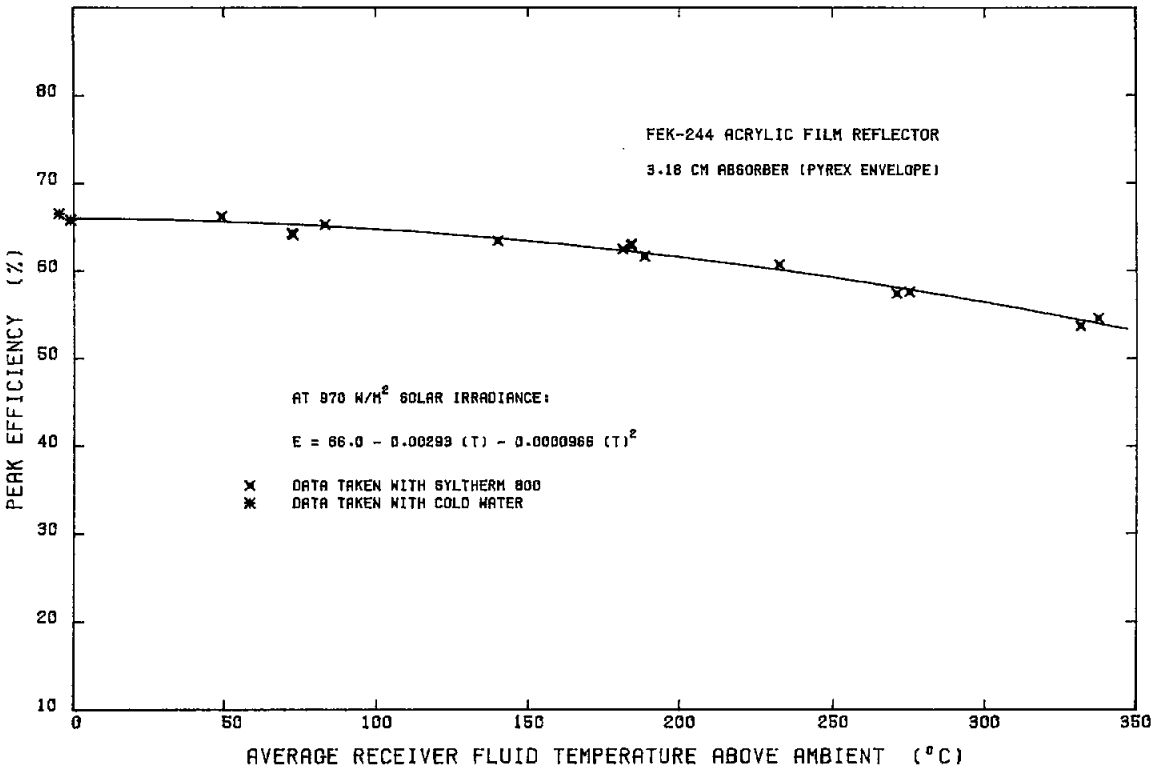

Figure 28. Solar Kinetics T-700A Efficiency vs Temperature Above Ambient

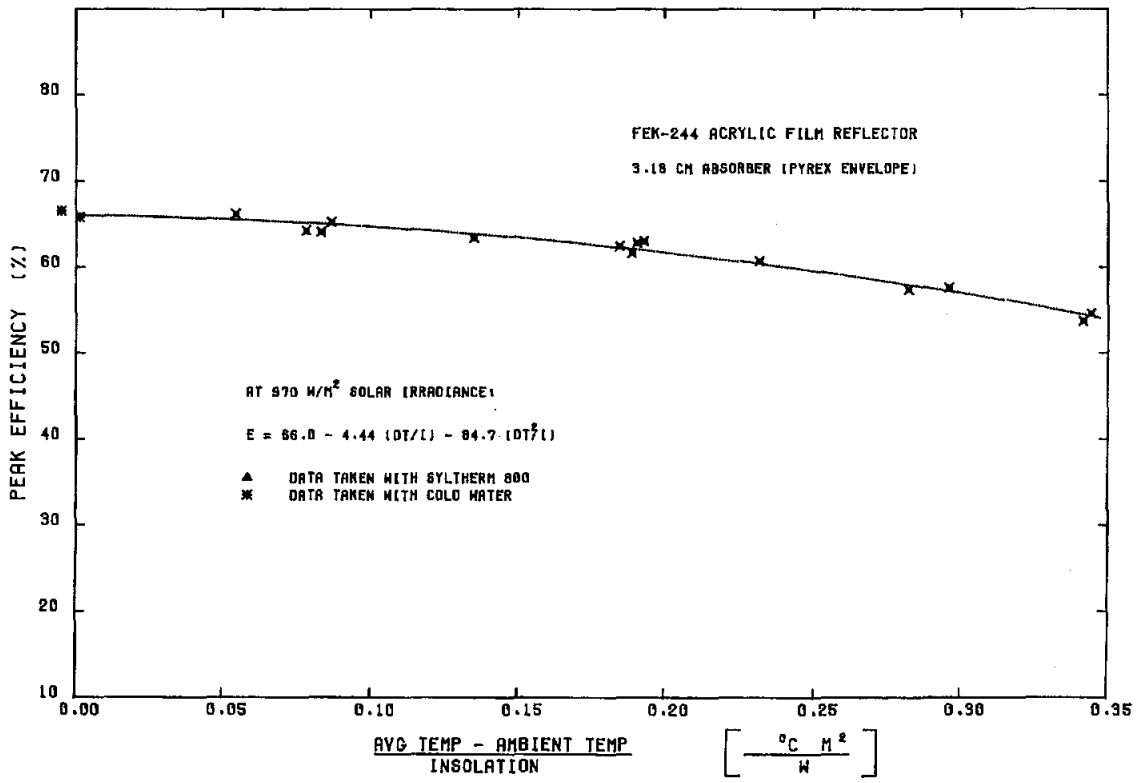

Figure 29. Solar Kinetics T-700A Efficiency vs Delta T/I

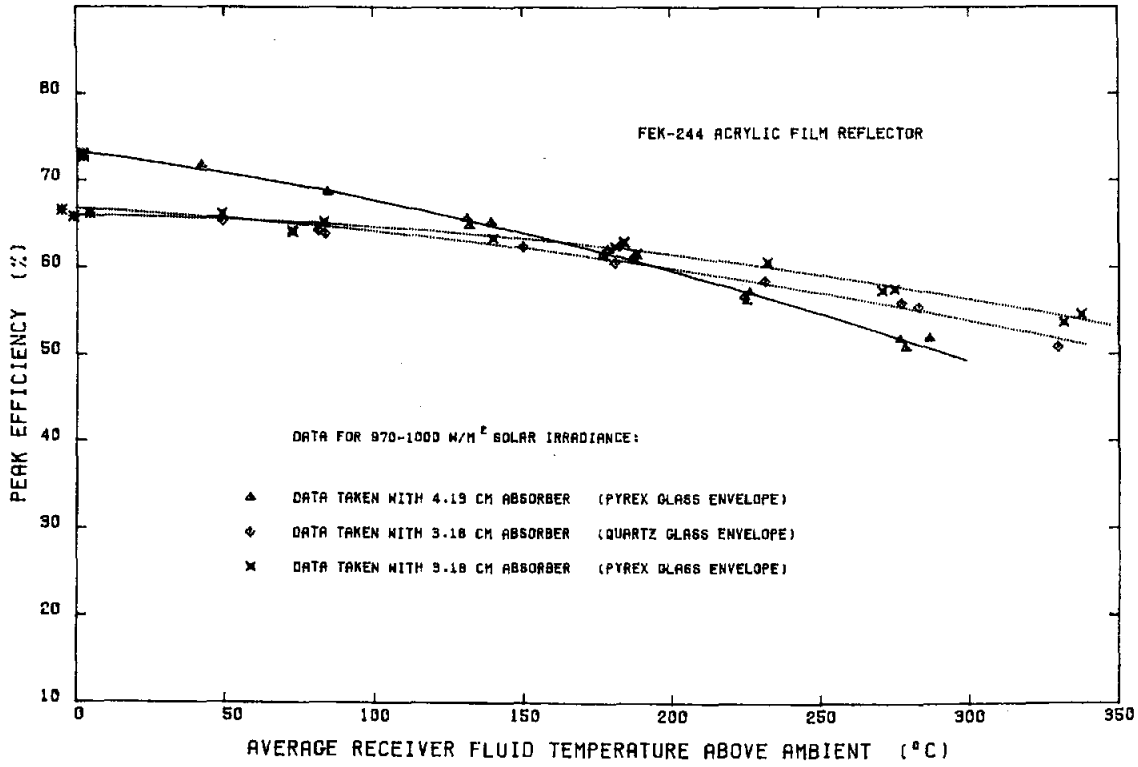

Figure 30. Performance Change With Receiver Configuration

If total energy recovery from a collector field over a period of time is to be estimated, definition of the collector's performance at other than zero incident angle is necessary. The all-day, fixed east-west axis efficiency data plots (such as Figure 11) provide some of this information, but such plots are not available for every possible operating temperature. One way of estimating the collector's performance at other than solar noon is to multiply the noon efficiency at the desired operating temperature by an incident angle modifier (K).

The 25 July low-temperature water test shown earlier in Figure 6 was used to determine the incident-angle modifier for the Solar Kinetics T-700A. Solar radiation angle of incidence actually occurring during the test is shown on the top abscissa scale in Figure 6, and covered the range from 0 to 67° during the test period. The data is plotted at 5° intervals in Figure 31; a second-order polynomial, least-squares fit to the test data produced the curve shown there. If the characteristics of the mirrors, receiver cover glass, and absorber tube surface were the same for all angles of incidence, the curve for K would follow the cosine curve also shown in Figure 31. Figure 32 shows the data from Figure 31 with the cosine factor removed; this is the collector's incident-angle modifier curve.

Using the glass reflector and the large (4.13-cm OD) receiver, incident-angle calculations were made from all-day efficiency tests at 20°, 100°, and 150°C. The tests and the incident-angle calculations were repeated using the FEK-244 acrylic reflector and operating temperatures of 20°, 100°, and 300°C. When data from all these tests (corrected for thermal loss) is overplotted on Figure 31, all the curves are nearly the same. Therefore, only a single curve is shown in Figure 31, as derived from the 20°C test shown in Figure 6.

Due to lack of time, not enough incident-angle measurements were made using the smaller (3.18-cm OD) receiver to derive an incident-angle modifer.

Receiver Differential Pressure Measurements

Heat-transfer fluid pressure drop across the receiver length gives some indication of the pumping power that will be required to circulate the fluid through an operational solar-collector field. Receiver differential pressure was measured on the Solar Kinetics T-700A with both the 4.13-cm and the 3.18-cm absorber tubes.

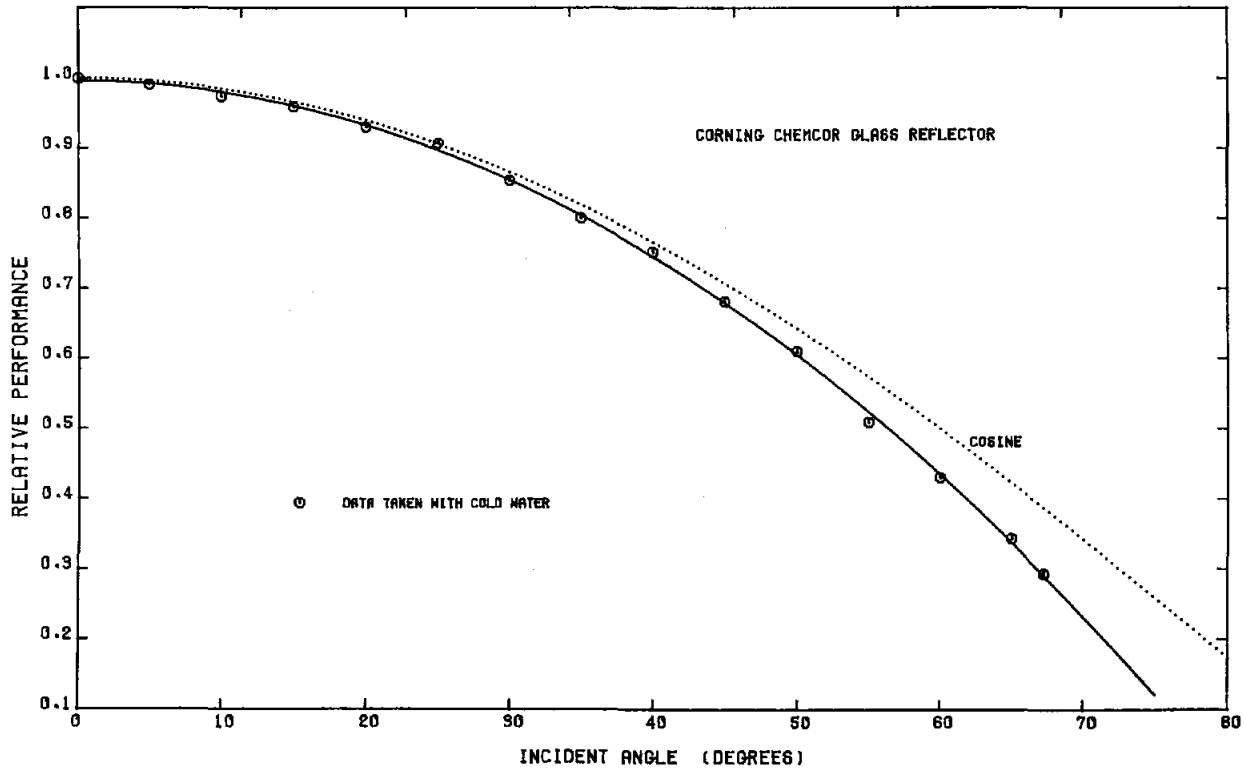

Figure 31. Solar Kinetics T-700A Performance vs Incident Angle

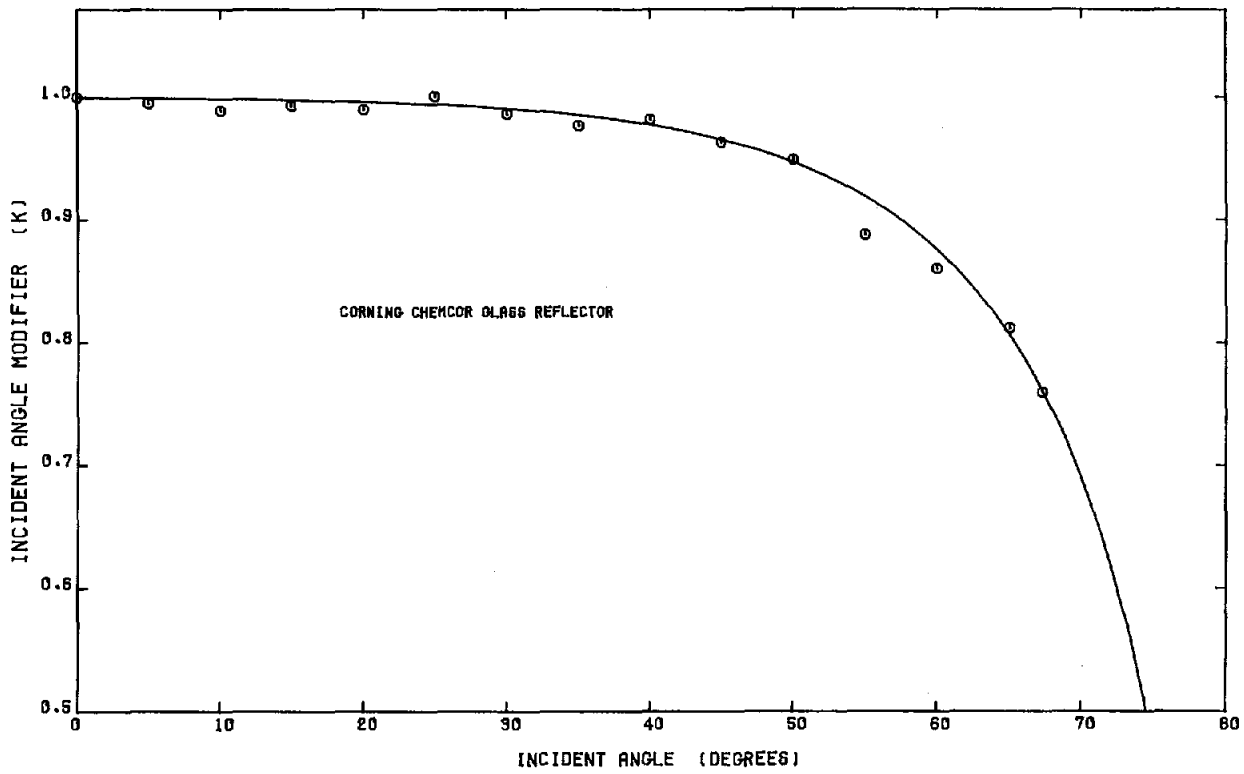

Figure 32. Solar Kinetics T-700A Incident Angle Modifier

Differential pressure measurement was made on the 4.13-cm-OD absorber tube (3.81-cm ID) at 100°, 200°, and 300°C with Syltherm 800 as the heat-transfer fluid, and at about 18°C with cold water as the heat-transfer fluid. No differential pressure measurements were made with Therminol 66; however, measurements on other receivers have shown the pressure drop with cold water is nearly identical to that with Therminol 66 at 150°C.

Figure 33 shows the differential pressure data for the 4.13-cm absorber tube. The data includes the pressure drop across the two flex hoses. Equations given in the figure relate differential pressure in kPa to fluid flow rates in liters per minute.

A similar set of measurements were made on the 3.18-cm-OD absorber tube (2.86-cm ID). The differential pressure test results for Syltherm 800 are shown in Figure 34; pressure drop through the two flex hoses is not included. The pressure drop is smaller for the 3.18-cm-OD tube than for the larger tube for two reasons: the flex hoses are not included in Figure 34, and the twisted tape present inside the larger tube was not installed in the smaller tube.

Differential pressure for the 3.18-cm-OD absorber tube was also measured with cold water; this data is shown in Figure 35. For this test, separate measurements were made to isolate the pressure contribution from the flex hoses; a curve is shown for the flex hoses as well as for the absorber tube.

Receiver Surface Temperature Measurements

In order to explain some of the test results obtained from the T-700A collector, we needed to know the relationship of the receiver surface temperatures to the temperature of the heat-transfer fluid. Accordingly, two Type-T thermocouples were welded to the absorber surface near the output end of the receiver. A mostly unsuccessful attempt was also made to measure the surface temperature of the glass absorber envelope.

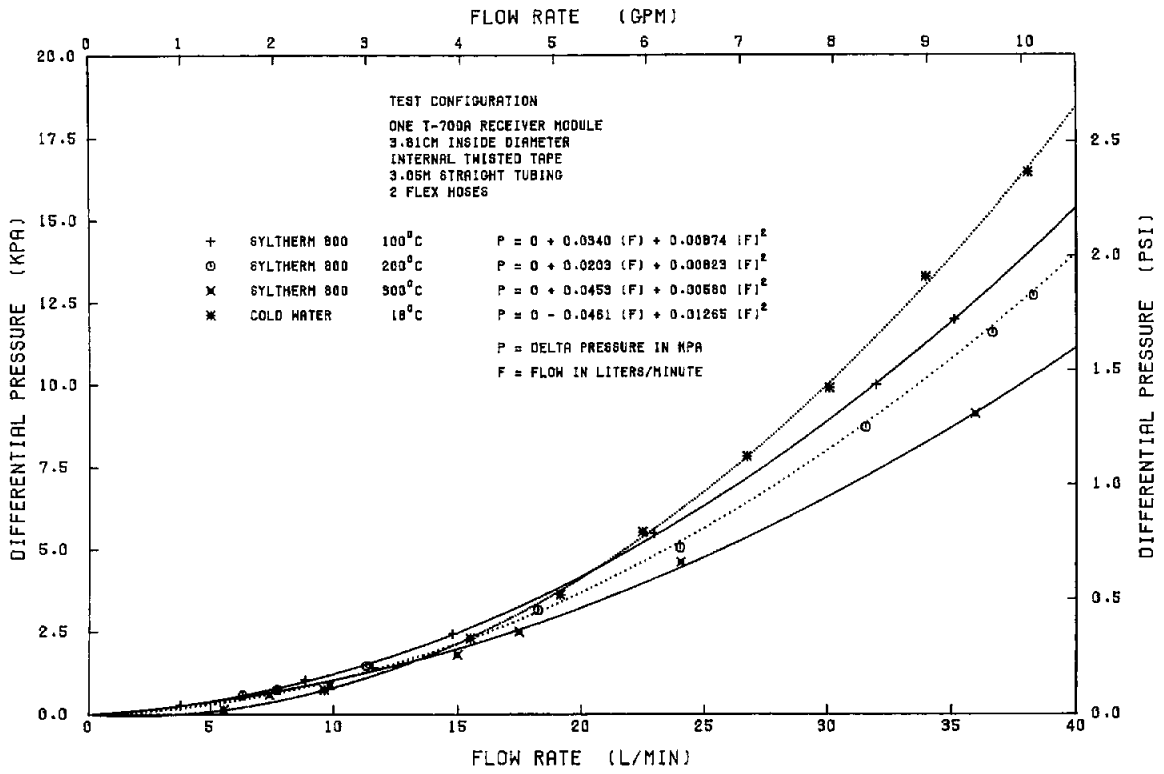

Figure 33. Solar Kinetics T-700A Receiver Differential Pressure (3.81-cm-ID tube)

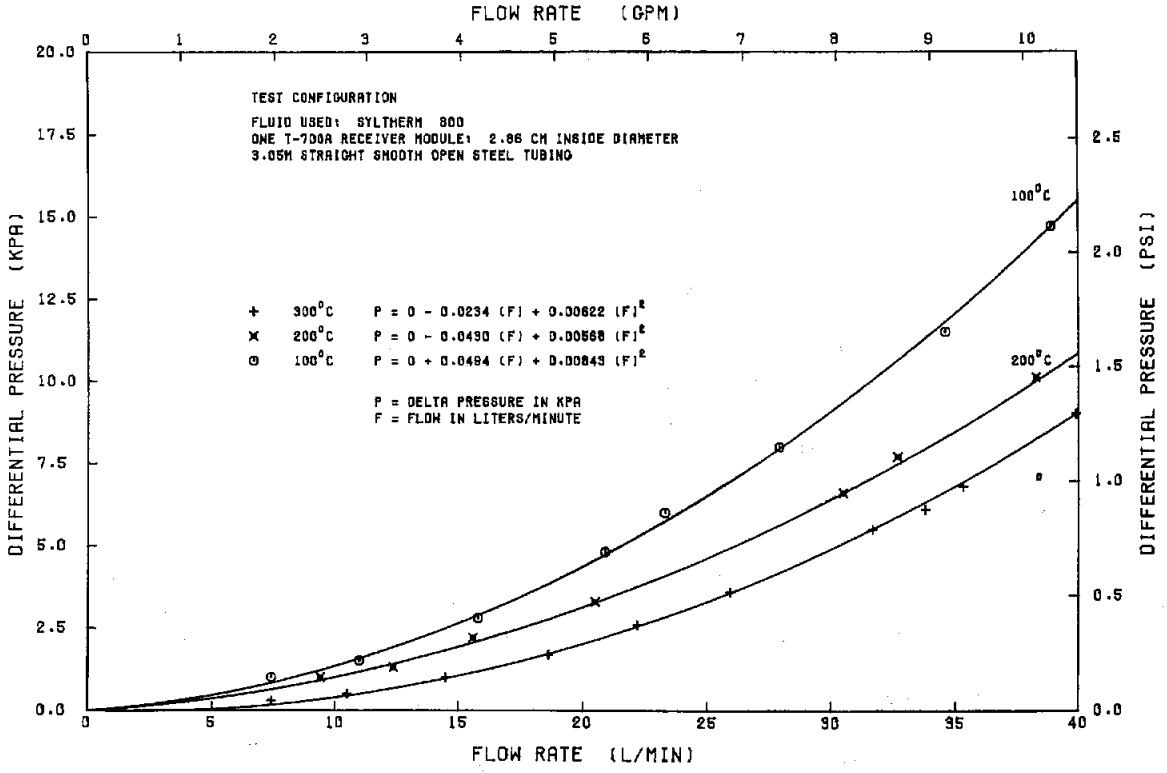

Figure 34. Solar Kinetics T-700A Receiver Differential Pressure (2.86-cm-ID tube)

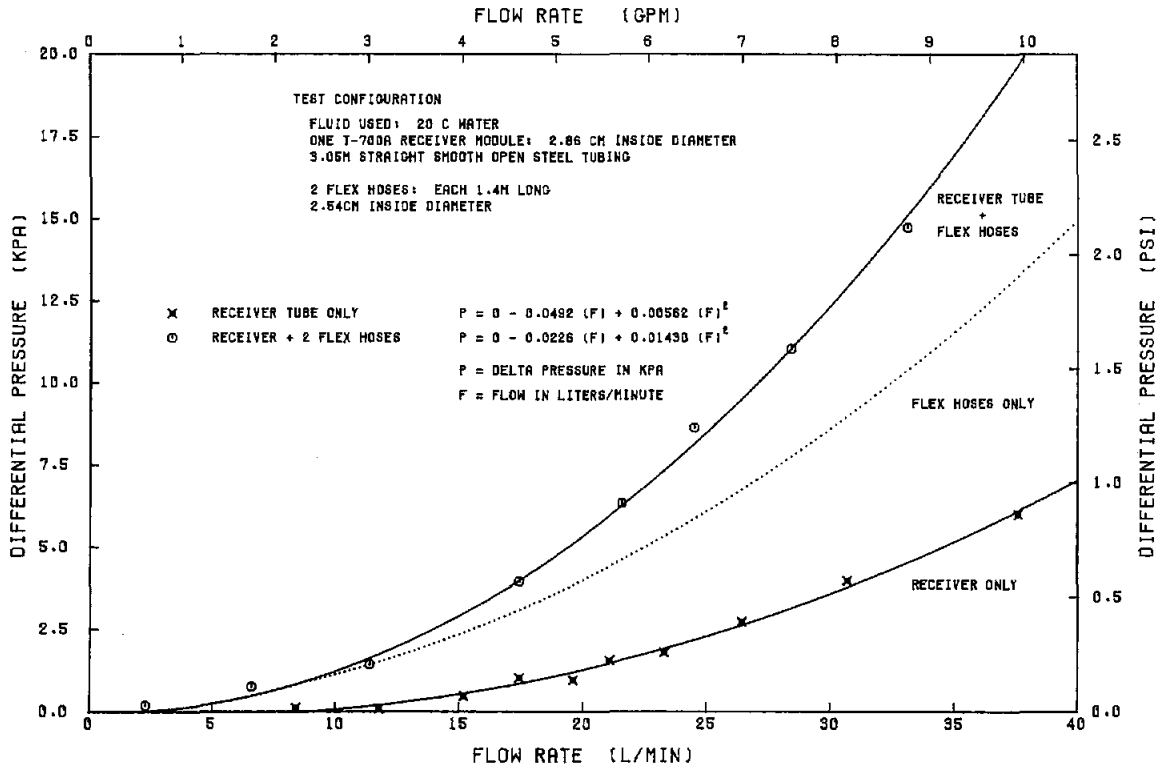

Figure 35. Solar Kinetics T-700A Receiver Differential Pressure (2.86-cm-ID tube with hoses)

Figure 36 shows the surface temperature measurements obtained during a test on 19 October 1981. The inlet temperature and the fluid-flow rate were maintained constant throughout the test period that began at about 1500 and extended to sunset. Measurements were made at 15- to 20-s intervals throughout the test period. The data shows that the absorber-surface temperature was much higher than the bulk-fluid temperature, even at a relatively high fluid-flow rate, and with a high Reynolds number (~45 000). Surface temperature decreased linearly with the solar irradiance.

Test results similar to those shown in Figure 36 were obtained at seven fluid temperatures ranging from 70° to 350°C, using Syltherm 800 as the heat-transfer fluid, and at 20°C using cold water as the heat-transfer fluid. Intercept values for zero solar irradiance were obtained during out-of-focus thermal-loss tests at each temperature. These data were combined in Figure 37, showing the variation in absorber surface temperature for a single, constant fluid-flow rate. The surface-fluid delta temperature decreases at higher temperatures for two reasons: the fluid viscosity decreases, allowing more fluid turbulence, better heat transfer, and higher Reynolds numbers; and the heat conductivity of the fluid becomes increasingly better as the temperature is increased. Surface-fluid delta temperature was much smaller with water as the heat-transfer fluid, reflecting both the better heat conductivity and low viscosity of water as compared to the Syltherm 800 synthetic oil.

A new set of curves similar to those in Figure 37 would be obtained for each different fluid-flow rate. Extremely limited test time was available, so only a few data points were obtained at other fluid-flow rates. These data indicate that surface-fluid delta temperatures of 60° to 70°C are quickly reached as the fluid-flow rate is reduced. At high levels of solar irradiance, surface-fluid delta temperatures less than ~15°C were unobtainable, even at 350°C fluid temperatures and Reynolds numbers as high as 70 000. Limited data was obtained on another collector with the same absorber diameter, using Therminol 66 as the heat-transfer fluid. Absorber surface-fluid delta temperatures were similar to those in Figure 37.

Figures 36 and 37 show that the absorber surface temperatures of a concentrating solar collector change linearly with irradiance. These surface temperature changes would directly affect thermal loss from the receiver assembly if there were no cover over the absorber. However, the collector being tested had a glass envelope surrounding the absorber tube, so that conduction and convection losses could not occur directly to the atmosphere. Direct radiation loss was also precluded because the glass was opaque to the infrared radiation from the absorber surface.

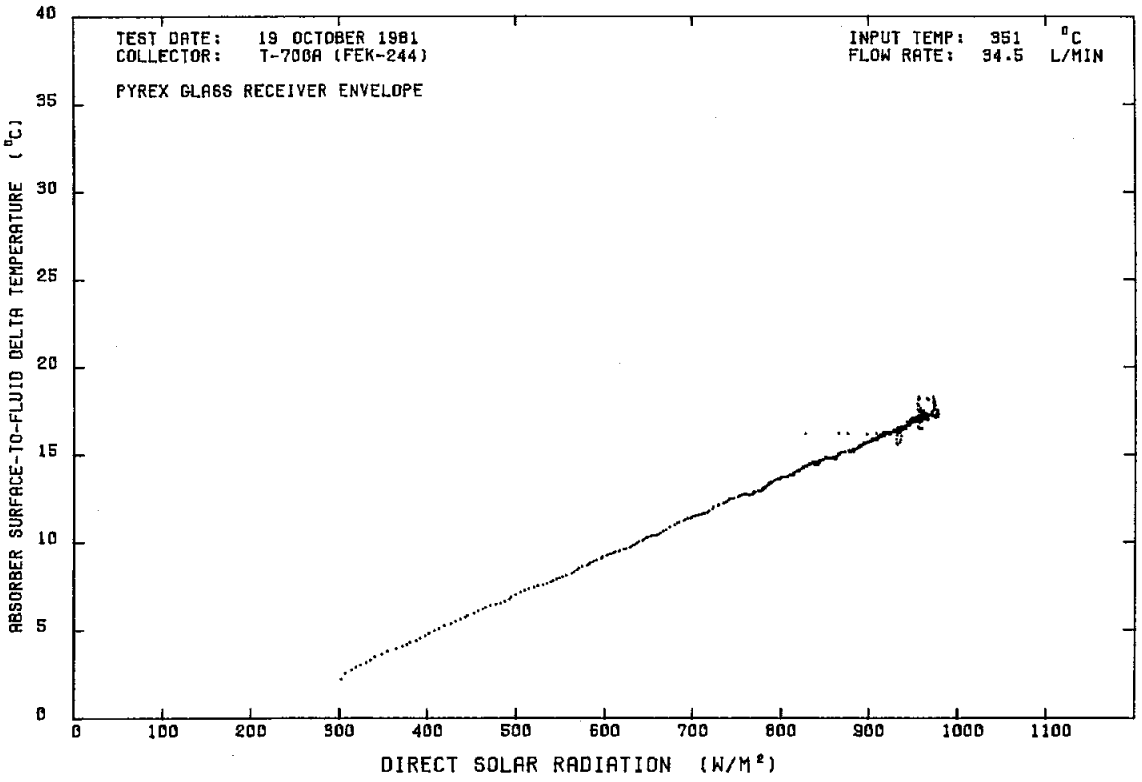

Figure 36. Solar Kinetics T-700A Absorber Surface Temperature vs Insolation

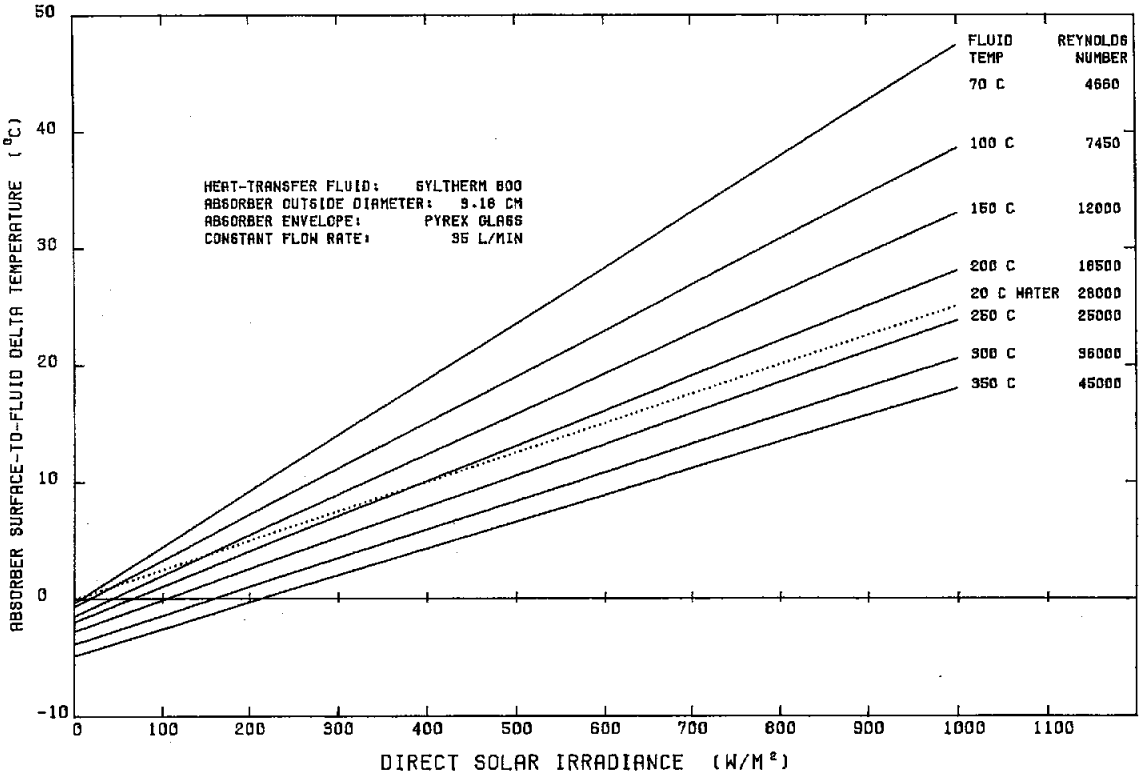

Figure 37. Solar Kinetics T-700A Absorber Surface Temperature vs Irradiance

Attempts were made to measure the surface temperature of the glass. These measurements are difficult to make; the surface temperatures are strongly affected by wind, and the temperatures change as a function of position around the circumference of the glass tube. When the glass surface temperature measurement is attempted with the collector in-focus, the resulting data is usually a measurement of the energy deposition in the measuring thermocouple from the concentrated light, rather than a measurement of the actual surface temperature of the glass. A more sophisticated technique than a thermocouple glued to the glass is required to obtain a reliable measurement. We obtained no usuable data on surface temperatures of the receiver glass under in-focus operating conditions.

Some interesting data was obtained from out-of-focus measurements of glass surface temperatures, using a hand-held surface-temperature probe. The distribution of surface temperatures around the circumference of the glass tube indicate that strong convection currents are present in the air inside the receiver assembly. These convection currents have been predicted from theoretical studies, and have probably been measured by others. For the receiver being tested, the annulus between absorber surface and inner glass surface was sized to minimize the combined effects of conduction and convection within the annulus.

The concentration of light on the large (4.13-cm OD) Solar Kinetics absorber was about 50; for the smaller (3.18-cm OD) absorber, the concentration was about 67:1. With 1000 W/m^2 solar-irradiance incident on the reflector system, and assuming all the concentrated light is intercepted by the receiver, the flux at the receiver is about 50 to 67 kW/m^2. Approximately 94% of the concentrated light is transmitted through the glass envelope to the absorber surface. About 3% to 4% of the light is lost because of reflections from the glass surfaces, leaving about 2% to 3% of the energy (1 to 2 kW/m^2) deposited within the glass envelope.

Even though we were unable to directly measure the surface temperature of the glass-receiver envelope when the collector was in-focus, it is obvious that deposition of 1 to 2 kW/m^2 of energy within the glass will change the glass temperature. That change of glass temperature should be approximately linear with changing solar irradiance, in the same way as the change in absorber surface temperature shown in Figure 37. In addition to the energy deposited in the glass directly from the concentrated light, additional energy is added to the glass from convection, conduction, and radiation heat-transfer from the heated absorber surface. These additions must also change as the absorber surface temperature changes.

All these energy depositions within the glass receiver envelope and the resulting glass-surface temperature changes are important to a discussion of receiver thermal loss in a later section of this report. Except for the small portion of thermal loss caused by conduction through absorber supports, all receiver thermal loss ultimately occurs at the receiver's outside surfaces, and is a function of the temperature of those surfaces.

Receiver Thermal Loss Test Results

Thermal loss from the Solar Kinetics T-700A 4.13-cm-dia absorber was measured in four different ways:

1. With the receiver shaded from direct and reflected sunlight, and the reflector aimed at the north sky.
2. With the receiver shaded from direct and reflected sunlight, and the reflector aimed south at the ground (near normal stow position).
3. With direct sunlight on the receiver, reflector aimed at the north sky, and collector defocused so that only diffuse reflected light from the mirror surfaces could reach the receiver.
4. Same as (3), but with the reflector aimed south at the ground (near normal stow position).

Thermal-loss test results are shown in Table 6, and are plotted in Figure 38. The thermal-loss test produced four distinct thermal-loss curves, as shown in Figure 38. Equations for the four curves are given in Table 7. The difference between the "shaded" curves and the "sun on the receiver" curves is easily explained. When sunlight (nonconcentrated, no reflection from mirrors) falls on the absorber-tube surface, the result is a small heat gain. The magnitude of the heat gain is just what would be expected from a small black-chrome, flat-plate collector with an area equivalent to that of the absorber tube. The difference between the curves corresponds closely to the illuminated area of the tube multiplied by the direct solar radiation. Direct solar radiation was used rather than total horizontal radiation because the receiver was shaded or illuminated in such a way that one-half or more of the sky was not within the view angle of the absorber.

Table 6. Solar Kinetics T-700A Receiver Thermal Loss Measurements, 4.13-cm-dia Absorber

Test Date	Receiver Tavg-Tamb (°C)	Direct Irradiance (W/m^2)	Flow Rate (L/min)	Wind Speed (m/s)	Thermal Loss (W/m^2)
9/06/80	116.4	960.1	20.6	3.0	25.3**
9/07/80	125.4	873.9	20.1	1.1	21.5*
9/07/80	124.9	935.9	20.1	3.8	31.8#
9/07/80	126.2	952.8	10.7	1.0	31.8#
9/07/80	126.5	960.7	10.8	1.2	41.8##
9/07/80	125.6	966.4	10.8	1.3	27.7**
9/07/80	125.8	967.6	10.8	4.5	15.1*
9/07/80	122.3	964.3	10.8	0.9	29.2#
9/07/80	167.7	943.5	10.9	1.7	51.9**
9/07/80	167.0	932.9	10.9	3.0	69.6##
9/07/80	167.8	906.6	10.9	1.8	57.8#
9/07/80	167.8	897.0	10.9	1.5	40.8*
9/07/80	168.2	846.4	11.0	1.8	55.7**
9/07/80	167.6	805.2	11.0	1.3	70.0##
9/08/80	215.6	953.9	23.7	3.4	94.7##
9/08/80	212.7	964.4	14.6	1.7	95.2##
9/08/80	212.7	964.5	14.6	2.5	80.8**
9/08/80	212.8	941.8	14.7	1.5	68.1*
9/08/80	212.9	916.0	14.7	3.8	69.3*
9/08/80	212.5	904.1	14.6	4.0	84.6#
9/08/80	211.5	898.3	14.7	1.9	96.6##
9/09/80	70.7	963.9	26.9	2.9	+0.7**
9/09/80	70.4	968.6	26.9	2.9	16.1##
9/09/80	65.7	968.8	15.3	1.7	16.9##
9/09/80	65.5	979.0	15.3	2.0	17.3##
9/09/80	64.1	975.4	15.3	1.8	0.1**
9/09/80	62.1	971.0	15.3	1.6	+9.2*
9/09/80	62.9	964.8	15.2	1.6	9.7#
9/09/80	63.9	953.8	15.3	2.3	19.5##

*Sun on receiver, reflector aimed at north sky.
**Sun on receiver, reflector aimed at south ground (stowed).
#Receiver shaded, reflector aimed at south ground (stowed).
##Receiver shaded, reflector aimed at north sky.

Loss entries marked + are heat gain rather than a loss.

Table 7. Solar Kinetics T-700A Thermal-Loss Equations, 4.13-cm-dia Absorber

Position	Equation
Shaded, north	Loss = + 0.0 + 0.1891 (dT) + 0.001231 $(dT)^2$
Shaded, south	Loss = − 6.577 + 0.1476 (dT) + 0.001330 $(dT)^2$
In sun, north	Loss = − 15.856 + 0.2036 (dT) + 0.001210 $(dT)^2$
In sun, south	Loss = − 26.809 + 0.1988 (dT) + 0.001169 $(dT)^2$
In Focus ($1005^{W/m^2}$)	Loss = 0.0 + 0.4462 (dT) + 0.001206 $(dT)^2$

Loss = W/m^2 of aperture
dT = °C above ambient air.

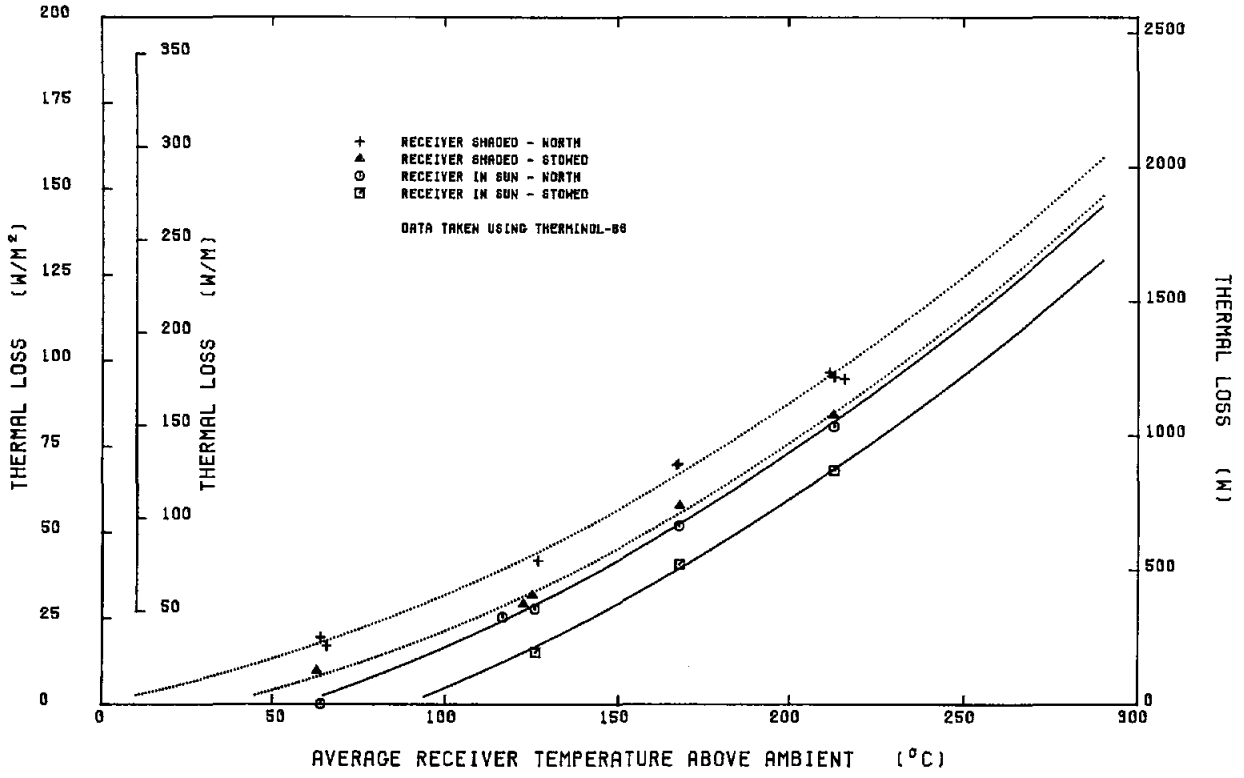

Figure 38. Solar Kinetics T-700A Receiver Thermal Loss

Conduction and convection losses should be approximately the same in each of the four tests. Radiation losses are probably not the same; radiation loss should be higher when the reflector is aimed at the cooler north sky than when aimed at the warmer ground surface to the south. Differences in the radiation loss probably account for most of the differences in the north-facing and the south-facing loss curves. Differences in the total sky radiation input to the absorber surface may also contribute, even when the absorber is shaded from direct solar radiation. Effective irradiance on the absorber surface is nearly zero when the absorber is shaded and aimed at the north sky.

The test data from the different collector positions illustrates the different answers that can be obtained from a thermal-loss test. The real question is not which of the measurements is the correct thermal loss—they are all correct, though all may not be very useful. A thermal-loss test procedure needs to be found that produces information to assist the collector design engineer in system improvements, is comparable for all collector tests, and can be used to assist in characterizing the thermal performance of an operating solar collector field.

The data in Table 6 and Figure 38 were taken with the aid of the AZTRAK rotating platform so that no changes in solar radiation-incident angle would occur during the tests. If this were not done, the effective solar radiation on the absorber surface would also have to be corrected for incident-angle effects in order to obtain consistent data. Since many collectors cannot be shaded, or cannot be aimed at the north sky, or cannot be aimed downward to the south, it is difficult to define a single thermal-loss test that will produce comparable test results in all cases. One possibility is the measurement of thermal loss at night, with the reflector aimed at the dark sky. The night measurement was found to be the same as the "receiver shaded, north sky" measurements made with the tracking platform during daylight hours.

The actual thermal loss that occurs when the collector is in focus is not the same as indicated by any of the four loss curves shown in Figure 38. The optical properties of the collector are assumed to be approximately constant with changing operating temperature. If there is no change in optical properties, the only reason the efficiency of the collector decreases with increasing operating temperature must be increasing thermal losses. A curve representing the thermal loss under in-focus operation can be derived from the measured efficiency data; the fifth (top) curve shown in Figure 39 is just such an "in-focus" loss curve, derived from the efficiency curve shown earlier in Figure 22. Figure 39 shows that the actual thermal loss occurring from an in-focus collector is higher than any of the measured losses. The lower four curves in Figure 39 are the measured loss curves previously shown in Figure 38.

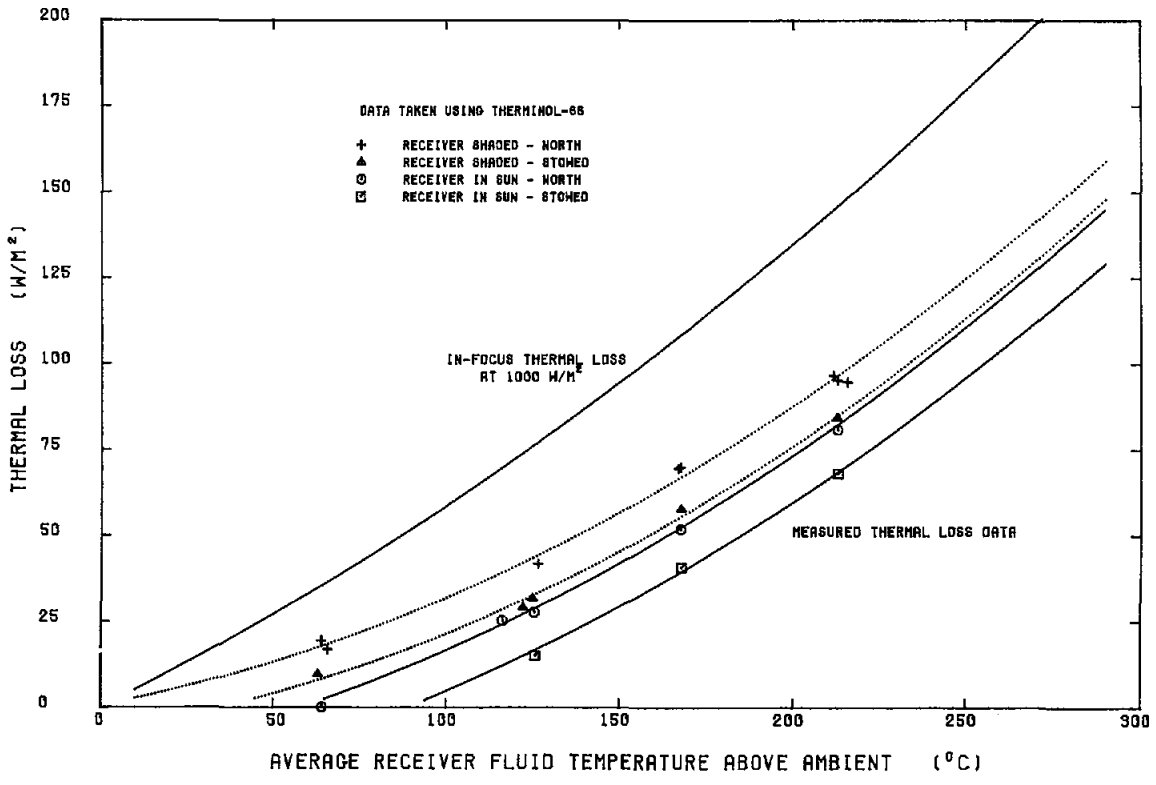

Figure 39. Comparison of Out-of-Focus and In-Focus Thermal Losses

Figure 39 shows the in-focus thermal loss crossing through zero loss at zero degrees temperature above ambient. This is almost certainly not true. As discussed earlier, the fluid temperature may be the same as the ambient air, but the receiver surface temperatures are much higher than the fluid temperature when in-focus. There is probably no single fluid temperature at which convective, conductive, and radiation thermal loss are all simultaneously zero, but there should be some fluid temperature at which the sum of the three losses is zero; that temperature is probably not equal to the ambient air temperature. The in-focus thermal-loss curve probably should be approximately parallel to the measured loss curve at all temperatures; that would mean that in-focus thermal loss still occurs when the heat-transfer fluid is at the same temperature as the ambient air. Zero thermal loss at zero temperature for the calculated in-focus loss curve in Figure 39 is an error that results when the low temperature measured efficiency point is treated as the optical efficiency. Actual optical efficiency is slightly higher and, if known, should produce the proper thermal loss at zero temperature. The error is not significant when considering real solar-collector fields, because it occurs below any useful operating temperatures.

A higher thermal loss during in-focus operation is reasonable, because even though the fluid temperatures may be identical, both the absorber-surface temperatures and the receiver glass-envelope temperature are higher when in-focus than during the out-of-focus thermal loss tests. An indication of the magnitude of the in-focus and out-of-focus surface temperature differences were shown earlier in Figures 36 and 37.

From the tests discussed above, it appears that the thermal loss from a concentrating solar collector is not a constant for a given fluid temperature, but changes with the nature of the heat-transfer fluid, with fluid-flow rate, and with the level of input solar irradiance.

Thermal loss from the small 3.18-cm absorber was also measured with both quartz-glass and Pyrex-glass envelopes. Thermal-loss measurements on the small absorber were made only under near-zero solar irradiance conditions (collector reflector aimed at the north sky with a shaded receiver) or true-zero irradiance (reflector aimed at the zenith at night). Both measurements were nearly identical. The test data obtained is shown in Table 8, and in Figure 40. Figure 40 also includes calculated in-focus loss curves obtained from the efficiency curves shown in Figures 25 and 28. As expected, the thermal loss from the smaller absorber diameter was less than that measured with the 4.13-cm-dia absorber. The lower loss is also reflected in the smaller slope of the efficiency curves, producing a higher efficiency at high temperatures than was possible with the large diameter absorber.

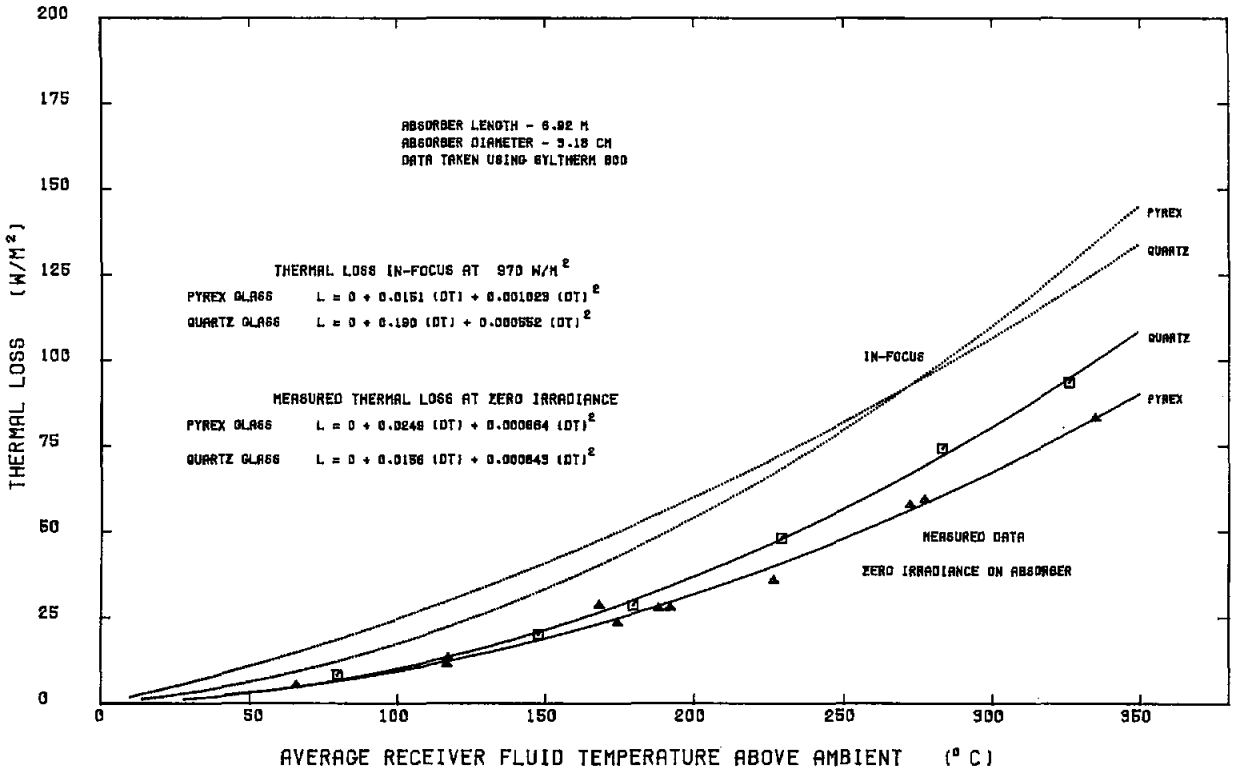

Figure 40. 3.18-cm Absorber Thermal Loss With Pyrex and Quartz Glass

Table 8. Solar Kinetics T-700A Receiver Thermal-Loss Measurements, 3.18-cm-dia Absorber

Test Date	Receiver Tavg-Tamb (°C)	Direct Irradiance (W/m^2)	Flow Rate (L/min)	Wind Speed (m/s)	Thermal Loss (W/m^2)
		Pyrex-Glass Envelope			
9/16/81	117.1	806.8	15.2	1.4	11.4
9/17/81	174.5	890.7	22.1	2.1	23.5
9/18/81	288.0	0.0	31.4	4.0	69.2*
9/18/81	286.5	70.0	31.3	3.2	67.5
9/18/81	272.3	867.5	30.4	2.0	57.8
9/21/81	81.3	0.0	12.0	0.3	9.3*
9/21/81	65.7	935.1	14.3	1.5	5.3
9/22/81	179.3	0.0	16.1	0.1	25.6*
9/22/81	168.3	797.2	15.9	1.3	28.7
10/08/81	192.2	0.0	17.3	0.7	29.2*
10/08/81	224.7	852.8	18.1	2.4	35.3
10/08/81	275.2	809.4	18.7	2.2	57.2
10/09/81	188.1	0.0	15.6	0.6	27.8*
10/09/81	267.3	780.7	15.6	2.1	58.5
10/19/81	335.0	0.0	34.8	1.1	83.1*
		Quartz-Glass Envelope			
10/29/81	79.2	910.8	37.2	4.4	2.9
10/29/81	81.4	936.3	16.0	0.9	1.4
10/29/81	147.7	991.0	17.3	2.1	20.1
10/29/81	179.6	1004.9	18.1	4.4	28.6
10/29/81	229.0	976.9	18.6	3.5	48.1
10/29/81	326.0	816.2	37.4	6.4	93.6
10/29/81	283.3	740.7	19.6	3.7	74.3
10/29/81	296.4	1.3	37.3	5.5	66.8

*Clear night sky, reflector aimed at zenith.

For all other tests in this table; receiver shaded, reflector aimed at north sky.

Efficiency Test Results With Variable Solar Irradiance

Most of the efficiency measurements at the CMTF are made with a direct normal solar irradiance between 900 and 1000 W/m^2. Collector performance will not be the same at lower levels of solar radiation. Variation of thermal loss with irradiance was discussed above. Heat gain from an in-focus collector also varies directly with changes in irradiance; since thermal loss is changing at the same time, both effects must be considered together to determine the collector performance with a variable solar-radiation input.

To answer some of the questions about concentrating collector performance under other than ideal solar conditions, a series of efficiency tests were made over the widest range of solar irradiance available. Stable, low levels of solar irradiance are rare in Albuquerque during most of the day. Stable values of solar irradiance as low as 300 W/m^2 do frequently occur in Albuquerque just after sunrise and just before sunset, when atmospheric dust, moisture, smoke, etc, attenuates the sunlight. Attenuation by clouds at any time is usually much too variable, producing such an unstable

output temperature that a valid efficiency measurement is impossible.

With the required intensity of sunlight restricted to the vicinity of sunrise and sunset, the tests were possible only because the collector was mounted on the AZTRAK rotating platform, so that a zero-incident angle for the efficiency tests could be obtained and maintained constant at any hour of the day.

Figure 41 is the result of an efficiency test performed on 24 April 1981, at a fluid-inlet temperature of 301°C. In order to achieve stable operating conditions at 300°C before sunrise, heating of the fluid system was started at 0200. Inlet temperature was maintained constant at 301°C throughout the day, from before sunrise until sunset. Fluid flow-rate was also maintained constant, while the output temperature was allowed to vary with changing solar radiation.

At sunrise, the insolation increased rapidly as the solar disc rose above the eastern hills. Direct normal irradiance was about 300 W/m^2 when the solar disc was fully above the horizon. Valid efficiency measurements below 400 W/m^2 were not possible because shadows of several utility poles and the corner of a building partially shadowed the collector's reflector.

The 24 April test was continued until just after 1100, with the AZTRAK maintaining the collector at a zero-incident angle. Efficiency slowly increased as the direct normal-solar irradiance increased. Efficiency testing was discontinued at 1116 in order to accomplish some other testing.

Measured efficiency is quite sensitive to the thermal stability of the fluid system. During the time from sunrise to peak irradiance near solar noon, the inlet-fluid temperature was maintained relatively constant, but the output temeprature increased continuously along with the increasing solar irradiance. A changing receiver temperature causes errors in the heat-gain calculations, since the equations assume thermal equilibrium. An increasing temperature causes the calculated efficiency to be less than the actual efficiency, while a decreasing temperature has the opposite effect. It is not possible with current equipment to change the flow rate to maintain a constant output temperature while also maintaining a constant input temperature, or to maintain a constant absorber delta-T. Because the temperature changes during the tests were relatively slow, the error was believed to be small, but a test was performed as a check.

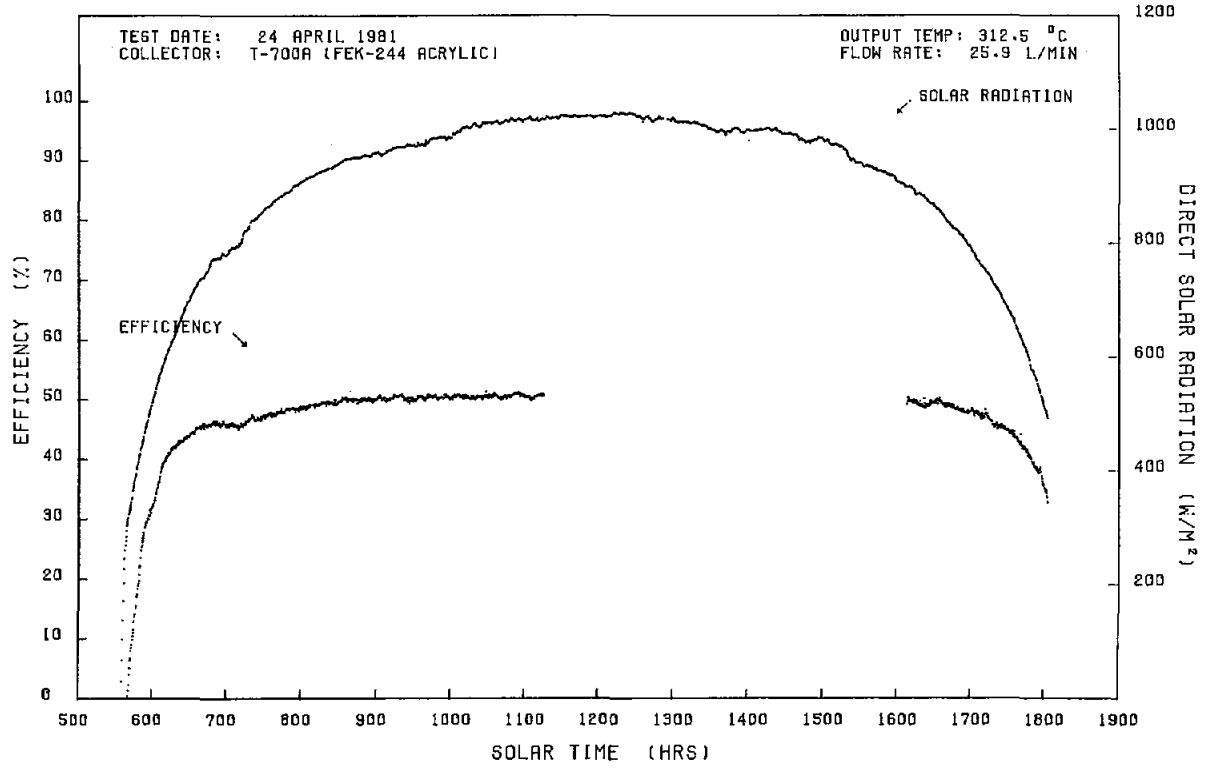

Figure 41. Solar Kinetics Parabolic Trough Efficiency Evaluation at 301.6°C Input

Beginning at 1600 (4:00 pm) on 24 April, the AZTRAK was returned to the zero-incident-angle tracking mode; inlet temperature was still at 300°C. Direct solar irradiance was 900 W/m^2 at 1600, decreasing to 500 W/m^2 at 1800 (6:00 pm), when the test was terminated because of building shadows reaching the reflectors. As expected, efficiencies measured during the afternoon's declining temperatures were not identical to those measured with increasing temperatures during the morning test, but were slightly higher. The difference was small, with a maximum difference of about 2 efficiency percentage points; during most of the day, the difference was much less. Similar errors would be present at all the temperatures used during these tests.

The efficiency plot for the afternoon test is shown on the right side of Figure 41. The data from the afternoon portion of Figure 41 is plotted again in Figure 42, clearly showing the change in collector efficiency as the solar irradiance changed.

Efficiency tests similar to those shown in Figure 42 were made at ambient temperature and at 100°, 150°, 200°, and 250°C. Data points from these efficiency tests are given in Table 9 for each 50-W/m^2 increase in solar irradiance at each of the test temperatures. Each of the data points listed in Table 9 is a 10-point average, as were all the earlier test data points in this report.

The test data from Table 9 is plotted in Figure 43, showing the variation in collector efficiency for each of the six temperatures as a function of direct-solar irradiance. Two sets of data points are shown for the 300°C curve; they are the morning (increasing temperature, lower points) and the afternoon (decreasing temperature, higher points) from the 24 April all-day efficiency test (Figure 41).

No measured data was obtained below 400 W/m^2 with the 4.13-cm absorber (500 W/m^2 at most test temperatures). The curves can be extended to zero efficiency with a simple calculation; zero efficiency occurs when the heat gain from the collector just equals the thermal loss. Assuming that the optical efficiency is approximately equal to the values measured with cold water (72.8%):

$$Q = \eta_o I \tag{4}$$

or

$$I = \frac{Q}{\eta_o} \tag{5}$$

where

Q = Thermal loss at temperature T
η_o = Collector optical efficiency
I = Direct normal solar irradiance at zero net heat gain.

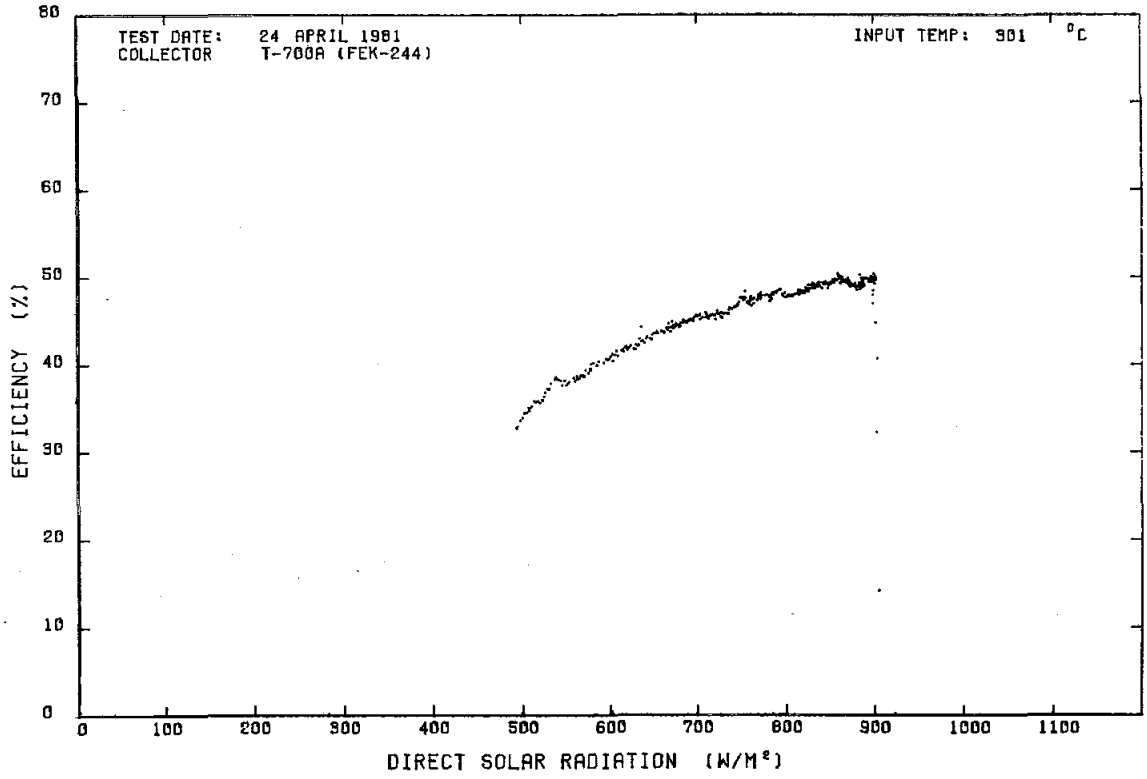

Figure 42. Solar Kinetics T-700A Efficiency vs Insolation (4.13 cm Dia Absorber)

Table 9. Variation of Efficiency With Irradiance, Syltherm 800 Heat-Transfer Fluid, FEK-244 Reflector, 4.13-cm Absorber

Test Date	Direct Irradiance (W/m^2)	Temp Out (°C)	Tavg –Tamb (°C)	Tavg-Tamb / I (°C·m^2/W)	Receiver Delta-T (°C)	Efficiency (%)
7/25/80	441.2	31.1	8.4	0.00195	7.02	77.6*
7/25/80	526.1	32.1	7.6	0.00145	8.36	77.9*
7/25/80	602.1	28.6	5.6	0.00930	4.74	77.9*
7/25/80	635.4	29.2	5.2	0.00815	5.22	77.4*
7/23/80	703.4	30.3	4.9	0.00705	6.19	77.3*
7/23/80	747.6	28.6	0.8	0.00106	4.49	78.5*
7/23/80	805.6	30.9	0.5	0.00614	6.28	78.4*
7/23/80	845.7	36.6	1.2	0.00147	10.34	78.4*
7/24/80	864.4	35.1	3.5	0.00401	10.01	78.8*
7/24/80	912.6	40.9	3.1	0.00333	13.83	77.9*
7/24/80	943.7	35.2	–3.4	–0.00355	9.12	77.5*
4/08/81	569.6	25.5	14.2	0.02490	7.08	71.9**
4/08/81	611.4	22.9	12.8	0.02090	3.88	72.2**
4/08/81	657.1	23.4	12.6	0.01920	4.19	72.6**
4/08/81	670.2	23.5	12.7	0.01890	4.27	72.6**
4/07/81	1023.9	29.8	2.3	0.00225	9.50	72.7**
5/29/81	459.5	108.4	92.0	0.2004	4.91	64.2
5/29/81	502.5	109.1	92.4	0.1839	5.60	65.7
5/29/81	554.3	110.0	92.4	0.1667	6.34	66.7
5/29/81	606.3	110.6	91.7	0.1512	7.05	67.8
5/29/81	654.9	111.1	91.5	0.1397	7.66	68.0
5/29/81	704.0	111.7	90.6	0.1287	8.25	68.1
5/29/81	749.5	112.4	89.7	0.1197	8.84	68.6
5/29/81	810.1	113.2	89.4	0.1104	9.61	68.8
5/29/81	855.3	113.7	89.5	0.1046	10.16	68.8
5/29/81	904.9	114.7	85.9	0.0950	10.80	68.9
5/29/81	962.4	115.9	83.1	0.0864	11.56	69.2
5/10/81	1018.0	113.7	84.3	0.0828	9.87	68.6
5/22/81	498.4	159.4	147.3	0.2956	5.36	59.6
5/22/81	519.4	159.8	147.4	0.2839	5.67	59.9
5/22/81	554.2	160.6	147.4	0.2661	6.20	60.8
5/22/81	594.5	161.3	147.3	0.2478	6.75	61.6
5/22/81	653.3	162.4	146.8	0.2247	7.57	62.7
5/22/81	702.6	163.2	145.8	0.2075	8.24	63.4
5/22/81	751.4	163.9	145.1	0.1931	8.90	63.8
5/22/81	801.4	164.9	145.2	0.1812	7.79	64.0
5/22/81	854.4	165.3	142.5	0.1668	10.53	64.4
5/22/81	904.5	165.9	141.7	0.1567	11.07	63.9
5/22/81	940.5	166.9	141.8	0.1507	11.76	65.1
5/27/81	504.0	208.4	191.9	0.3809	5.30	53.0
5/27/81	547.9	209.2	191.9	0.3502	6.04	54.9

Table 9. (cont)

Test Date	Direct Irradiance (W/m^2)	Temp Out (°C)	Tavg –Tamb (°C)	Tavg-Tamb / I ($°C \cdot m^2/W$)	Receiver Delta-T (°C)	Efficiency (%)
5/27/81	606.6	210.1	191.3	0.3154	6.83	55.9
5/27/81	654.5	210.8	190.9	0.2916	7.54	57.0
5/27/81	693.4	211.5	190.2	0.2744	8.00	57.8
5/27/81	754.5	212.6	189.6	0.2513	8.98	58.8
5/27/81	795.5	213.3	187.0	0.2351	9.65	59.6
5/27/81	845.6	213.7	182.2	0.2155	10.48	60.5
5/27/81	895.4	214.2	182.1	0.2034	10.85	60.9
5/27/81	953.9	215.5	181.0	0.1898	11.87	60.5
5/27/81	983.3	215.7	181.2	0.1843	12.06	61.0
5/23/81	502.5	256.1	244.2	0.4860	4.36	41.5
5/23/81	553.7	257.1	244.5	0.4416	5.33	45.5
5/23/81	600.8	257.9	244.7	0.4074	6.04	47.4
5/23/81	650.1	258.7	244.8	0.3766	6.74	48.8
5/23/81	695.3	259.5	244.7	0.3520	7.43	50.2
5/23/81	707.0	259.8	245.0	0.3466	7.61	50.5
5/23/81	749.6	260.7	245.2	0.3271	8.28	51.7
5/23/81	809.9	261.7	244.5	0.3019	9.15	52.8
5/23/81	853.6	262.4	243.7	0.2855	9.89	53.9
5/23/81	895.2	263.2	240.0	0.2681	10.61	55.1
5/23/81	936.3	264.0	239.2	0.2555	11.21	55.6
5/23/81	991.3	265.0	237.5	0.2396	11.97	56.1
5/23/81	998.1	265.3	236.2	0.2366	12.16	56.5
			(Sunrise)			
5/24/81	553.9	304.6	293.1	0.5292	3.90	35.8
5/24/81	615.3	306.3	293.5	0.4771	5.06	41.0
5/24/81	650.2	307.1	293.7	0.4517	5.55	42.6
5/24/81	699.5	308.1	293.7	0.4199	6.14	44.0
5/24/81	756.4	309.1	293.2	0.3856	6.99	45.8
5/24/81	801.3	309.1	293.2	0.3659	7.39	45.8
5/24/81	854.2	309.9	293.2	0.3433	8.09	46.9
5/24/81	900.9	310.8	289.8	0.3217	8.79	48.4
5/24/81	950.3	311.4	285.1	0.3000	9.65	50.0
5/24/81	1004.9	312.4	280.6	0.2792	10.48	50.5
			(Sunset)			
5/24/81	899.3	310.1	278.7	0.3099	9.68	49.9
5/24/81	852.3	310.3	277.0	0.3250	8.96	49.4
5/24/81	800.2	310.4	278.4	0.3478	8.24	47.8
5/24/81	752.8	309.1	275.8	0.3663	7.80	47.4
5/24/81	699.0	308.9	278.8	0.3988	6.96	45.3
5/24/81	647.8	307.1	277.6	0.4285	6.15	43.2
5/24/81	600.5	306.9	278.0	0.4630	5.24	40.8
5/24/81	564.4	306.6	278.6	0.4936	4.68	38.6
5/24/81	501.8	305.0	278.2	0.5546	3.72	35.9

*Data taken with cold water, glass reflector.
**Data taken with cold water, FEK-244 reflector.

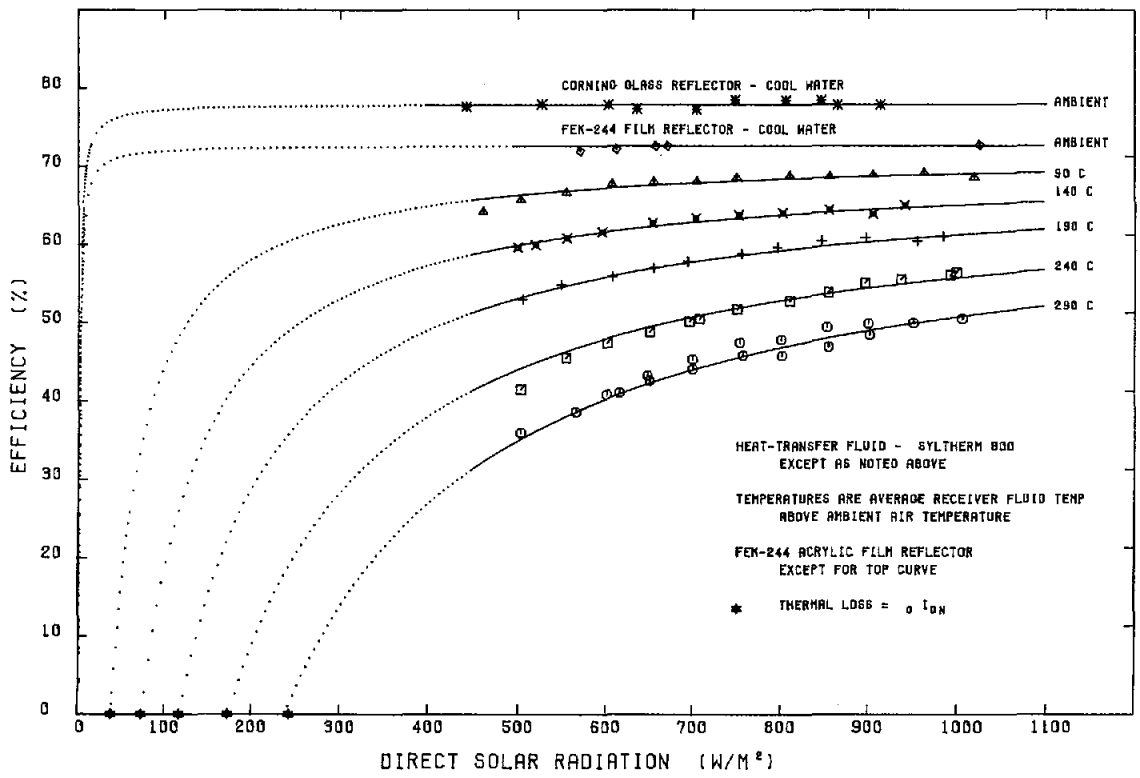

Figure 43. Solar Kinetics T-700A Efficiency vs Insolation and Temperature

Direct-solar irradiance at zero heat gain was calculated for each operating temperature used; these points are shown as zero efficiency points in Figure 43. The thermal loss Q in Eqs (4) and (5) was assumed to be a variable with irradiance, as shown later in this report. Equations (4) and (5) were iterated until there was no further change in Q or I. No actual measurement at zero efficiency was made with the 4.13-cm absorber because of shadows on the reflector at sunrise and sunset.

A polynominal least-squares curve fit, as used for the other curves in this report, did not match the data shown in Figure 42 very well. The set of curves that best fit the data were hyperbolic; these hyperbolic curves are shown in Figure 43. The set of equations is given in Table 10. A hyperbolic shape for the curves is obtained because operating efficiency would approach optical efficiency if the solar radiation input increased without limit; the curve would pass through zero efficiency when the thermal loss equals the heat gain, and approach negative infinity as the solar radiation decreases toward zero.

Table 10. Equations of Efficiency vs Solar Irradiance, FEK-244 Acrylic-Film Reflector, 4.13-cm-dia Absorber

Temp Above Ambient (°C)	A	B
290	66.5	15790
240	67.5	11747
190	69.4	8109
140	70.2	5123
90	71.8	2727
0	72.7	72.7
0	78.0	78.0*

*Corning glass reflector

Form of Equation: $\eta = A - (B/I)$
η = Collector efficiency in %
I = Direct normal solar irradiance.

Figure 44 shows a more familiar presentation of the test data from the low solar-irradiance test series. A polynomial least-squares curve fit to the test data was used to draw the set of curves; the set of equations is given in Table 11.

Instead of the two sets of curves and equations used to draw Figures 43 and 44, a single equation can be derived from the test data that will give the collector's efficiency as a function of both temperature and irradiance. Discussion of the model equation problem for collector efficiency is given in Appendix B. Analysis of the test data produced an equation that is an excellent fit to the complete range of data in Table 9:

$$\text{Efficiency} = 73.67 - 0.0239\,(dT) - 18.0952\,(dT/I) - 0.1311\,(dT^2/I) \quad (6)$$

Equation (6) is the same as (B4) from Appendix B. The equation can reproduce all the test data points shown in Table 9 with a maximum deviation of 1.9 efficiency percentage points (about 3% error). Over most of the range of test data the error is much less, with a standard error of estimate of 0.773 percentage points. Any value of delta-T from zero to 300°C, and any value of irradiance from zero to 1050 W/m^2 can be used in Eq (6).

Table 11. Equations of Efficiency vs Temperature Above Ambient, FEK-244 Acrylic-Film Reflector, 4.13-cm-dia Absorber

Direct Normal Solar Irradiance (W/m^2)	A	B (x 10^{-2})	C (x 10^{-4})
500	73.0	5.29	2.86
600	73.3	5.32	2.03
700	73.1	4.30	1.97
800	73.0	3.35	2.05
900	73.0	3.22	1.81
1000	73.0	3.43	1.59

Form of Equation: $\eta = A - B(dT) - C(dT)^2$

η = Collector efficiency in %
dT = Average temperature above ambient air temperature.

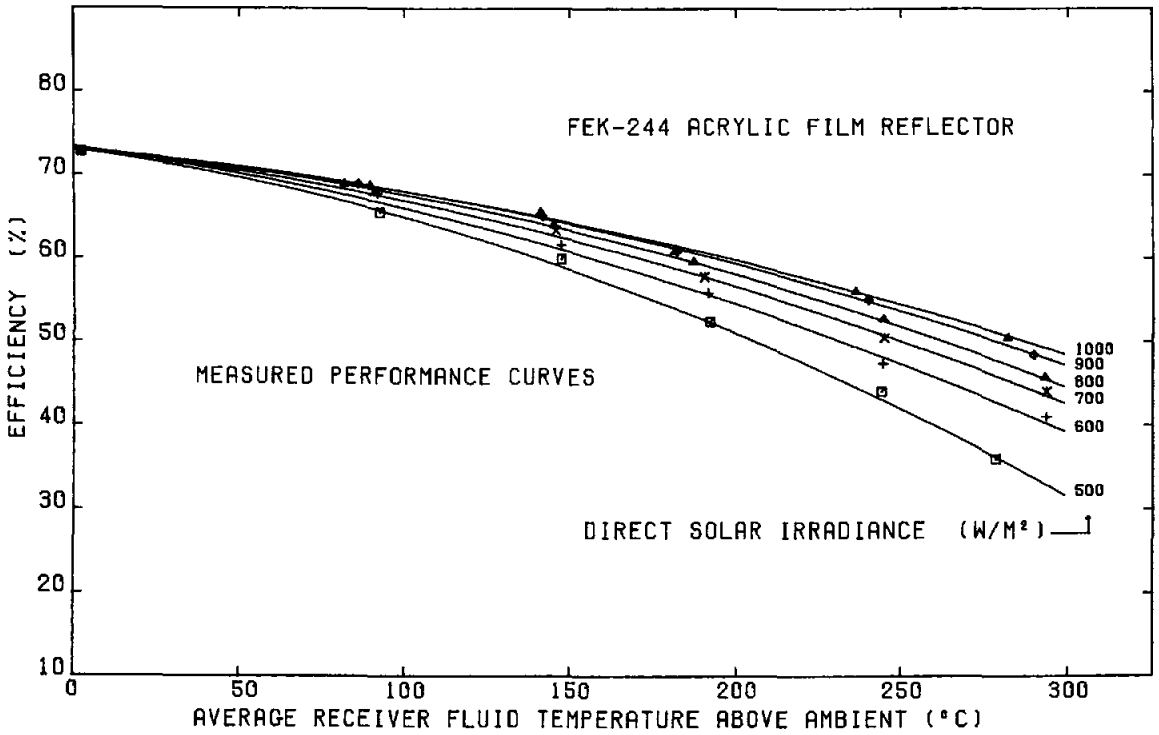

Figure 44. Solar Kinetics T-700A Efficiency vs Temperature and Insolation

Equation (6) can reproduce all the curves shown previously in Figures 43 and 44, but the characteristics of the collector can be better understood by plotting a three-dimensional surface that simultaneously shows the relationship between collector efficiency, temperature, and solar irradiance. Figure 45 is a plot of Eq (6), characterizing the performance of the Solar Kinetics T-700A collector module with an FEK-244 acrylic reflector and a 4.13-cm-dia absorber.

Obtaining the complete set of test data required to draw Figures 43, 44, and 45 for every collector tested is not practical. Too many days of testing are required to accumulate the set of data shown in Table 9. The test crew also objects to the 17-h days required to complete a test such as that shown in Figure 41. We therefore investigated the possibility of calculating the collector response from a smaller set of test data. Appendix C recounts the details of this investigation. The search was successful; a procedure was developed that reproduces the measured test data quite closely.

Using the three equations ((C3), (C4), and (C5)) developed in Appendix C, calculations were made to determine the efficiency of the T-700A collector for direct-solar irradiance from 400 to 1000 W/m^2; results of the calculations are plotted in Figure 46 (same as Figure C3, Apendix C). If the calculated performance curves in Figure 46 are compared with the measured performance curves in Figure 44, the maximum difference is ~ 1.5 efficiency percentage points at the higher temperatures (~ 3% error).

The calculations used to produce data for Figure 46 can also be used to provide a set of data for input to a multiple linear-regression program. For this purpose, Eqs (C3), (C4), and (C5) from Appendix C were used to generate an array containing 112 sets of data, with delta-T at 50°C intervals from zero to 350°C, and with irradiance at 100-W/m^2 intervals from zero to 1100 W/m^2 at each temperature. A multiple linear-regression program provided a curve fit to the data. The equation obtained from the calculated data set (Eq (7)) is almost identical to Eq (6), which was derived from the measured data set in Table 9.

$$E = 73.58 - 0.0278\,(dT) - 18.851\,(dT/I) - 0.1233\,(dT^2/I) \quad (7)$$

Over a collector operating range of temperatures from 50° to 300°C, and with an irradiance from 300 to 1000 W/m^2, the maximum difference between Eqs (6) (test data) and (7) (calculated data) is 0.8 efficiency percentage points (less than 2%). The procedure developed in Appendix C makes it possible to calculate the approximate collector performance for any solar irradiance and for any temperature within the operating range by using only three sets of measured data:

- A thermal-loss curve, measured under out-of-focus conditions, at zero-solar-irradiance incident on the absorber.
- An efficiency curve obtained at a high-level, constant-solar irradiance. An in-focus thermal-loss curve can be derived from this data.
- A near-ambient-air-temperature efficiency measurement to approximate the collector's optical efficiency. We have not found any other satisfactory way to approximate the optical efficiency from data taken at elevated temperature.

The test series discussed above and the associated calculations were made using the 4.13-cm-dia absorber originally furnished with the T-700A collector module. The procedure used to calculate the collector performance under different operating conditions should apply to other collectors of similar design. However, no data was available on another collector of any kind.

Ideally, several completely different collectors of different design and constructed by different manufacturers would be tested to determine if they would respond to a variable solar irradiance in the same way as the T-700A. Because closure of the CMTF test facility was imminent, no other collectors were scheduled or available for such a comparison test. However, after the variable solar-irradiance tests, the T-700A was fitted with a smaller receiver that made its thermal response different. Measured thermal loss at 300°C was only about half that of the larger absorber diameter. Concentration ratio was increased because of the smaller absorber diameter (67:1 vs 51:1); the smaller diameter allowed more spillage of concentrated light, causing the optical efficiency to be lower. Two different versions of the small receiver were available, using quartz-glass and Pyrex-glass receiver envelopes. Therefore, two additional test series were run for comparison with the test data shown in Figures 43 and 44.

Figure 47 shows test data from one of these tests with the small receiver and a Pyrex-glass absorber envelope. Throughout the test, a clear view of the horizon was available without the sunrise and sunset shadows that had interfered with most earlier tests. With no shadows, it was possible to follow the collector response through the zero efficiency point.

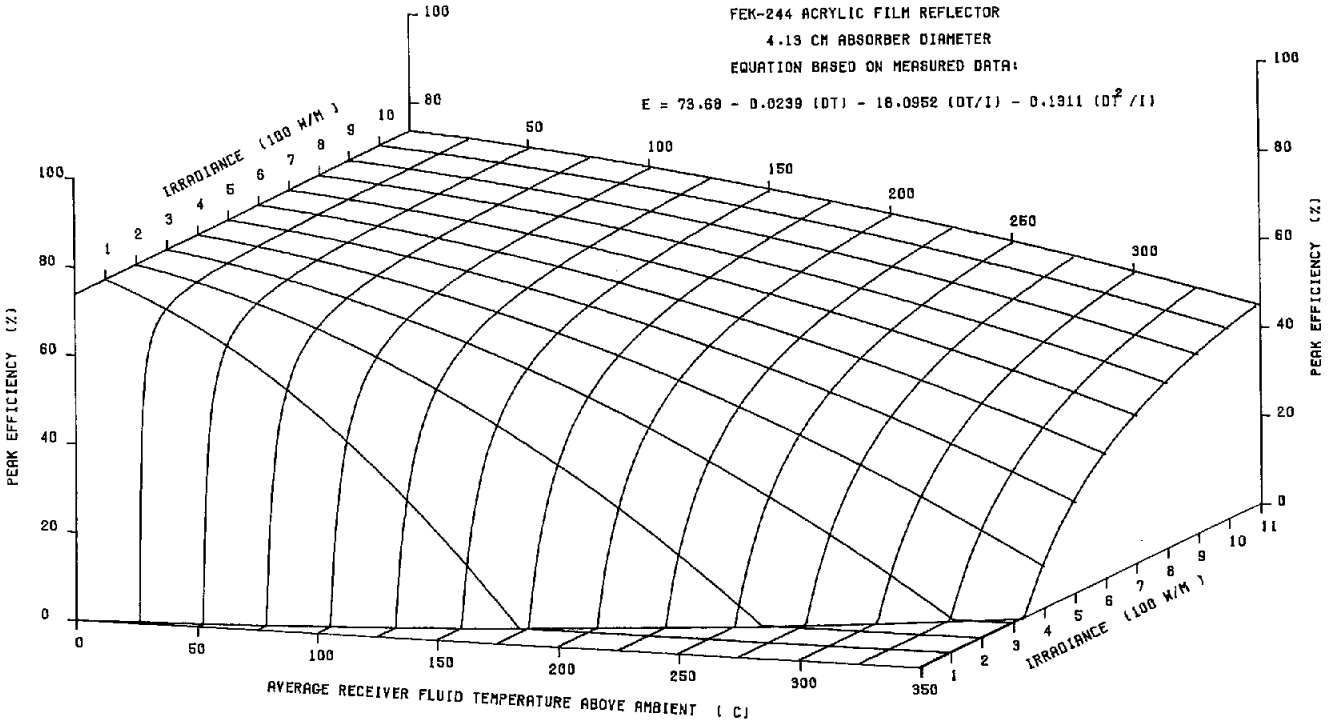

Figure 45. Solar Kinetics T-700A Efficiency vs Temperature and Irradiance (4.13-cm absorber tube)

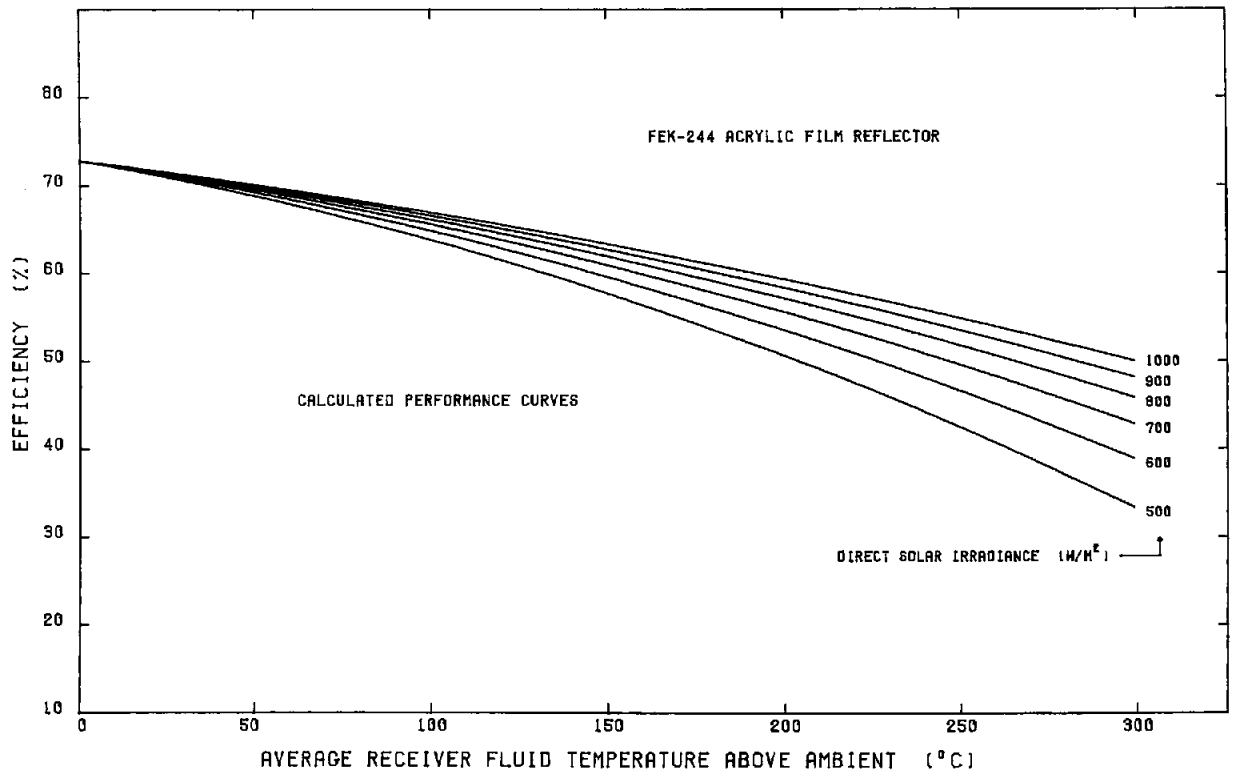

Figure 46. Solar Kinetics T-700A Efficiency vs Temperature and Irradiance

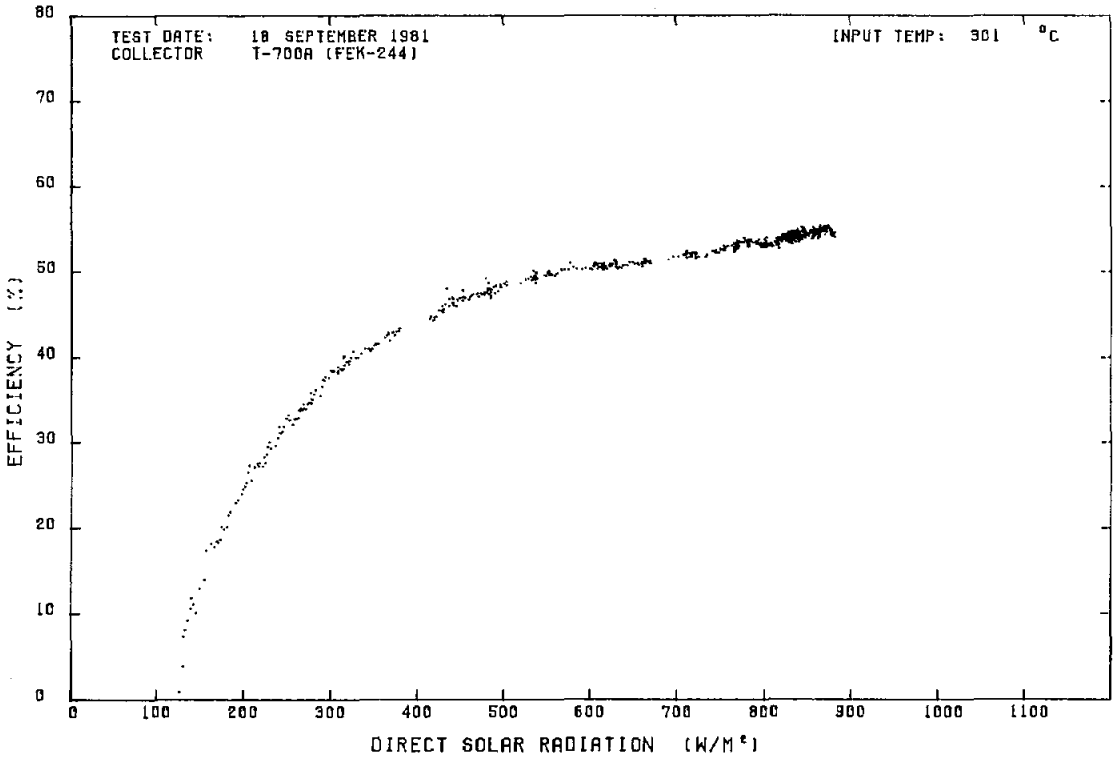

Figure 47. Solar Kinetics T-700A Efficiency vs Insolation (3.18 cm Dia Absorber)

Zero efficiency occurs when the heat gain just balances the thermal loss. At zero efficiency, the absorber-surface temperature should be approximately the same as the bulk-fluid temperature, since there is no net heat flow to or from the fluid. At a fluid temperature of 300°C, Figure 37 shows a zero surface-fluid delta temperature at about 150 W/m^2 solar irradiance; zero efficiency occurred in Figure 47 at about 130 W/m^2. From the thermal-loss data and approximate optical efficiency, zero-collector efficiency should occur at about 115 W/m^2 solar irradiance.

There were a few problems with the test shown in Figure 47 that make it less than ideal. The test is shown here because it was the only occasion in which a curve was obtained over the complete range of collector efficiency. During the test, the solar irradiance changed rapidly below ~ 300 W/m^2, causing the fluid-system temperature stability to be less than normally considered acceptable. The input temperature was stable, but the output temperature was increasing rapidly because of increasing solar irradiance. An increasing temperature would cause the efficiency measurement to be slightly low. Also, the focus was later found to be less than optimum, and a slight adjustment raised the peak efficiency at 300°C by 3 percentage points. Both items would tend to lower the measured zero-efficiency point closer to that calculated from thermal-loss data. Even with these problems, the agreement between the three estimates of the solar irradiance required to achieve zero efficiency isn't too bad, since each of the three were obtained from different kinds of tests and run on different days. The zero-efficiency point is certainly not important for collector operation purposes, but it is useful in checking for consistency between the various measurements and calculations.

Test data similar to that shown in Figure 47 was obtained at the following inlet fluid temperatures: 26°, 60°, 200°, 300°, and 350°C. In most cases, the test data did not extend below 400 W/m^2 solar irradiance. Test points from these tests are shown in Table 12, and plotted in Figures 48 and 49.

Test data from Table 12 was used in a multiple regression computer program to obtain a performance equation (see Appendix B). The equation resulting from the data analysis was:

$$\text{Efficiency} = 66.12 - 0.0142\,(dT) - 2.5009\,(dT/I) - 0.0646\,(dT^2/I) \quad (8)$$

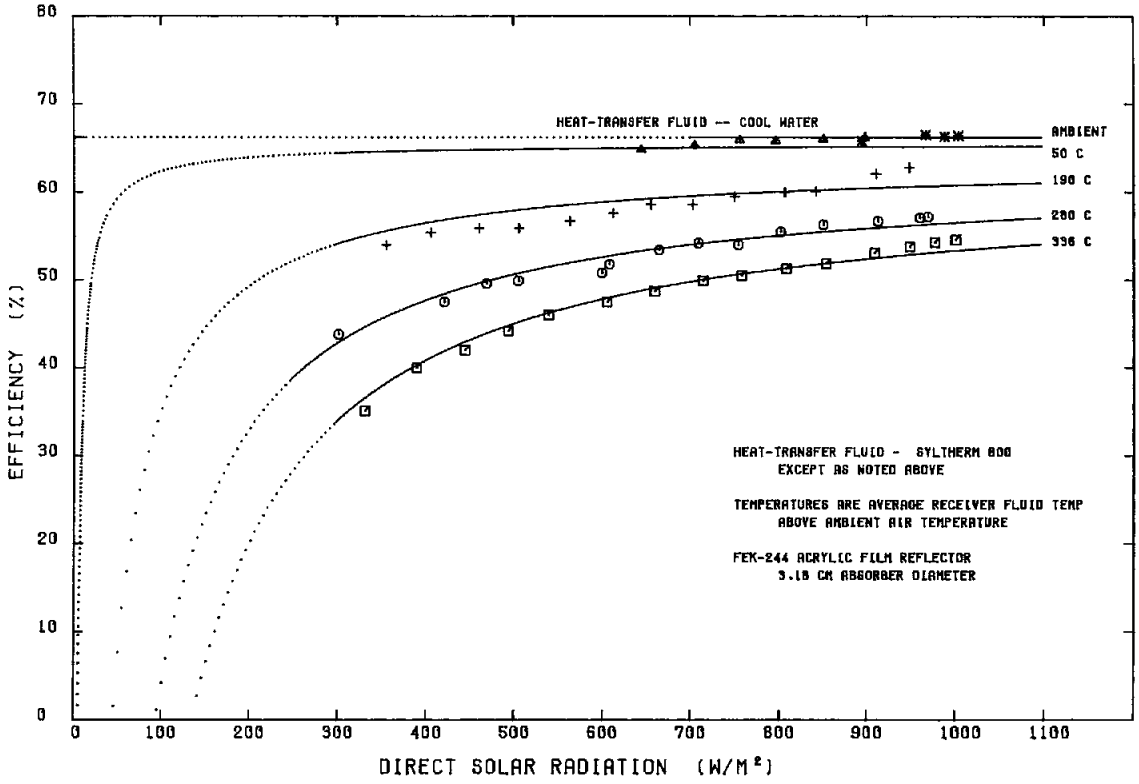

Figure 48. Solar Kinetics T-700A Efficiency vs Insolation and Temperature

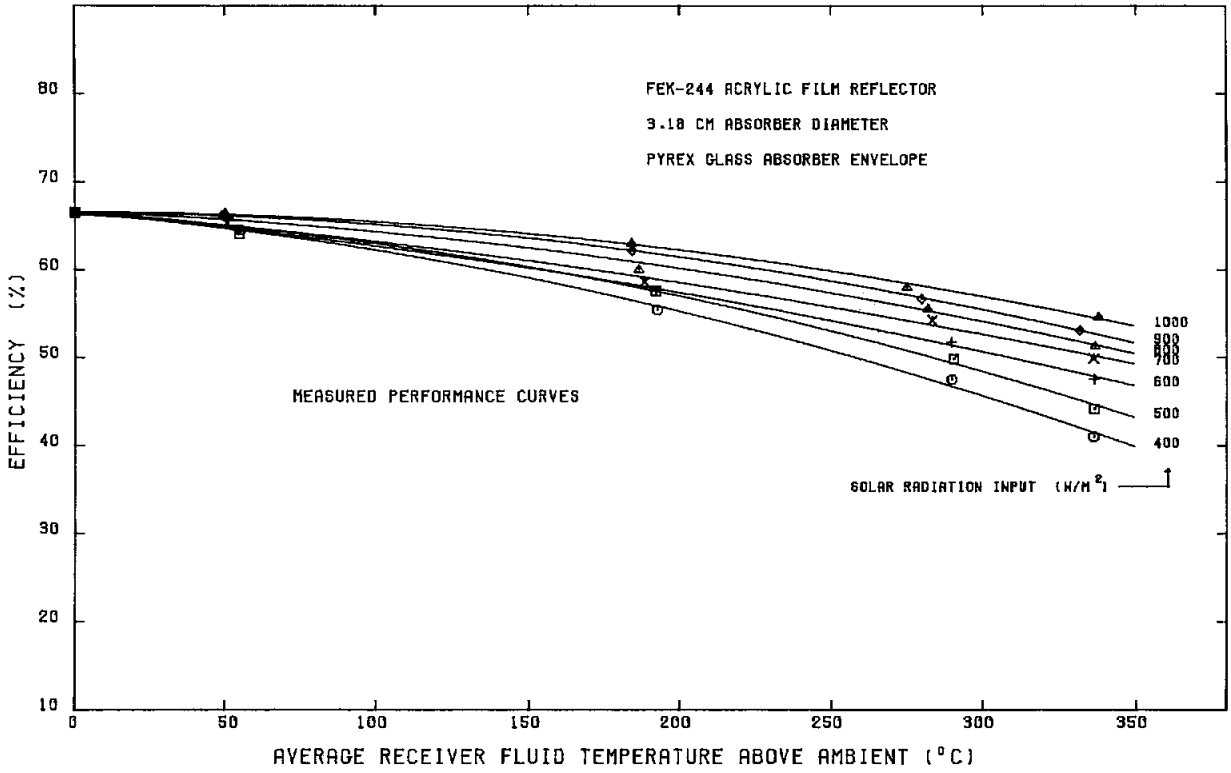

Figure 49. Solar Kinetics T-700A Efficiency vs Temperature and Insolation

Table 12. Variation of Efficiency With Irradiance, Syltherm 800 Heat-Transfer Fluid, FEK-244 Reflector, 3.18-cm Absorber, Pyrex-Glass Envelope

Test Date	Direct Irradiance (W/m^2)	Temp Out (°C)	Tavg –Tamb (°C)	Tavg-Tamb / I (°C·m^2/W)	Receiver Delta-T (°C)	Efficiency (%)
7/08/81	893.7	34.1	1.1	0.0012	6.17	65.8*
10/20/81	966.3	23.4	–5.0	–0.0052	3.54	66.5*
10/20/81	987.6	23.7	–0.4	–0.0004	3.60	66.3*
10/20/81	1003.1	26.1	–0.2	–0.0002	5.91	66.4*
10/13/81	320.0	66.9	54.3	0.1752	2.80	63.0**
10/13/81	347.7	68.9	55.3	0.1591	3.32	63.8**
10/13/81	430.2	68.4	55.2	0.1284	4.17	64.5
10/13/81	495.7	69.4	54.7	0.1103	4.80	64.1
10/13/81	555.6	69.7	54.3	0.0977	5.43	64.4
10/13/81	597.5	70.1	54.0	0.0905	5.81	64.6
10/13/81	644.8	70.7	53.9	0.0835	6.28	64.8
10/13/81	704.8	71.5	50.7	0.0720	6.90	65.3
10/13/81	755.5	72.0	51.3	0.0679	7.45	65.9
10/13/81	796.1	72.4	51.5	0.0648	7.84	65.8
10/13/81	850.1	72.9	50.3	0.0592	8.39	66.0
10/13/81	897.5	73.4	49.1	0.0547	8.88	66.2
10/09/81	108.1	201.2	190.8	1.7650	0.04	2.7**
10/09/81	354.7	204.2	192.8	0.5436	2.70	54.0**
10/09/81	405.0	204.9	192.6	0.4756	3.10	55.4+
10/09/81	460.1	205.3	192.4	0.4183	3.60	55.9+
10/09/81	505.3	205.8	192.5	0.3811	3.96	55.9+
10/09/81	562.9	206.4	191.3	0.3417	4.39	56.7+
10/09/81	612.5	206.9	191.9	0.3134	4.94	57.6
10/09/81	655.4	207.4	191.6	0.2923	5.37	58.6+
10/09/81	702.5	207.8	188.3	0.2681	5.75	58.6
10/09/81	750.0	208.2	188.6	0.2514	6.09	59.5
10/09/81	806.3	208.8	186.3	0.2310	6.63	60.0
10/09/81	841.4	209.1	186.4	0.2215	6.95	60.1
10/09/81	909.8	209.9	184.2	0.2025	7.96	62.1
10/09/81	947.7	210.2	183.3	0.1934	8.20	62.8
10/19/81	300.7	294.7	289.4	0.9534	1.87	43.8**
10/19/81	420.4	295.5	289.7	0.6898	3.19	47.5**
10/19/81	468.4	295.8	289	0.6194	3.61	49.6
10/19/81	504.6	296.1	290.3	0.5754	3.90	49.9
10/19/81	599.3	296.5	290.0	0.5187	4.40	50.8
10/19/81	608.1	297.1	289.6	0.4763	4.87	51.8
10/19/81	664.6	297.6	286.7	0.4315	5.47	53.4
10/19/81	709.1	298.3	283.3	0.3996	5.92	54.2
10/19/81	754.0	298.9	280.4	0.3719	6.29	54.0
10/19/81	801.6	299.2	281.8	0.3516	6.87	55.5
10/19/81	850.1	299.7	281.9	0.3317	7.39	56.3
10/19/81	911.9	300.8	279.8	0.3068	7.99	56.7
10/19/81	959.8	301.1	276.5	0.2881	8.71	57.1
10/19/81	968.6	301.2	274.8	0.2837	8.81	57.2

Table 12. (cont)

Test Date	Direct Irradiance (W/m^2)	Temp Out (°C)	Tavg –Tamb (°C)	Tavg-Tamb / I (°C·m^2/W)	Receiver Delta-T (°C)	Efficiency (%)
10/19/81	330.2	353.1	336.1	1.0170	1.88	35.1**
10/19/81	388.9	353.8	336.1	0.8656	2.49	40.0**
10/19/81	443.7	354.4	336.2	0.7586	3.03	42.0
10/19/81	493.0	354.9	336.3	0.6826	3.54	44.2
10/19/81	538.9	355.4	336.4	0.6245	4.02	46.0
10/19/81	605.2	355.9	336.3	0.5559	4.67	47.5
10/19/81	659.4	356.4	336.3	0.5101	5.22	48.7
10/19/81	714.1	357.0	336.1	0.4707	5.79	49.9
10/19/81	757.5	357.5	335.9	0.4367	6.22	50.5
10/19/81	807.7	358.2	336.6	0.4167	6.74	51.3
10/19/81	853.3	358.5	332.3	0.3895	7.21	51.9
10/19/81	908.1	359.3	331.6	0.3651	7.80	53.1
10/19/81	948.2	359.7	333.7	0.3520	8.35	53.8
10/19/81	976.6	360.2	337.0	0.3450	8.66	54.3
10/19/81	1002.1	360.2	337.1	0.3470	8.71	54.6+
Calculated values of irradiance for efficiency = zero						
	4.4		50.0			0.0
	13.8		100.0			0.0
	28.4		150.0			0.0
	48.3		200.0			0.0
	74.0		250.0			0.0
	115.8		300.0			0.0
	144.4		350.0			0.0

*Data taken with cold water.
**Single data point, not a 10-point average.
+Temperature stability marginal.

The curves shown in Figures 48 and 49 were drawn with Eq (8); the test data points are from Table 12. The match between test data and the curve is not as good as was obtained with the large receiver but, considering the difficulty experienced in getting repeatable measurements on the flexible small receiver, the agreement is not too bad. Maximum deviation of the equation from the test data points is just over two efficiency percentage points.

Figure 50 is a complete plot of the measured data Eq (8) over the full range of temperature and irradiance. The curve has the same general shape as that seen in Figure 45, but there is a noticeable difference at high temperatures and low irradiance.

The response of the collector was also calculated, using the procedure shown in Eqs (C3) through (C5) of Appendix C. The calculations used the measured thermal loss curves and in-focus thermal-loss curves from Figure 40. From the calculated data set another performance equation was obtained; it is nearly the same as Eq (8).

$$\text{Efficiency} = 67.21 - 0.0119\,(dT) - 2.4867\,(dT/I) - 0.0664\,(dT^2/I) \quad (9)$$

Agreement was excellent between the equation obtained from the measured data (8) and the equation obtained from calculated data (9). Over the collector operating range of temperatures from 50° to 350°C and irradiance from 300 to 1000 W/m^2, the maximum difference between the two equations is 1.7 efficiency percentage points (about 3%).

Test time was available to obtain only a few data points on the small receiver using a quartz-glass envelope. The expected response of the collector with this receiver was calculated, and the measured points plotted on the calculated curves (Figure 51). The measured points are all within 1 efficiency percentage point of the corresponding calculated curve.

The physical characteristics of the three receivers used on the T-700A during this test series were all slightly different, and the measured efficiency and thermal-loss curves were significantly different. Since the procedure developed to calculate the collector performance changes with temperature and irradiance was successful in reproducing all three sets of performance curves, the method will probably also work for other parabolic-trough collectors. Further theoretical work and corresponding tests are needed to determine if the procedure applies to solar collector designs other than parabolic troughs. Thermal-loss mechanisms in some collector designs are significantly different from those of parabolic troughs; a linear variation of thermal loss with solar irradiance may not apply to those collectors. A transmission lens type of concentrator (such as a Fresnel lens system) may also be more sensitive to the solar spectrum shift that usually accompanies low levels of solar irradiance.

Variable Solar Irradiance and Delta-T/I

The test data from Table 9 was plotted in Figure 44 as a set of efficiency curves vs temperature above ambient. The test data can also be plotted in the form of delta-T/I curves; this was done in Figure 52. Previous test data for the FEK-244 reflector (shown earlier in Figure 23) was taken at an average irradiance of 970 W/m^2, and would fall between the 900 and 1000 W/m^2 curves in Figure 52.

Observe that the separation between the curves for the different values of solar irradiance is just as large as those seen in Figures 43 and 44. A delta-T/I presentation cannot be used to display a very wide range of irradiance because, for any given operating temperature, the quantity delta-T/I becomes increasingly larger as irradiance is reduced. When irradiance approaches zero, the ordinate in Figure 52 would have to be of infinite length to display the curves. A plot of efficiency vs delta-T/I is thus not suitable to show the complete operating range of a concentrating solar collector.

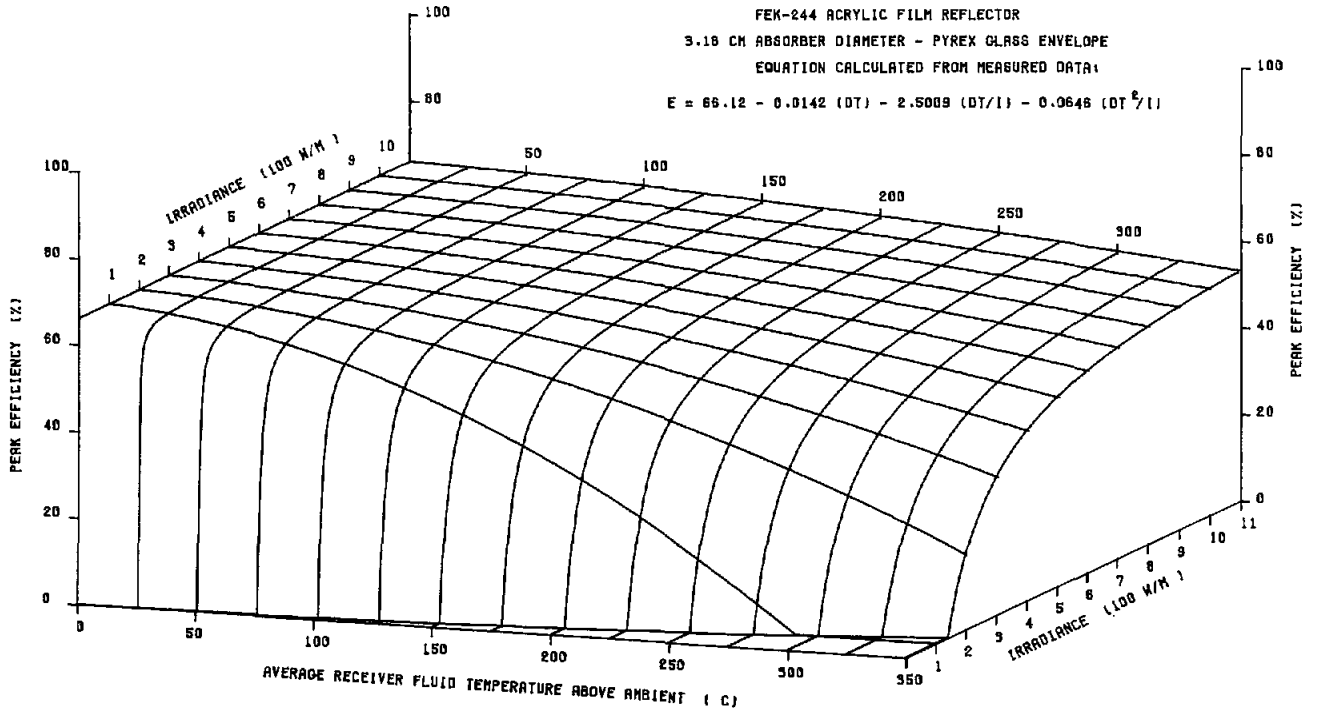

Figure 50. Solar Kinetics T-700A Efficiency vs Temperature and Insolation

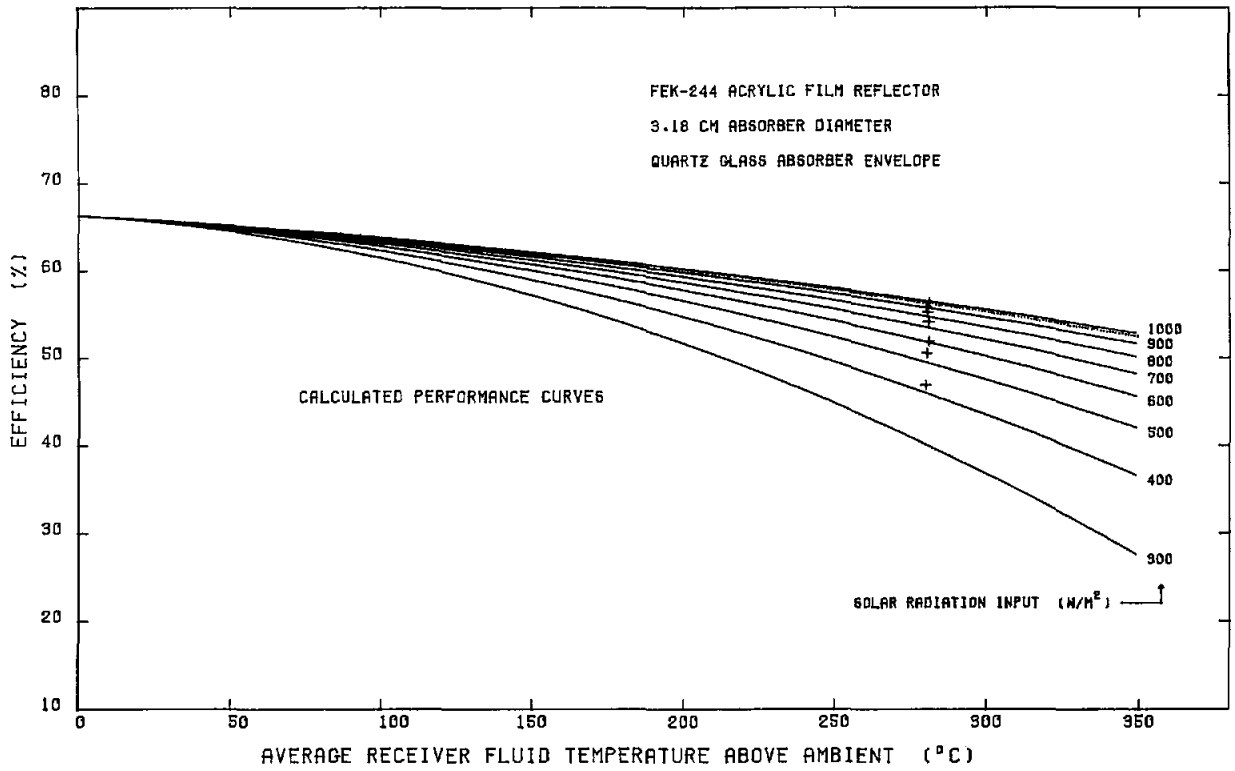

Figure 51. Solar Kinetics T-700A Efficiency vs Temperature and Insolation

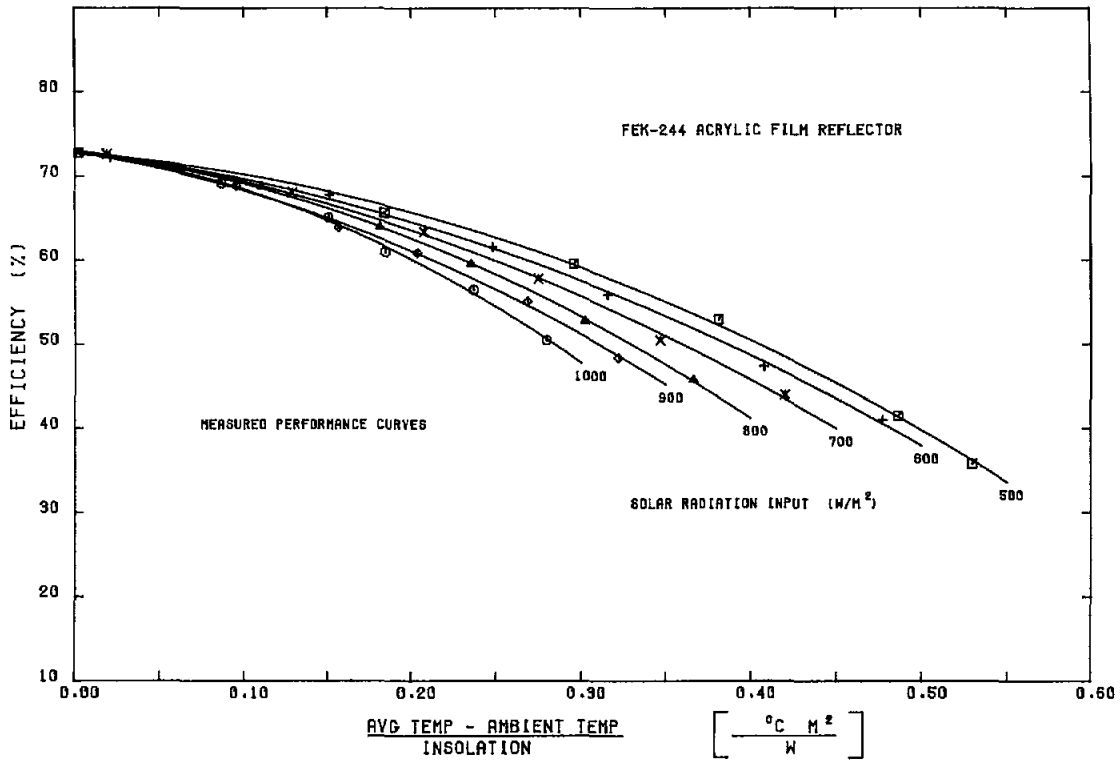

Figure 52. Solar Kinetics T-700A Efficiency vs Delta T/I and Insolation

When only a single value of solar irradiance is used to derive the efficiency equation, the delta-T/I presentation does NOT correctly account for variations in efficiency caused by changes in solar irradiance. Because the solar irradiance I appears in delta-T/I equation (such as those shown in Figures 14, 17, 20, 23, and 26), there is a great temptation to insert any values of temperature and irradiance that are of interest, and calculate the resulting efficiency. This procedure is incorrect; in fact, the I in the delta-T/I equation is not usually an independent variable at all, but is a constant equal to the solar irradiance existing when the data was measured, as it is in all the curves shown in Figure 52. The delta-T/I curves and equations shown earlier in this report (and most of those published by other solar collector test laboratories) are based on a very narrow range of irradiance, so that the correct efficiency can be calculated only for the same narrow range of irradiance.

A curve equation in the delta-T/I format can be derived in which the irradiance is an independent variable (see Appendix B). However, this can be done correctly only if test data is available to show the actual variation of collector response with irradiance, and if a multiple, nonlinear regression technique is used to generate the efficiency equation. Normally this has not been done with past collector tests, and the I in the delta-T/I equations and plotted test data can be used only as a nearly-constant value when only nearly-constant values of irradiance were present in the original test data. Most collector tests report the quantity delta-T/I over a considerable range of delta-T, but with all values measured over a very small range of irradiance (see Tables 1 through 5 for typical peak efficiency measurements). Data such as in Tables 1 through 5 contain essentially no information on how the collector might perform at other values of irradiance.

If the delta-T/I equation from Figure 23 is plotted over the full range of temperature and irradiance, the plot will have the same general shape as that in Figure 45. However, only the portion of the curve near 970 W/m^2 will be correct, because no other information was available for the curve fit. The division by irradiance in two terms of the efficiency equation will produce the general hyperbolic shape in the figure, but there is an infinite family of hyperbolic curves and the chances of obtaining the RIGHT hyperbolic shape are negligible. Exactly the same kind of problem exists if we extrapolate the curves of temperature outside the region covered by actual test data. The general form of the equation will continue the parabolic shape of the temperature curve to any extreme of temperature but, again, when outside the range of actual test data, it is not likely that a correct value of efficiency will be obtained. The solar collector test standard ASHRAE 93-77 prohibits extrapolating beyond the test limit of temperature; this prohibition should be expanded to include irradiance as well.

As an example of the kind of error that can result from the extrapolation of test results caused by using an arbitrary value of I in a delta-T/I equation, consider the set of operating conditions listed below:

Direct solar irradiance	=	615.3 W/m^2
Input temperature	=	300.7°C
Output temperature	=	306.3°C
Temperature above ambient	=	293.5°C
Delta-T/I	=	0.4771°C·m^2/W

If the 0.4771 delta-T/I shown above is substituted into the delta-T/I efficiency equation used to draw the 1000 W/m^2 delta-T/I curve in Figure 52:

$$\text{Efficiency} = 72.8 - 23.3\,(dT/I) - 200.2\,(dT/I)^2 = 16.1\% \quad (10)$$

The calculated efficiency point is shown in Figure 53, marked on the extension of the 1000 W/m^2 curve with a star. The corresponding measured efficiency point is shown at the same value of delta-T/I on the 600 W/m^2 curve, marked with a "+". The actual measured efficiency for the operating conditions given above was 41%; the measured data is the second entry for 24 April in Table 9. The measured efficiency is a factor of 2.5 higher than that predicted by substituting 615.3 W/m^2 into the 1000 W/m^2 delta-T/I curve. The error decreases as the solar irradiance used approaches the original test value; the calculated point is 61% low at 600 W/m^2, 34% low at 700 W/m^2, 18% low at 800 W/m^2, and 8% low at 900 W/m^2.

The errors also decrease rapidly at lower operating temperatures. Most flat-plate collectors would be operating below a delta-T/I of 0.1 in Figure 53; the errors would be quite small. At low temperatures and a concentration ratio of one, delta-T/I can be used with a wide variation in irradiance without serious errors. At high-temperatures and high concentration ratios, delta-T/I fails because thermal loss becomes an ever-larger fraction of the total heat gain; delta-T/I is also not a constant at a given temperature, but is changing with the irradiance. The delta-T/I presentation of efficiency data, when based only on nearly-constant values of irradiance, is highly misleading for use with a concentrating collector operating at high temperatures. (Refer to Figure B1 in Appendix B for a complete plot of delta-T/I error vs temperature and irradiance.)

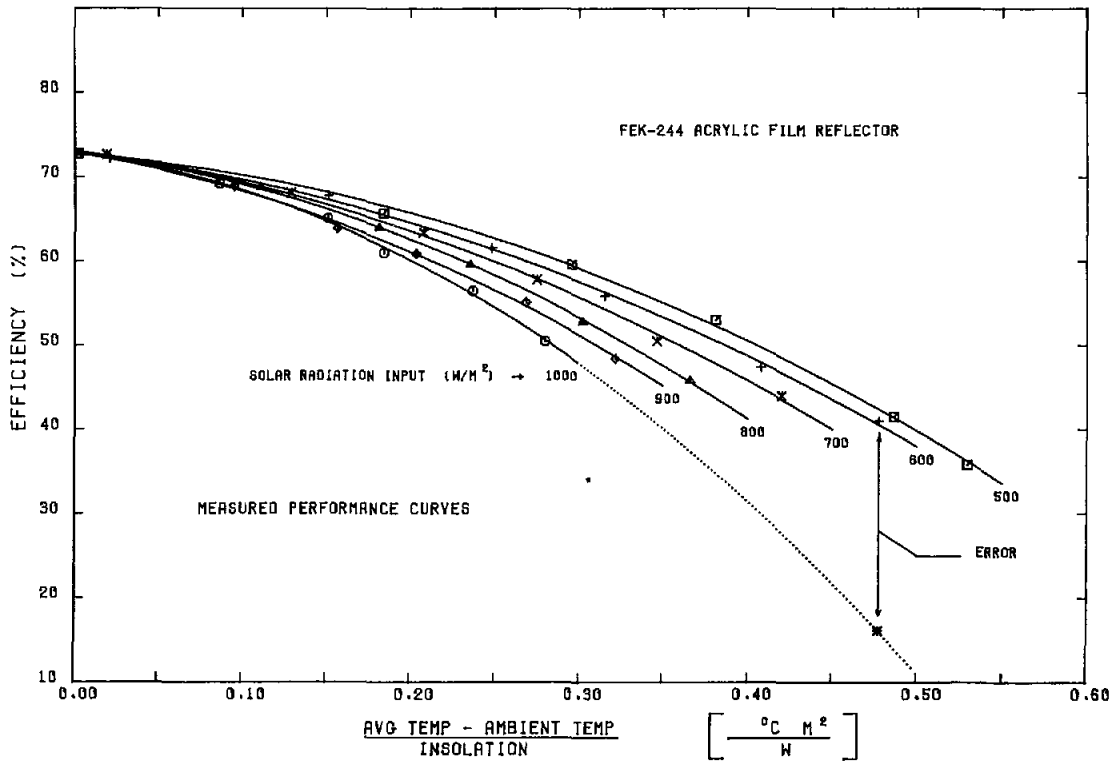

Figure 53. Error Resulting From Extrapolation of Delta T/I

Delta-T/I curves are not the only ones that can be misused; they are just the easiest. An inspection of Figure 44 shows that the same set of operating conditions outlined above, if applied to Figure 44, would result in an overestimate of 10 percentage points in operating efficiency at 600 W/m^2, rather than the 25-point underestimate found with Figure 53.

The errors outlined above are not necessarily the same for other collectors. Since we are dealing with equations extrapolated outside the range of test data, the actual shape of the curves in those regions is not predictable. However, an extrapolation of temperature means an extension of a slowly changing parabolic shape, which might make the error fairly small if the extension is small. An extrapolation of irradiance means an extension along a hyperbolic path, where the errror depends critically on the exact location along the curve; an error could range from very small to very large for the same change in irradiance.

Calculated Annual Thermal Performance

To supplement the peak efficiency data obtained from the tests in this report, estimates of the annual thermal performance of the T-700A collector have been made. The annual performance estimates use Typical Meteorological Year (TMY) data tapes for five cities: Albuquerque, Fort Worth, Fresno, Charleston, and Boston. Previously published documents contain annual thermal performance predictions for the T-700A with Corning-glass reflectors[4] and for the T-700 with FEK-244 acrylic-film reflector[5]. However, the T-700 collector used for Reference 5 was an earlier model, not identical to the T-700A used in this test series.

The procedure used to calculate the annual thermal output is given in Reference 6. The calculations shown in Reference 6 contain no corrections for changes in collector efficiency at low solar-irradiance levels since this data was not available when the document was being prepared. Change in collector performance as a function of solar irradiance was recognized as a possible source of error in Appendix A of Reference 6. If collector efficiency had been calculated for the T-700 collector using measured performance curves, such as Eq (6) or those shown in Figure 43, instead of a delta-T/I equation based on a single value of I, annual thermal output from the collector would be somewhat larger than that shown in Reference 4 and 5.

For this report, the annual thermal performance of the T-700A collector was calculated in two different ways. One calculation was made using the 1000 W/m^2 delta-T/I efficiency equation from Figure 52 in the same way as outlined in Reference 6. The second calculation was made using Eq (6) (also shown in Figure 45). Equation (6) was derived from measured data over a full range of delta-T and irradiance, and correctly predicts the response of the collector to varying levels of temperature and solar irradiance. Data from both sets of calculations are shown in Appendix D, in a format similar to that used in References 4 and 5.

The new calculations of annual thermal performance show that a delta-T/I equation based on a single value of irradiance underestimates the energy available; the annual estimate is about 7% to 10% low for cities that have high levels of direct solar irradiance during most of the year, such as Albuquerque and Phoenix. The estimate can be as much as 30% low for cities like Boston and Charleston that have a much lower average solar irradiance level, and thus larger errors of the type shown in Figure 53. The error is smaller at lower temperatures (see Appendix D).

A performance estimate could be prepared using the equations for efficiency vs output temperature or efficiency vs temperature above ambient. These equations also are not correct with an arbitrary value of irradiance. If used, the energy output would be overestimated rather than underestimated, as when using the delta-T/I method. The only way to get the right answer is to use an equation that includes both delta-T and irradiance as independent variables.

Summary of Results and Conclusions

The Solar Kinetics T-700A collector module achieved the highest efficiencies ever measured at the CMTF on a commercially available solar collector, both with glass mirrors and with FEK-244 acrylic-film mirrors.

In addition to tests with the two types of reflector materials, the collector was also tested with absorbers of two different diameters. Tests covered the complete temperature range from ambient to 360°C (680°F). A summary of the collector performance at approximately 970 W/m^2 direct normal solar irradiance is shown in Table 13 below, and in Figure 54 through 57.

The glass mirrors offer higher performance for greater initial cost. The small receiver was not wide enough to capture all the concentrated light, causing the low-temperature efficiency to be less than that with the large receiver. However, the lower thermal loss associated with the smaller surface area of the small receiver resulted in a higher operating efficiency for tempertures above ~ 170°C. A quartz-glass receiver envelope did not further improve the efficiency of the small diameter receiver.

A large number of tests performed on the T-700A were not intended to determine peak performance at noon on a perfect day, but were designed to obtain information on collector operation during less ideal conditions and to further our general understanding of how these machines work. Some important data was obtained:

1. Receiver-surface temperatures change linearly with solar irradiance. When a collector is focused, surface temperatures are significantly higher than fluid temperatures at all fluid flow rates.
2. Receiver thermal loss depends on receiver surface temperatures rather than on heat-transfer fluid temperatures.
3. Because of the surface temperature changes, the thermal loss from a parabolic-trough collector also changes significantly with changes in solar irradiance.
4. The changing ratio of heat gain to thermal loss causes the collector efficiency to change with changing solar irradiance.
5. Current practice of publishing equations and performance curves of collector efficiency and receiver thermal loss, without regard to level of solar irradiance, leads to serious errors when these data are used to predict performance of collector fields operating in the real world (see Appendix D). The delta-T/I presentation of collector efficiency data, using essentially a single value of irradiance as has been done in the past, does not help because the I in delta-T/I is not a variable, but is a constant value (see Figure 53 for an example).
6. The T-700A collector tests covered a wide range of solar irradiance. Equations were derived from the test data that correctly predicted collector performance at any temperature within the range of tests and at any level of solar irradiance. The equations give collector efficiency as a function of both delta-T and direct normal solar irradiance. In graphical form, a plot of the equations depicts a three-dimensional surface. A plot of the equation for the T-700A, as obtained from test data with FEK-244 acrylic-film reflectors and a 4.13-cm-dia absorber, is shown in Figure 45. A similar plot for the collector using the small absorber was shown in Figure 50.

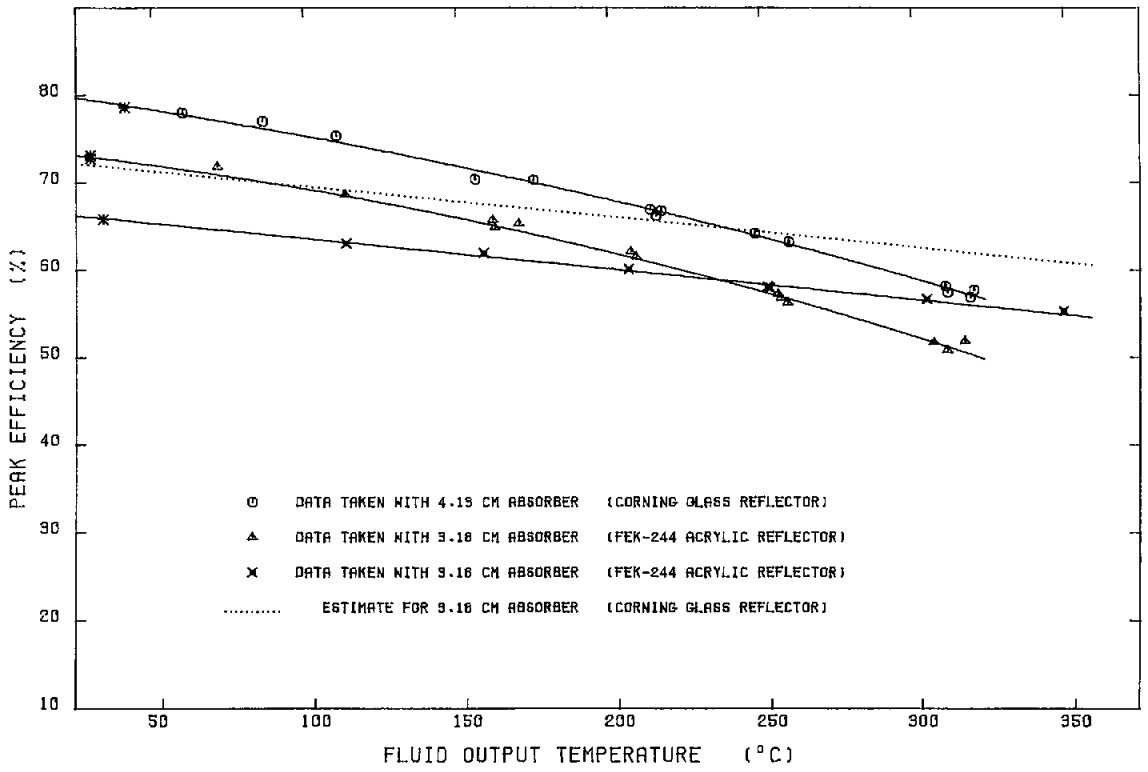

Figure 54. Solar Kinetics T-700A Efficiency Performance Comparison (Efficiency vs Fluid Output Temperature)

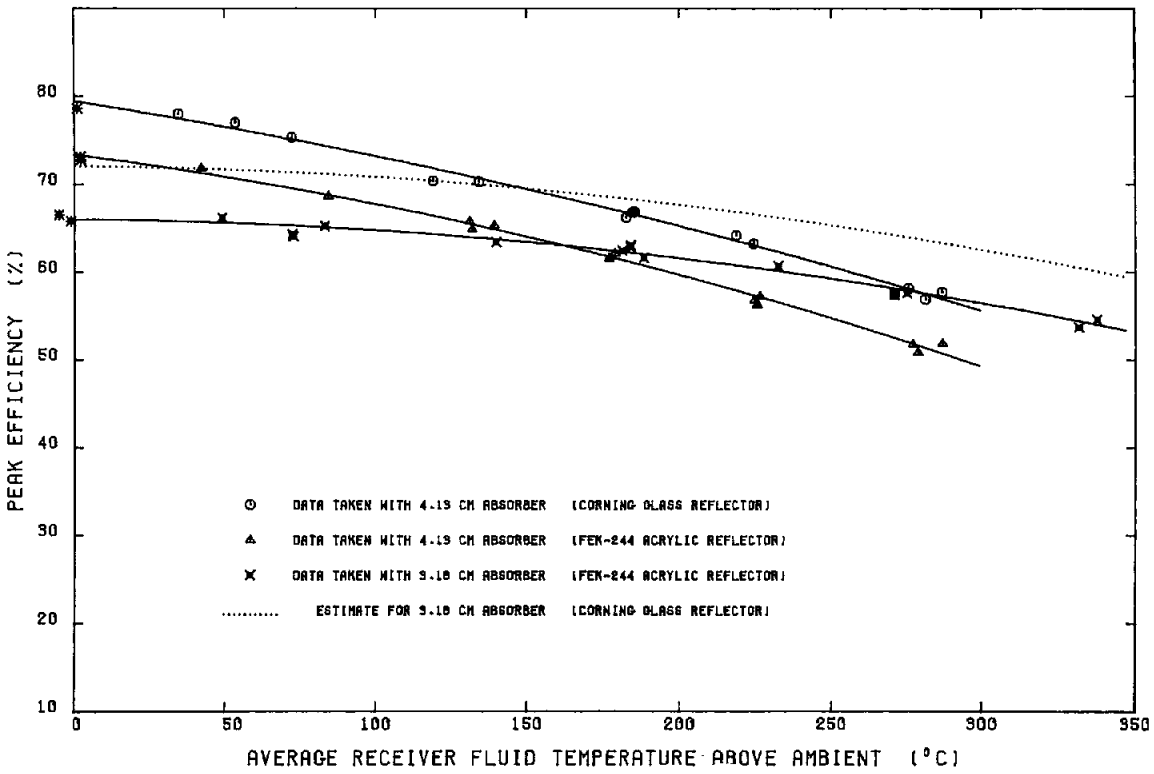

Figure 55. Solar Kinetics T-700A Efficiency Performance Comparison (Efficiency vs Average Receiver Fluid Temperature Above Ambient)

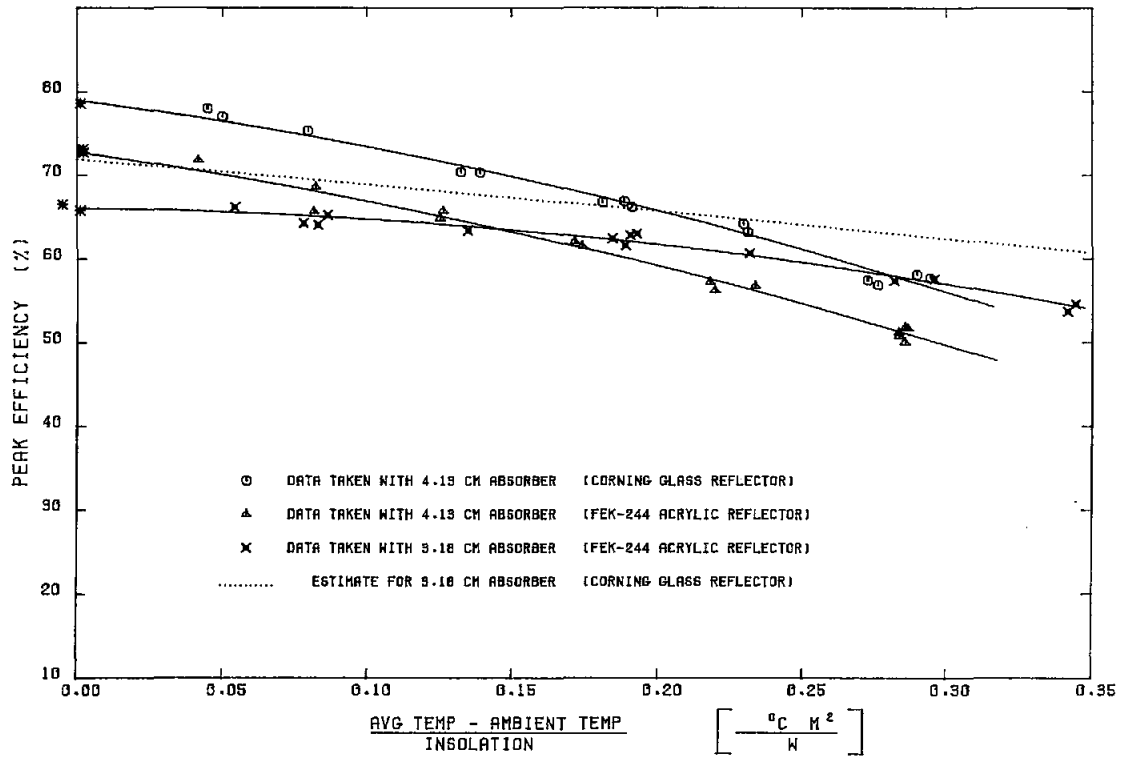

Figure 56. Solar Kinetics T-700A Efficiency Performance Comparison (Efficiency vs Delta T/I)

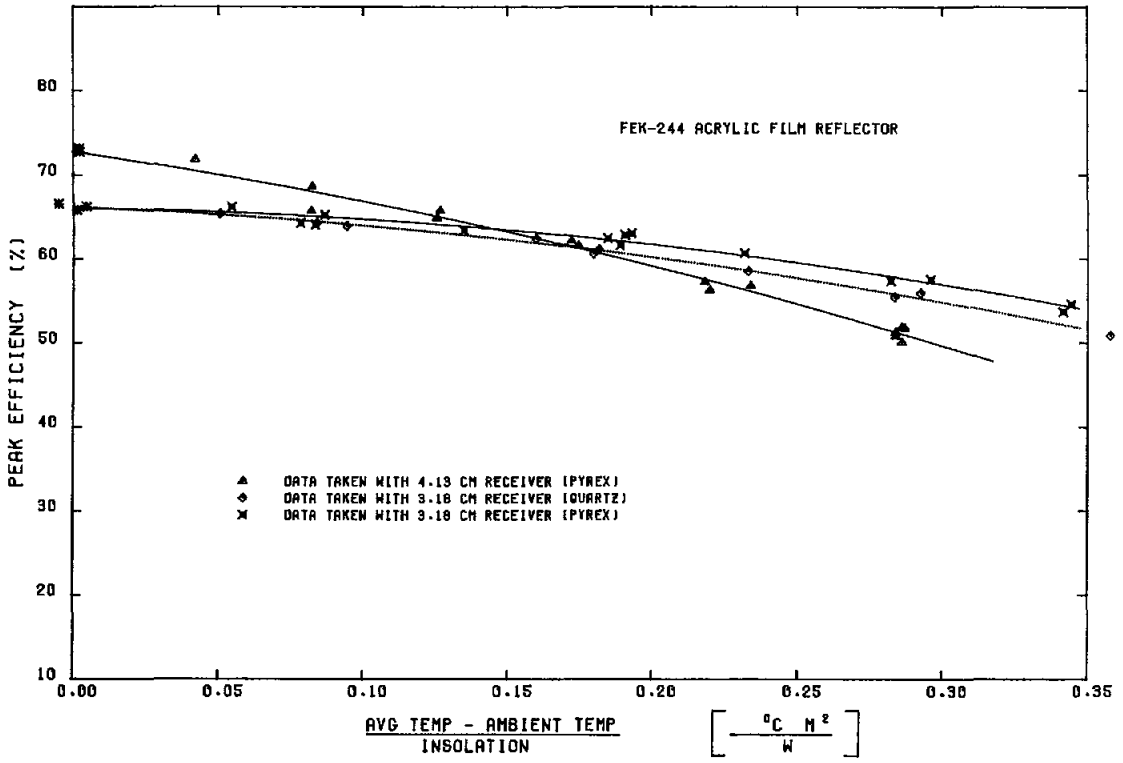

Figure 57. Performance Change With Receiver Configuration

Table 13. Peak Efficiency of T-700A Collector at 970 W/m²

Configuration	Temp	Efficiency	Temp	Efficiency
Glass mirror, large receiver	Ambient	79%	300°C	59%
Glass mirror, small receiver	Ambient	73%*	300°C	63%*
Acrylic mirror, large receiver	Ambient	73%	300°C	52%
Acrylic mirror, small receiver	Ambient	67%	300°C	56%

*Not measured; estimated from test data.

A procedure has been developed that can be used to calculate the performance of a parabolic-trough collector at any temperature within its operating range, and at any level of solar irradiance. Only three sets of test data need to be accumulated as inputs to the calculations. In order that realistic operational performance can be predicted, future tests of parabolic-trough concentrating solar collectors should include these tests:

1. A thermal-loss curve measured under out-of-focus conditions with zero solar-irradiance incident on the absorber.
2. An efficiency curve obtained at constant solar irradiance. An in-focus thermal-loss curve can be derived from this data.
3. A near-ambient-temperature efficiency measurement to approximate the collector's optical efficiency. We have found no satisfactory way to determine the ambient-air-temperature collector efficiency from data taken at elevated temperature.

The three sets of test data shown above were obtained on four different versions of the T-700A collector module. Using the procedure shown in Appendix C, the data sets were used to derive performance equations for each variation of the collector configuration. These equations predict collector efficiency for any delta temperature from 0 to 350°C, and at any value of direct normal solar irradiance from 0 to 1100 W/m². Graphical plots of the equations derived from calculated data are shown in Figures 58 through 62; plots of the two equations derived from measured data were shown earlier in Figures 45 and 50. Equations derived from calculated data are nearly the same as those derived from measured data. The efficiency equations are shown on each plot; coefficients for all the equations are listed in Table 14.

The collector performance equations shown in Table 14 and in Figures 58 through 62 should be used to obtain collector efficiency under all operational conditions. The other efficiency equations shown on the earlier curves throughout this report are valid only at the value of solar irradiance shown with each equation.

Recommendations

1. Future tests of parabolic-trough concentrating solar collectors should include the three tests listed above so that collector performance can be obtained over a useful range of irradiance, rather than under only ideal peak noontime conditions.
2. Use of the efficiency plot vs delta-T/I should be discontinued for concentrating collectors. The graphic plot cannot be used over the full performance range of the collector; also the form of the equation is unsuitable. A three-variable equation of efficiency vs delta-T, delta-T/I, and delta-T^2/I appears to be the best presentation available to show peak efficiency data.
3. If test data was obtained only over a small range of irradiance, the average test value of irradiance should be noted directly on the efficiency plot and referenced when the efficiency equation is used.
4. Further theoretical work and tests should be accomplished to determine how other collector designs respond to the variable solar irradiance that will occur on every day of their operating lifetimes.

Table 14. Performance Equations for T-700A Collector Modules

Reflector	Absorber Tube (cm)	Constant	dT	dT/I	dT^2/I
Glass	4.13	77.6352	–0.0061	–19.0694	–0.1225
Glass	3.18	73.1933	–0.0107	– 2.4884	–0.0664*
FEK-244	4.13	73.6766	–0.0239	–18.0952	–0.1311**
FEK-244	4.13	73.5797	–0.0278	–18.8510	–0.1233
FEK-244	3.18	66.1212	–0.0142	– 2.5009	–0.0646**
FEK-244	3.18	67.2062	–0.0119	– 2.4867	–0.0664
FEK-244 (quartz)	3.18	66.3979	–0.0097	– 1.5532	–0.0843

Equations calculated from efficiency and thermal loss data except:
*Optical Efficiency not measured, estimated from other test data.
**Equation from curve fit to actual test data.

Equations give collector efficiency in percent when: Delta-T is in °C above ambient air temperature, irradiance is in W/m^2

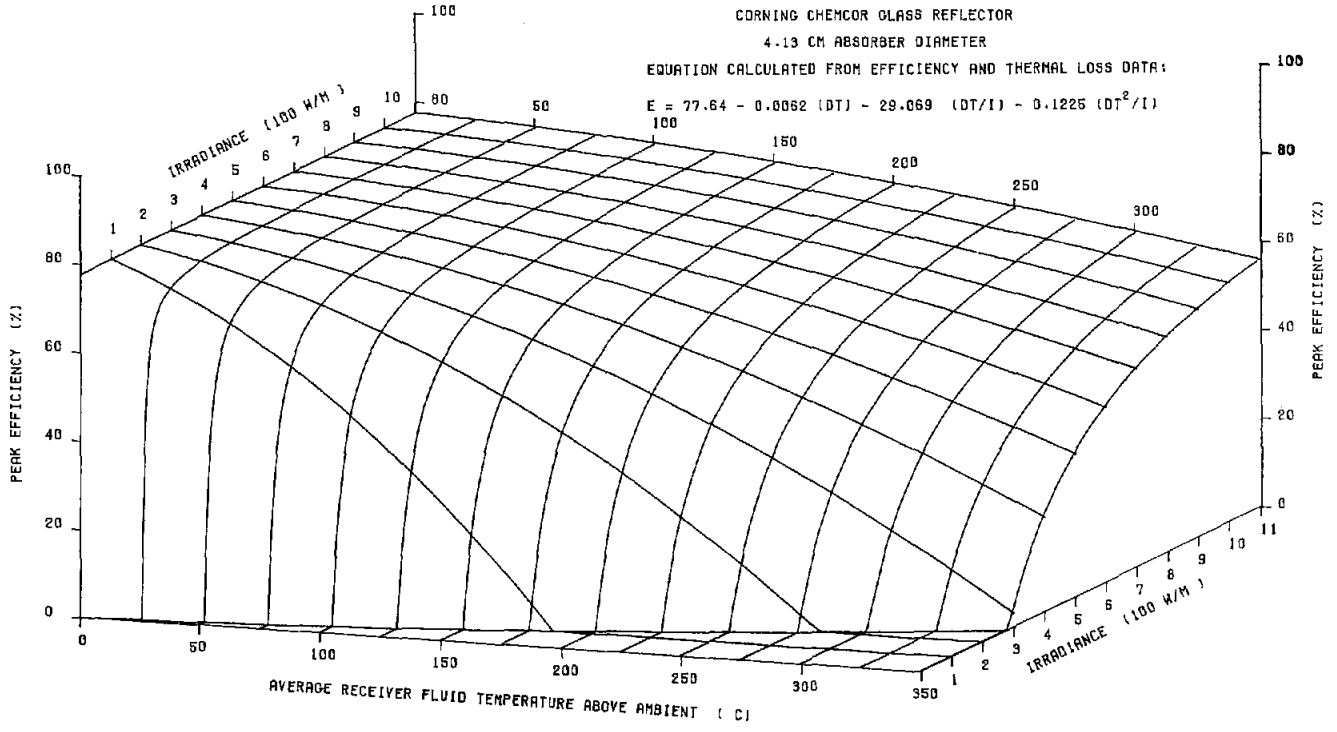

Figure 58. Solar Kinetics T-700A Efficiency vs Temperature and Irradiance (4.13-cm tube with glass reflector)

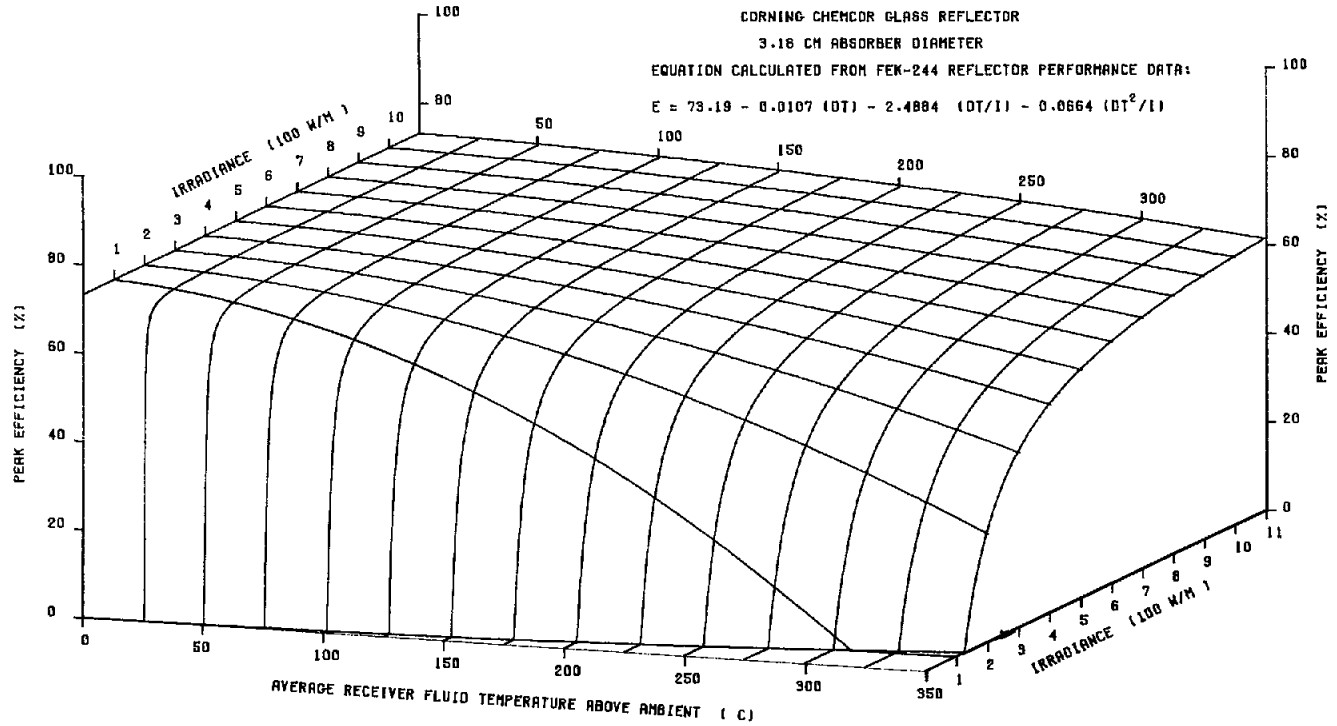

Figure 59. Solar Kinetics T-700A Efficiency vs Temperature and Irradiance (glass reflector with 3.18-cm tube)

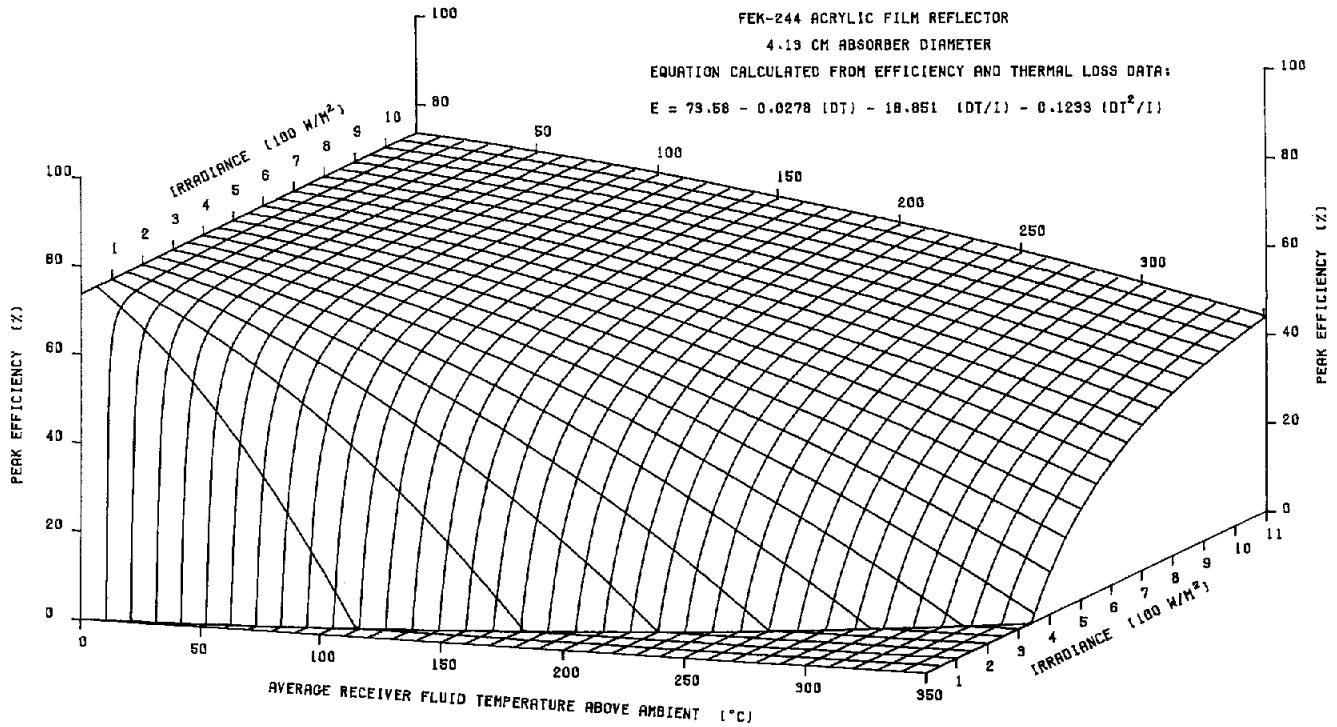

Figure 60. Solar Kinetics T-700A Efficiency vs Temperature and Irradiance (film reflector with 4.13-cm tube)

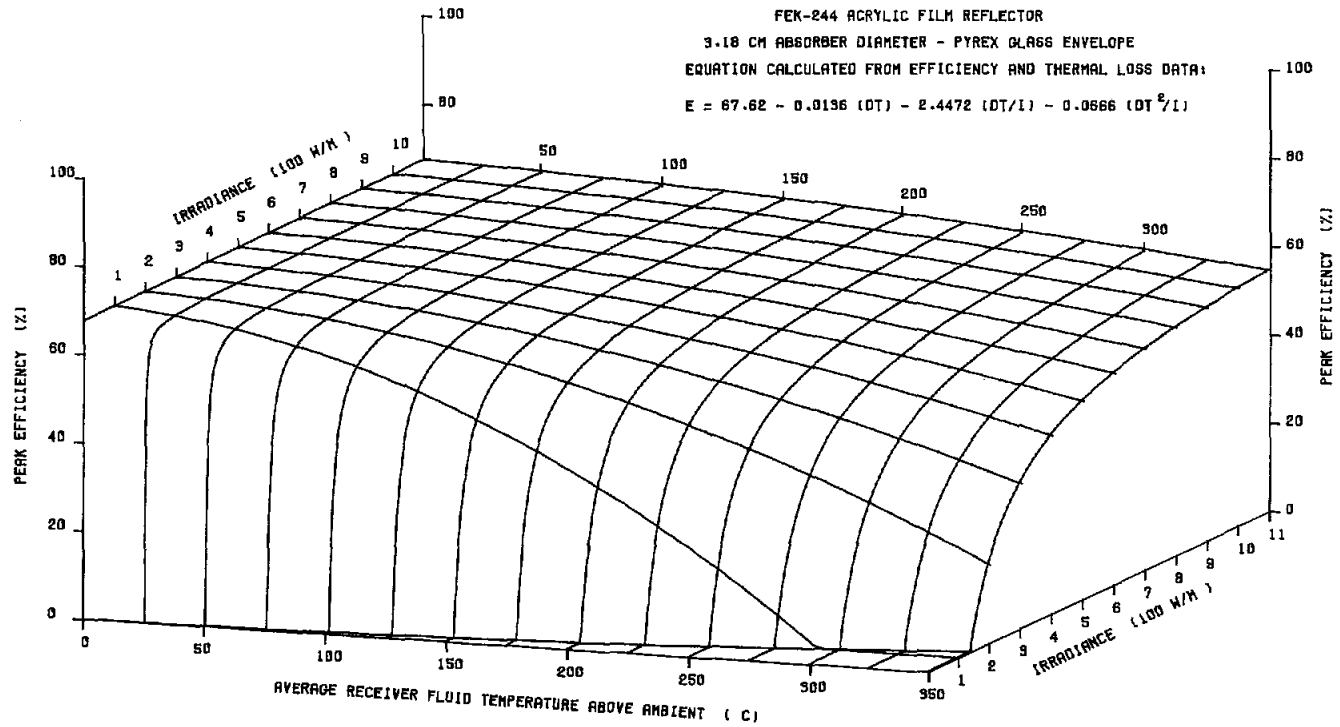

Figure 61. Solar Kinetics T-700A Efficiency vs Temperature and Irradiance (3.18-cm tube with film reflector and Pyrex envelope)

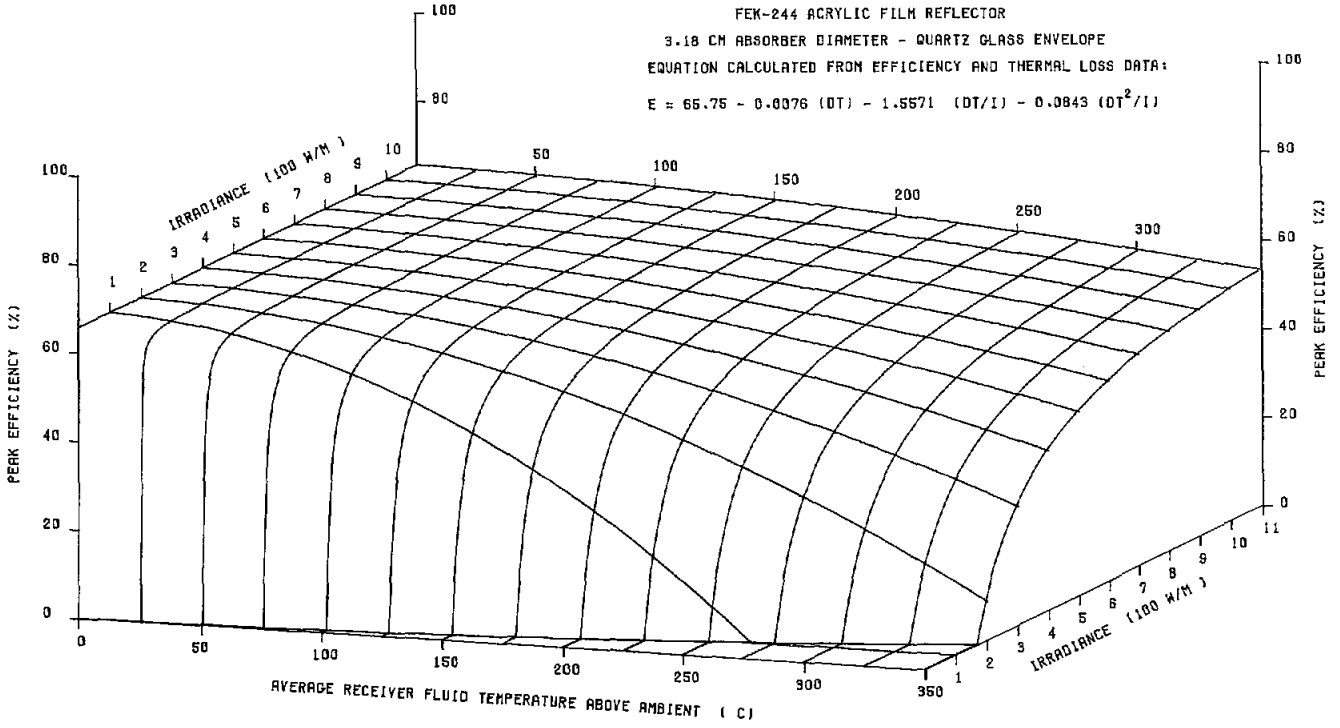

Figure 62. Solar Kinetics T-700A Efficiency vs Temperature and Irradiance (3.18-cm tube with film reflector and Quartz envelope)

APPENDIX A

Collector Module Information Sheet

Manufacturer:	Solar Kinetics, Inc. 3300 Century Circle Irving, Texas 75060 (214) 721-1070
Operating Temperature:	20° - 350°C (68° - 662°F)
Module Size:	6.1 x 2.13 m (240 x 84 in)
Aperture:	12.80 m^2 (137.76 ft^2)
Module Construction:	Monocoque Bulkheads: Aluminum castings Face Sheets: T6 aluminum sheet
Rim Angle:	90 degrees
Reflector:	Corning Tempered-Glass Mirrors Second-Surface Silvered Reflectance: 0.94 3M FEK-244 Acrylic-Film Mirrors Second-Surface Aluminized Measured Reflectance: 0.84 (660 nm)
Focal Length:	55.9 cm (22 in.)
Concentration Ratio:	Aperture Width/Receiver Diameter 51:1 (4.13-cm-OD absorber) 67:1 (3.18-cm-OD absorber)
Receiver:	Absorber Diameter: 4.13 cm (1.625 in.) Black-Chrome-Plated Steel Tubing Measured Absorptance: 0.94 Measured Emittance: 0.20 (300°C) 6.35-cm-dia Pyrex-Glass Envelope Absorber Diameter: 3.18 cm (1.257 in.) Black-Chrome-Plated Steel Tubing Measured Absorptance: 0.94 Measured Emittance: 0.20 (300°C) 5.21-cm-dia Quartz-Glass Envelope 5.21-cm-dia Pyrex-Glass Envelope
Sun Tracking:	Single-Axis Elevation Tracking Shadow-Well Sun Sensor
Tracking Drive System:	Hydraulic

APPENDIX B

The Collector Efficiency Equation

The equation of efficiency vs delta-T/I shown in Figure 23 for the T-700A with FEK-244 reflectors and 4.13-cm-dia absorber was obtained by a polynomial least-squares regression technique. This procedure produces an equation containing both delta-T and irradiance, but irradiance is not an independent variable because no range of irradiance data is normally used in the regression calculations. The equation from Figure 23 is:

$$\text{Efficiency} = 72.8 - 49.8\ (dT/I) - 88.1\ (dT/I)^2 \qquad (B1)$$

Each term in the equation serves as a model of the physical processes occurring during collector operation. The first term is a constant and should be approximately equal to the collector's optical efficiency. The other two terms in the equation have negative coefficients, which reduce the efficiency as a function of thermal loss (dT terms) and irradiance (I). The first power of dT should model the linear convection and conduction thermal loss. Nonlinear thermal loss by radiation should theoretically be a function of the fourth power of the absolute temperature, but we may be able to represent the radiation loss over the relatively small range of temperature we are interested in with only a function of dT^2. Figure 43 shows that the efficiency variation with irradiance is hyperbolic in form. The division by I in the second and third term of equation (B1) should produce the general hyperbolic shape of the curve; however, having a second power of I in the third term is theoretically incorrect.

Because Eq (B1) was derived only from peak noon efficiency data at an essentially constant irradiance (Table 3 for the test data), it is not likely to provide a good estimate of the collector's performance under other operating conditions. One example of the error inherent in the equation was shown earlier in Figure 53. Figure B1 shows an error plot of Eq (B1) as compared to Eq (B4) below, which correctly predicts efficiency over the full range of collector operating conditions. Figure B1 shows that Eq (B1), when derived only from peak noon efficiency test data, may closely predict peak noon efficiency values, but it is an extremely poor model of the collector's overall performance.

Test data listed in Table 9 was used in a multiple regression computer program (MICROSTAT, Reference 7) with Eq (B1) as the model to be fitted. The equation obtained was quite different from the dT/I equation shown in (B1) that was obtained, using only peak efficiency data from Table 3, at a nearly-constant value of irradiance. From the data in Table 9, the equation was:

$$\text{Efficiency} = 76.94 - 84.98\ (dT/I) + 22.07\ (dT/I)^2 \qquad (B2)$$

Equation (B2) reproduces the test data in Table 9 much more closely than does Eq (B1), but the fit is not very good. When the efficiency values predicted by Eq (B2) are compared to the test data, there is a repeating pattern of error in which the predicted value is about 6 efficiency percentage points high at low values of I, and becomes too low at high values of I. The pattern repeats at each set of temperatures.

If Eqs (B1) and (B2) are compared, the first term (constant) in (B2) is too large (about 4 points higher than measured), the second term in (B2) is almost twice as large as in (B1), and the third term in (B2) is positive to compensate for the large second term. Since the third (squared) term in the equation is suppose to represent nonlinear thermal loss, a positive coefficient is at odds with what is really happening. Equation (B2) is better than (B1), but it is not a good model of the collector performance.

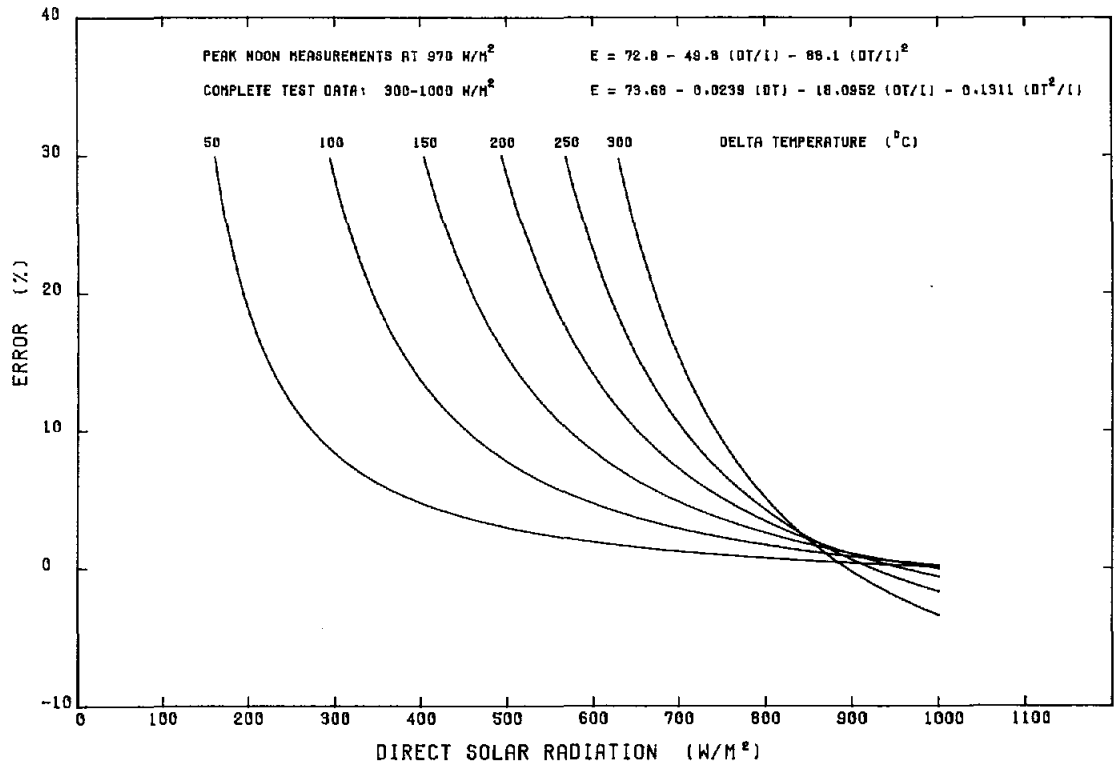

Figure B1. Efficiency Error in Peak-Noon Delta-T/I Equation

Others have also attempted to derive a single equation that would correctly predict a concentrating solar collector's performance under any operating condition. Reference 8 contains a performance equation for a T-700 collector (and others) that was derived from "all-day" test runs such as those shown in Figures 8 and 11. Unfortunately, the analysis was made on an earlier version of the T-700 collector, and thus did not include the near-optical efficiency measurements and the data in Table 9. The equations in Reference 8 produce a set of curves similar to those in Figures 43 and 44, but because of the limited range of delta-T and irradiance test data used in the curve fits, the computed efficiencies are not as close to the test data as we would like, and do not correctly cover the full range of irradiance. The obvious next step was to use all the available data in a curve fit with the model equation from Reference 8. Using the data from Table 9, the equation obtained from the multiple regression analysis was:

$$\text{Efficiency} = 70.55 - 13.39\ (dT/I) - 0.1728\ (dT^2/I) \quad \text{(B3)}$$

Equation (B3) is a better fit to the test data than was (B2) or (B1). The squared function in the third term is now properly restricted to dT, leaving irradiance as a first-power function. The constant term is too low (2.5 points lower than measured), but in general the deviations from the test data are about half those with Eq (B2). There is still evidence of a repeating pattern to the deviations from the test data. The equation reproduces the test data over the range from 400 to 1000 W/m^2, and temperatures from 50° to 300°C to within −3, +2 efficiency points (about ±4%). Not a bad fit, but we can still do better.

The stepwise feature of the MICROSTAT multiple regression computer program was then used to successively try data values containing I, T, dT, dT^2, dT/I, dT^2/I, and dT^4/I in various combinations to produce a number of performance equations. When a term containing only delta-T was added to Eq (B3), an exceptionally close fit to the test data was obtained. None of the other model variations were any better than (B3); in every case, the correlation coefficients for I, T, dT^2, and dT^4/I were very small. The best fit equation obtained was:

$$\text{Efficiency} = 73.67 - 0.0239\ (dT) - 18.0952\ (dT/I) - 0.1311\ (dT^2/I) \quad \text{(B4)}$$

With Eq (B4), the deviations from the test data were again cut almost in half. Maximum deviation from test data was 1.9 efficiency percentage points (about 3%). Over most of the range of test data, the error was much less with a standard error of estimate of 0.77 percentage points. Equation (B4) appears to be a good model of the collector performance over the complete range of operational conditions (from 0 to 300°C delta-T, and 0 to 1050 W/m^2 direct solar irradiance).

Table B1 compares the three collector performance models shown in Eqs (B2), (B3), and (B4).

An identical regression analysis was performed on the test data shown in Table 12, obtained from the small diameter absorber. Results of the analysis were similar to those shown in Table B1. Finally, the regression analysis was made for each variation of the collector module, using data calculated with the procedure shown in Appendix C. Table B2 shows some of the results of the multiple regression analysis on all the collector modules. Performance equations from the analysis are shown in Table 14, in the Summary section of this report.

In Table B2, the curve fit for the calculated data is better than that from the test data, because the calculated data is a smooth function, without the random scatter found in the test data.

Table B1. Results of Multiple Regression Analysis Collector Performance Models, FEK-244 Reflector, 4.13-cm Absorber

Model Eq	Independent Variables	Standard Error of Estimate	R^2	Max Deviation From Test Data	Sum of Sq Residuals
(B2)	dT/I, $(dT/I)^2$	2.810	0.965	5.8*	592
(B3)	dT/I, dT^2/I	1.565	0.989	2.7	184
(B4)	dT, dT/I, dT^2/I	0.773	0.997	1.9	44

*Repeating pattern with I at each dT. Units are percentage points.

Table B2. Results of Multiple Regression Analysis for Several T-700A Collector Modules

Collector Module	Standard Error of Estimate	R^2	Max Deviation From Data	Sum of Sq Residuals
Glass, 4.13 cm	0.949	1.000	1.5	97
Glass, 3.18 cm	0.391	1.000	0.6	16
FEK-244, 4.13 cm	0.773	0.997	1.9*	44
FEK-244, 4.13 cm	0.401	1.000	0.6	17
FEK-244, 3.18 cm	0.833	0.998	2.1*	41
FEK-244, 3.18 cm	0.434	1.000	0.7	20
FEK-244, 3.18 cm (quartz)	0.346	1.000	0.5	13

*Actual test data used. All others, calculated.

APPENDIX C

Calculation of Collector Performance From Limited Test Data

As part of the Solar Kinetics T-700A test series, the efficiency was measured with cool water as the heat-transfer fluid. The receiver fluid temperature was maintained as close as possible to the ambient air temperature. Operation at ambient air temperature does not reduce the thermal loss to zero, but the thermal loss should be small enough that the measured efficiency is close to the optical efficiency. Using water rather than oil as the heat-transfer fluid also helps reduce the thermal loss, because the better heat conductivity of water reduces the surface temperature (see Figure 37).

If we know the collector's approximate optical efficiency, then efficiency at any other temperature can be found by subtracting thermal loss at the desired temperature from heat gain as determined at optical efficiency. The difficulty is determination of the actual thermal loss from an operating collector.

Thermal loss tests on the T-700A resulted in four distinct thermal-loss curves (see Figure 38). Attempts were made to calculate the collector's operating efficiency at temperature by using each of the four thermal-loss curves in turn. When efficiency was calculated using any of the four measured thermal-loss curves, the calculated efficiency values were always larger than efficiencies actually measured, indicating that the thermal losses being used were too small. Figure C1 (the two curves are taken from Figure 39) shows that the actual thermal loss occurring when the collector is in focus is larger than indicated by any of the measured loss curves. Accordingly, operating efficiency was calculated using the in-focus loss curve from Figure C1; this gave efficiency values that checked with test data at about 1000 W/m^2 solar irradiance (calculated efficiencies at 970 W/m^2 had to be right because the in-focus thermal loss curve was derived from that particular efficiency curve).

However, when efficiency was calculated for lower values of solar irradiance, efficiency became increasingly too small as the irradiance was reduced, showing that the thermal loss was too large at low values of irradiance. Surface-temperature measurements (Figure 37) also support the idea of a smaller thermal loss at lower values of irradiance. We needed to determine the nature of the transition from a high value of thermal loss on an in-focus collector to the lower loss measured when out of focus.

The in-focus thermal loss curve in Figure C1 was derived from an efficiency curve obtained from tests near 1000 W/m^2. This idea was taken one step further by calculating an in-focus thermal loss curve from each of the efficiency curves in Figure 44, thus giving an in-focus thermal-loss curve for each 100 W/m^2 step of irradiance from 500 to 1000 W/m^2.

When the set of calculated in-focus thermal-loss curves are overplotted on Figure C1, these calculated thermal loss curves fit neatly between the 1000 W/m^2 in-focus thermal-loss curve and the zero irradiance thermal loss-curve. (Zero irradiance thermal loss is represented by the shaded, north-facing measured thermal loss curve.) This set of thermal loss curves is shown in Figure C2. The thermal loss appears to vary in an approximately linear fashion, increasing as the input solar irradiance increases, so that the 500 W/m^2 curve falls just about half-way between the zero insolation curve and the 1000 W/m^2 curve.

It is not surprising that thermal loss should vary directly with the level of solar irradiance, since thermal loss depends on surface temperatures rather than on absorber fluid temperature. Other tests have shown that absorber surface temperatures are appreciably higher than fluid temperature, and also change with fluid-flow rate and level of solar irradiance (see Figures 36 and 37). Figures 36 and 37 also show that the surface temperature change is linear with changing solar irradiance. A linear variation of surface temperature does not necessarily mean that changes in thermal loss will be linear also, but it may be close enough for practical use.

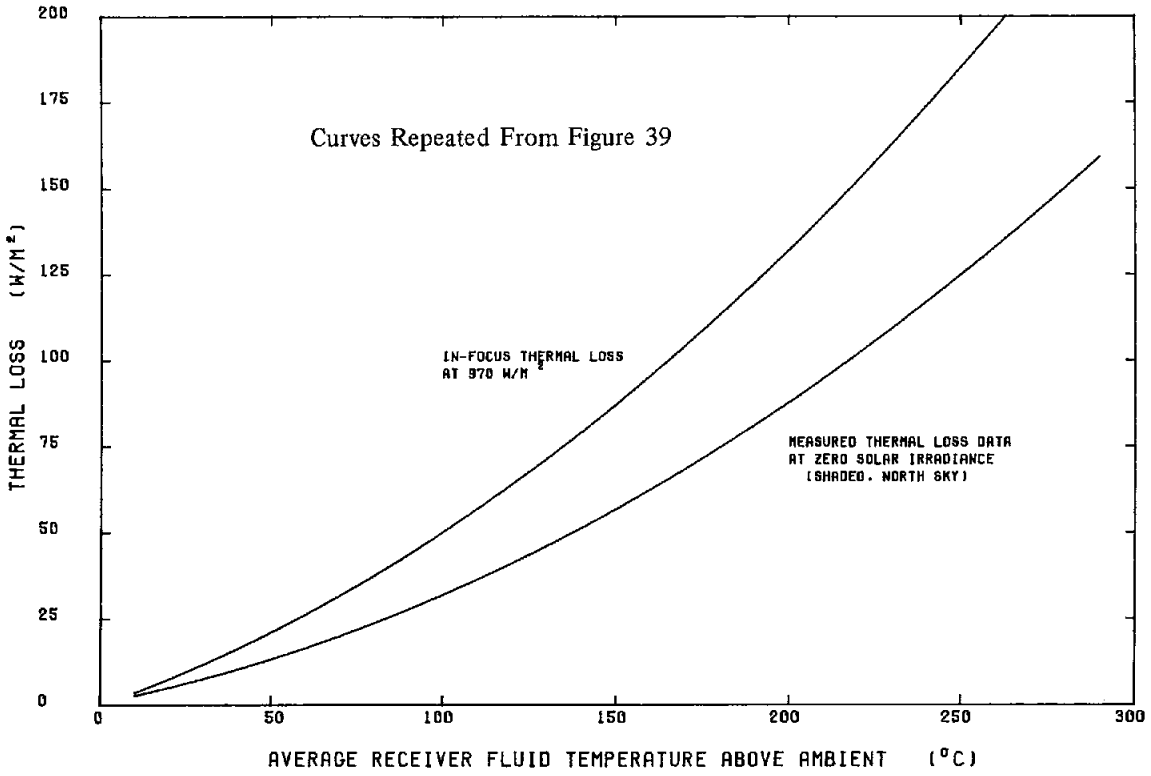

Figure C1. Receiver Thermal Loss In-Focus and Out-of-Focus

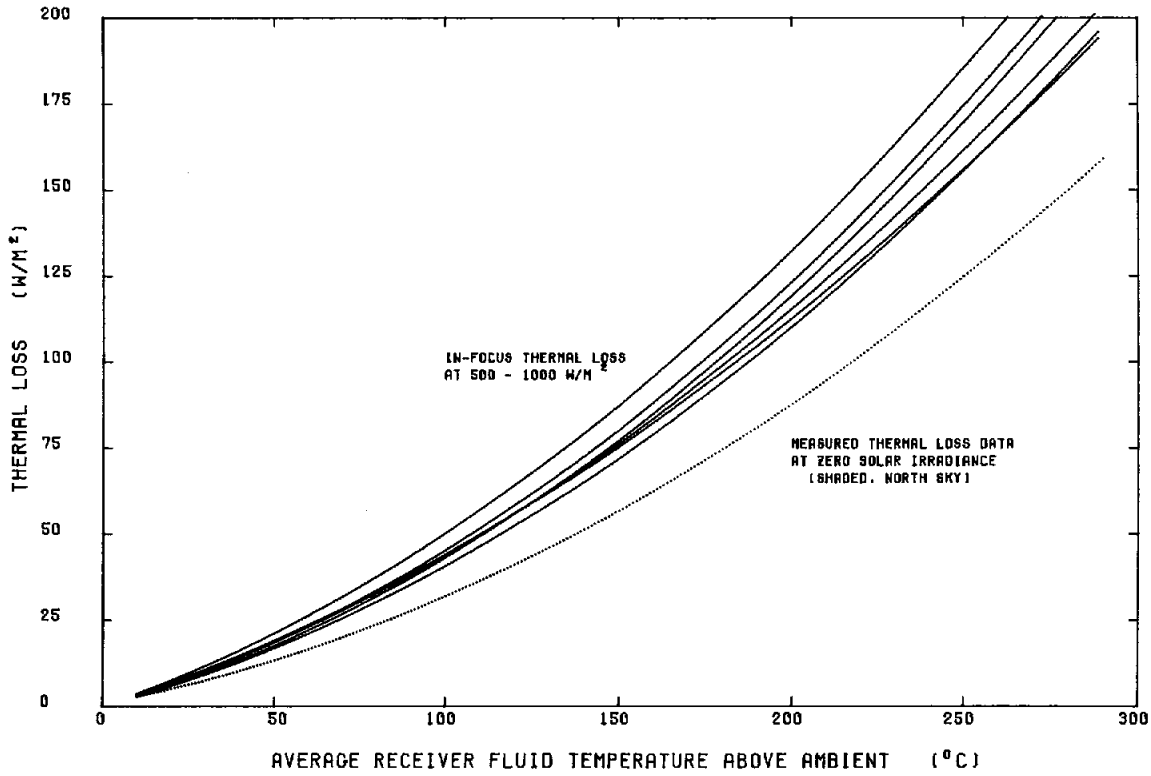

Figure C2. Family of In-Focus Receiver Thermal Loss Curves

If in-focus thermal loss varies approximately linearly with changes in solar irradiance, then thermal loss for any irradiance can be obtained by scaling between only two loss curves, one derived from efficiency testing at a constant high level of irradiance such as 1000 W/m^2 and a measured thermal loss curve obtained at an effective zero irradiance. Determination of thermal loss could be done by scaling graphically between the 0 and 970 W/m^2 curves in Figure C1, but it is more convenient to calculate the thermal loss using the equations of the two loss curves, repeated here from Table 7.

$$\text{Loss at } 970 \text{ W/m}^2 = 0 + 0.343001\ (dT) + 0.001588\ (dT^2) \quad \text{(C1)}$$

$$\text{Loss at } 0 \text{ W/m}^2 = 0 + 0.189190\ (dT) + 0.001231\ (dT^2) \quad \text{(C1)}$$

The thermal loss at any irradiance I can be expressed:

$$L_I = L_o + (L_{test} - L_o)\ I/I_{test} \quad \text{(C3)}$$

where:

L_I = thermal loss, in-focus at irradiance I
L_o = thermal loss at zero irradiance
L_{test} = thermal loss, in-focus at irradiance existing during reference efficiency test
I = irradiance at which performance is to be calculated.

We can also easily calculate the heat gain available at any desired level or irradiance when the collector is operating at optical efficiency (η_o). It is simply:

$$Q_I = \eta_o\, I \quad \text{(C4)}$$

For the purposes of this calculation, the efficiency measured at ambient air temperature with cool water is assumed equal to the optical efficiency. This is not true, because the receiver-surface temperatures are higher than the fluid temperatures, and the thermal losses are not zero. The resulting error is estimated to be small (5% or less).

If the in-focus thermal loss, determined from Eq (C3), is subtracted from the heat gain determined from Eq (C4), the result will be a net heat gain for that set of operating conditions. The net heat gain divided by the input irradiance is the required efficiency value.

$$\eta = \frac{Q_I - L_I}{I} \quad \text{(C5)}$$

where

η = collector efficiency at irradiance I
Q_I = heat gain at optical efficiency, irradiance I
L_I = thermal loss at irradiance I
I = irradiance at which performance is desired.

Figure C3 shows the results of a set of calculations using the three equations above to determine the efficiency of the T-700A collector at input solar-radiation levels from 400 to 1000 W/m^2. If the calculated performance curves in Figure C3 are overlaid on the measured performance curves in Figure 44, the maximum difference is found to be about 1.5 efficiency percentage points at the higher temperatures ($\sim$ 3% error).

The calculations used to produce data for Figure C3 can also be used to provide a set of data for input to a multiple linear-regression computer program. For this purpose, Eqs (C3), (C4), and (C5) were used to generate an array containing 112 sets of data, with delta-T at 50°C intervals from 0 to 350°C, and with irradiance at 100 W/m^2 intervals from 0 to 1100 W/m^2 at each temperature. A multiple linear-regression analysis provided a curve fit to the data. The equation obtained from the calculated data was

$$\text{Efficiency} = 73.58 - 0.0278\ (dT) - 18.851\ (dT/I) - 0.1233\ (dT^2/I) \quad \text{(C6)}$$

Equation (C6) is almost identical to the equation obtained earlier from the actual test data in Table 9 (shown previously as Eq (6)):

$$\text{Efficiency} = 73.67 - 0.0239\ (dT) - 18.095\ (dT/I) - 0.1311\ (dT^2/I) \quad \text{(C7)}$$

Over a collector operating range of temperatures from 50° to 300°C and with an irradiance from 300 to 1000 W/m^2, the maximum difference between Eq (C7) (test data) and (C6) (calculated data) is 0.8 efficiency percentage points (less than 2%). When Eq (C6) is plotted as a 3-D graph (see Figure 60), there is no visible difference between the plot and that plotted earlier from the actual test data (Eq (C7), Figure 45).

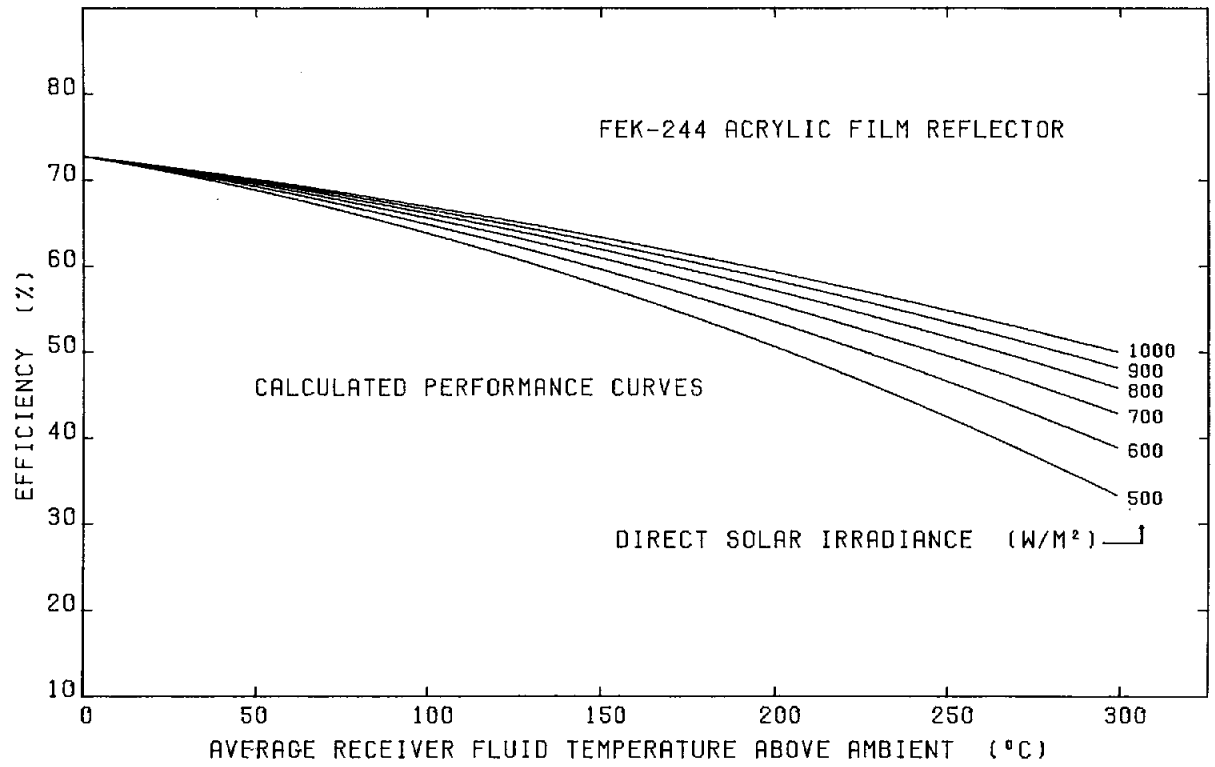

Figure C3. Solar Kinetics T-700A Efficiency vs Temperature and Irradiance

The set of calculations outlined above, using Eqs (C3), (C4), and (C5), was made for all the variations of the T-700A collector module; a multiple-regression analysis was made for each (see Appendix B). The complete set of performance equations from the regression analysis is given in Table 14 in the Summary section of this report.

A comparison was also made between the performance equation obtained from the test data for the small absorber and the equation obtained from the calculations for the same module. The equation from test data was

$$E\ (\text{test}) = 66.12 - 0.0142\ (dT) - 2.5009\ (dT/I) - 0.0646\ (dT^2/I) \qquad (C8)$$

The corresponding equation from calculations is:

$$E\ (\text{calc}) = 67.21 - 0.0119\ (dT) - 2.4867\ (dT/I) - 0.0664\ (dT^2/I) \qquad (C9)$$

Over the collector operating range of temperatures from 50° to 350°C and with an irradiance from 300 to 1000 W/m^2, the maximum difference between Eqs (C8) and (C9) is 1.7 efficiency percentage points (~3%).

Thus, the approximate collector performance can be calculated for any solar irradiance and at any temperature within the operating range by using only three sets of measured data:

1. A thermal loss curve, measured under out-of-focus conditions, at zero solar-irradiance incident on the absorber.
2. An efficiency curve obtained at a high-level, constant solar irradiance. This curve is used to determine the in-focus thermal loss at that particular value of solar irradiance.
3. A near-ambient air-temperature efficiency measurement to approximate the collector's optical efficiency. We have not found any other satisfactory way to approximate the optical efficiency from data taken at elevated temperature.

Data Analysis Computer Programs

Most large computer systems have sophisticated statistical-analysis packages available that can reproduce the equations derived from the test data in this report. In the interest of simplifying the data analysis for collector manufacturers and others without access to large computers, a statistical-analysis package called MICROSTAT (Reference 7) was obtained and used for this report. The MICROSTAT package includes all the statistical-analysis routines that would be needed for most tasks, including a data management system and a stepwise, multiple linear-regression program. The scatterplot of standardized residuals from a curve fit is highly useful for experimental work.

The MICROSTAT version used was configured for the North Star microcomputer, an 8-bit, Z-80 based machine. Only 32K of memory space and a single 5-in-floppy disc were needed, even though some of the data files generated and analyzed contained more than 600 items of data. There are other statistics packages available and many other small computers from a number of manufacturers. Most of the other available microcomputers and software packages are capable of reproducing the data collection and data analysis found in this report.

Data generation and analysis (as used in this appendix) is easy to automate on any microcomputer. For this report, a simple, short BASIC program was written to derive data for the in-focus thermal loss curves and to generate the calculated data files from Eqs (C3) through (C5). Multiple regression analysis of these data files produced the collector performance equations such as (C6).

The programs used to generate the data files can be easily duplicated by others; however, copies of the BASIC program can be made available to those interested. Contact the authors of MICROSTAT or other software houses for further information on data analysis software.

APPENDIX D

Estimates of Annual Thermal Performance

Introduction

During the last year, Sandia National Laboratories, Albuquerque has issued reports predicting the annual thermal performance of 14 different solar collectors. All these collectors were commercially available, concentrating solar collectors that have potential for use in industrial-process heat or similar applications. The formal program sponsoring the collector tests and associated performance reports was concluded prior to the completion of tests on the Solar Kinetics T-700A collector; therefore, calculations for the T-700A are being included in this report rather than as a separate report. Calculations were made for only one version of the collector: FEK-244 acrylic-film reflector with 4.13-cm-dia absorber.

A more detailed account of the methods used to make the predictions is given in Reference 6. The program is limited to thermal performance only and does not include consideration of other factors, such as:

1. Losses at the ends, at gaps, and from shadowing caused by collector field packing
2. Collector warm-up penalties
3. Degradation of performance
4. Cost of the collector
5. Losses in the energy-transport system and system warm-up penalties
6. Reliability
7. Cost of installation
8. Cost of operation and maintenance
9. Wind effects

Collector Operating Parameters

Physical parameters of the T-700A collector are given in Appendix A of this report. Initial calculations of T-700A performance were made in the same way as for all the previous collectors. These calculations were made as outlined in Reference 6, using the following three parameters, as defined by the tests covered earlier in this report. Results of this set of calculations are labeled CASE 1.

1. Peak efficiency—the efficiency of the collector when the sun's rays are at normal incidence to the aperture plane (equivalent to solar noon), expressed as a function of delta-T/I. Delta-T is defined as the temperature difference (°C) between the average heat-transfer fluid temperature and the ambient air temperature. I is the direct normal irradiance of the sun (watts/square meter). An equation and curve for the peak efficiency was shown earlier in Figure 23:

$$\text{Efficiency } (\%) = 72.8 - 49.8\ (dT/I) - 88.1\ (dT/I)^2 \qquad (D1)$$

2. Receiver thermal loss—the heat lost per unit aperture area, expressed as a function of delta-T. The shaded, north-facing thermal loss curve from Table 7 was used:

$$\text{Thermal Loss } (W/m^2) = 0 + 0.1891\ (dT) + 0.001231\ (dT)^2 \qquad (D2)$$

3. Optical loss coefficient (K_o)—K_o, in conjunction with the end-loss coefficient (K_E) and the "cosine effect," determine the incident angle modifier, K. Specifically, $K = K_o K_E \cos \phi$ (see Reference 1). Incident angle-modifier data for the T-700A is shown in Figure 32.

Annual thermal performance estimates resulting from use of the three parameters (above) were expected to be in error, since changes in collector efficiency with changing solar irradiance was not considered. A second calculation of annual thermal performance was made, using

$$E = 73.6766 - 0.0239\ (dT) - 18.0952\ (dT/I) - 0.1311\ (dT^2/I) \qquad (D3)$$

Equation (D3) was derived from actual test data, and was shown earlier in this report as Eqs (6), (C7), and (B4). The incident-angle modifier used was the same as in the first set of calculations. Results of the second set of calculations are labeled CASE 2.

Prediction of Thermal Performance

The performance parameters defined above were the input data describing the collector response; solar irradiance and other weather data were provided by Typical Meteorological Year (TMY) data tapes. TMY gives average weather and solar data for each hour of the day. From these inputs, a computer program calculated the thermal output of the collector for each month of the TMY in units of kilowatt-hours per square meter (kWh/m^2) of collector area. The calculation was made for five locations: Fresno, California; Albuquerque, New Mexico; Fort Worth, Texas; Charleston, South Carolina; and Boston, Massachusetts. Calculations were made for three different collector output temperatures and for both E-W and N-S collector axis orientations. The entire set of calculations was done twice; once for each of the two sets of collector performance parameters.

Figures D1 through D5 are graphical displays of computer prediction results of thermal output, using a single delta-T/I efficiency equation and a single thermal-loss equation (designated CASE 1, no correction for variable efficiency and thermal loss with irradiance). The figures show the monthly thermal output for each location, output temperature, and collector orientation. The monthly thermal outputs were summed to give an annual output for each parameter variation; a summary of the predicted annual thermal output is given in Table D1. All the thermal output estimates assume one square meter of collector aperture in the middle of a collector row of infinite length, with no end or gap losses and no shadowing caused by collector field packaging.

The information in Figures D1 through D5 and Table D1 is equivalent to the estimates previously published for other solar collectors.

Figures D6 through D10 show the results of the same calculations when collector efficiency and thermal loss are allowed to change with solar irradiance (designated CASE 2), using Eq (D3); both delta-T and solar irradiance are independent variables. A summary of the predicted annual thermal output is given in Table D2.

Comparison of Results

Table D3 shows a comparison of the two methods of calculating the collector thermal output. Calculating annual thermal output using a single equation of efficiency vs delta-T/I causes significant errors, because the delta-T/I equation is valid only at a single value of solar irradiance—that which existed when the efficiency data was measured. Graphic illustrations of the error that can result from using a delta-T/I equation at other than the original irradiance are shown in Figures 53 and B1.

Table D1. CASE 1 Predicted Annual Thermal Output ($kWh/m^2 \cdot yr$) (Using Single Loss and Efficiency Equations)

City	Solar Energy Available	Output Temperature 100°C Orientation		200°C Orientation		300°C Orientation	
		E-W	N-S	E-W	N-S	E-W	N-S
Fresno	2260	1094	1283	905	1034	686	759
Albuquerque	2583	1268	1437	1074	1190	848	914
Fort Worth	1733	848	958	682	750	445	526
Charleston	1350	654	706	494	518	328	331
Boston	1172	542	573	402	409	257	252

Table D2. CASE 2 Predicted Annual Thermal Output ($kWh/m^2 \cdot yr$) (Using Variable Loss and Efficiency Equations)

City	Solar Energy Available	Output Temperature 100°C Orientation		200°C Orientation		300°C Orientation	
		E-W	N-S	E-W	N-S	E-W	N-S
Fresno	2260	1142	1354	980	1146	765	876
Albuquerque	2583	1316	1505	1138	1287	905	1004
Fort Worth	1733	894	1019	756	851	576	634
Charleston	1350	704	770	578	623	418	440
Boston	1172	591	635	478	504	338	346

Table D3. Comparison of CASE 1 and CASE 2 (E-W axis)

City	CASE 1 ($kWh/m^2 \cdot yr$)	CASE 2 ($kWh/m^2 \cdot yr$)	Delta ($kWh/m^2 \cdot yr$)	CASE 2 > CASE 1 (%)
		300°C Output Temperature		
Albuquerque	848	905	57	6.7
Fresno	686	765	79	11.5
Fort Worth	495	576	81	16.4
Charleston	328	418	90	27.4
Boston	257	338	81	31.5
		200°C Output Temperature		
Albuquerque	1074	1138	64	5.6
Fresno	905	980	75	8.3
Fort Worth	682	756	74	10.9
Charleston	494	578	84	17.0
Boston	402	478	76	18.9
		100°C Output Temperature		
Albuquerque	1268	1316	48	3.8
Fresno	1094	1142	48	4.4
Fort Worth	848	894	46	5.4
Charleston	654	704	50	7.6
Boston	542	591	49	9.0

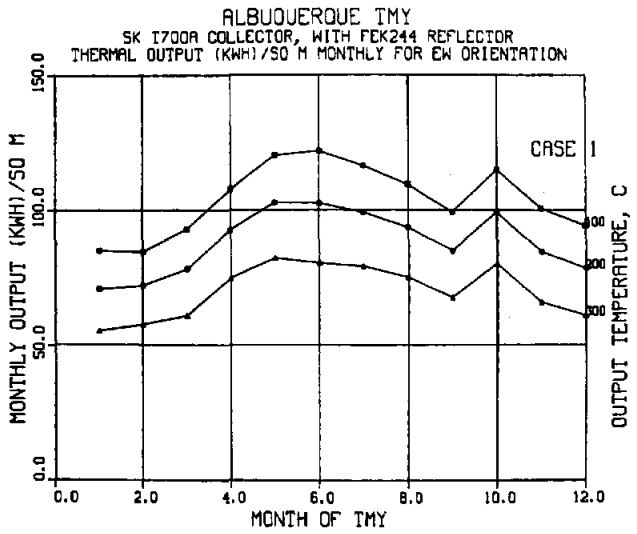

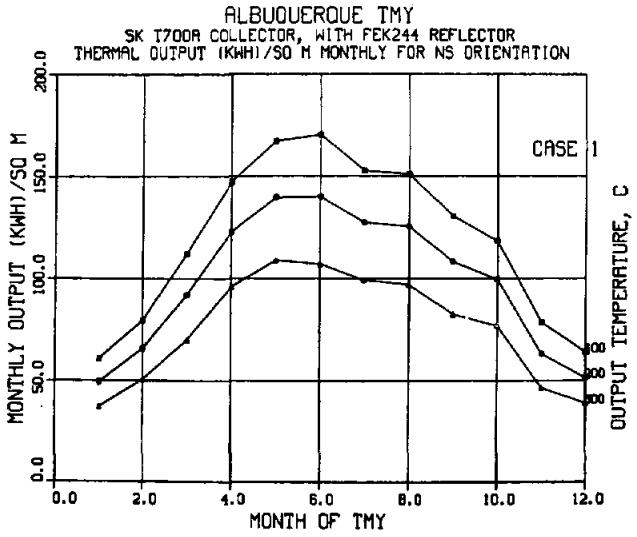

Figure D1. Annual Thermal Output for Albuquerque (CASE 1)

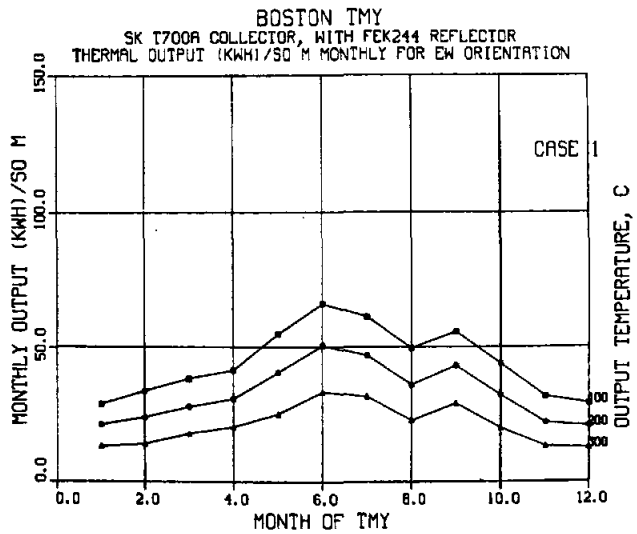

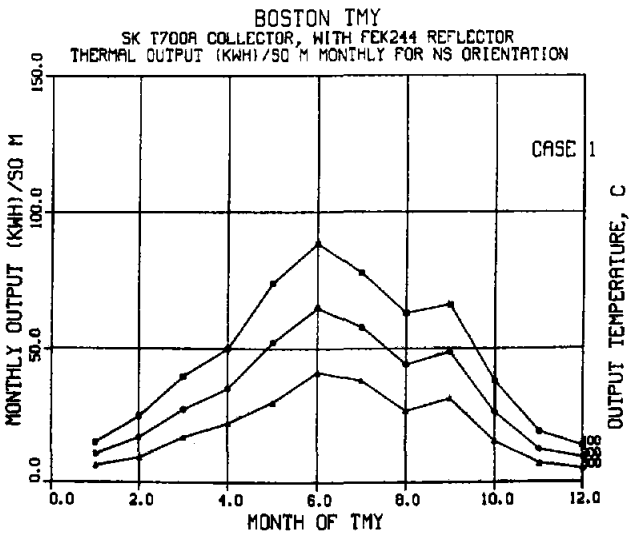

Figure D2. Annual Thermal Output for Boston (CASE 1)

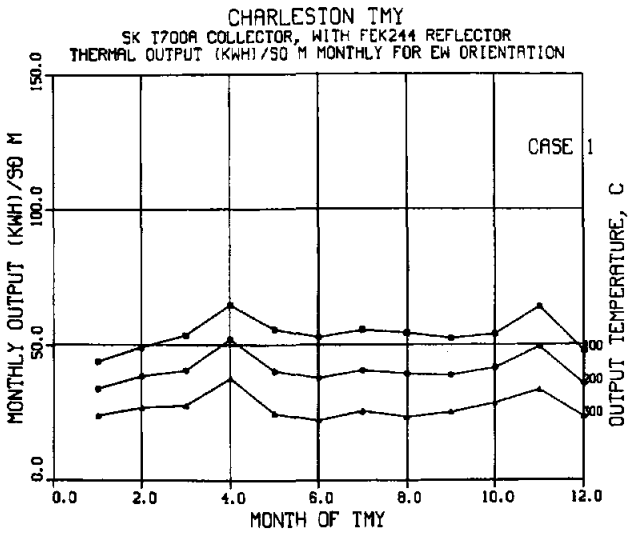

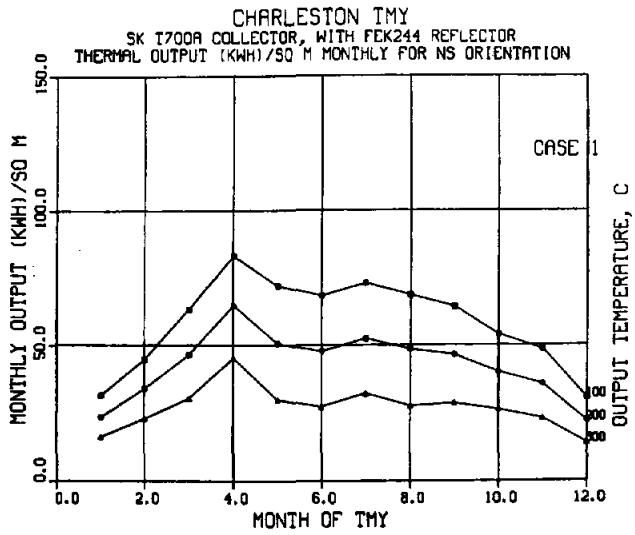

Figure D3. Annual Thermal Output for Charleston (CASE 1)

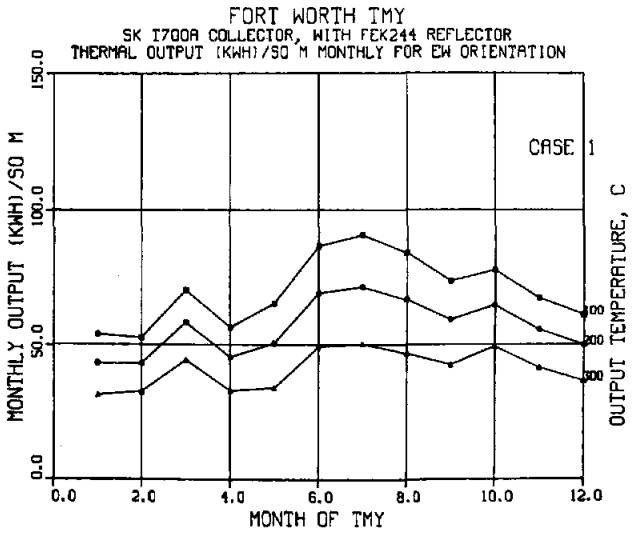

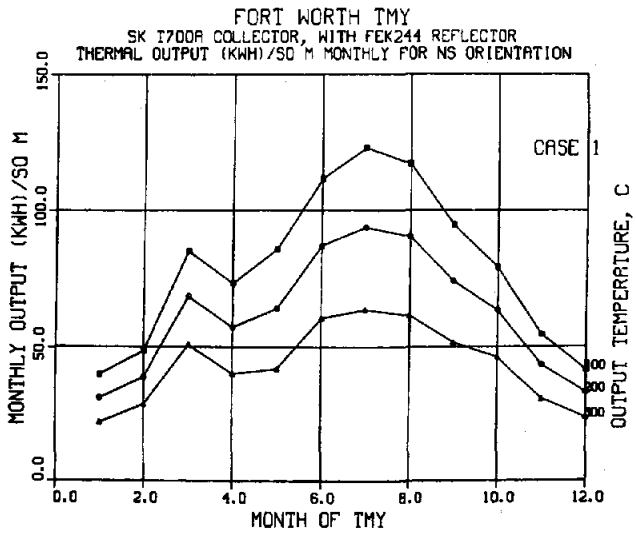

Figure D4. Annual Thermal Output for Fort Worth (CASE 1)

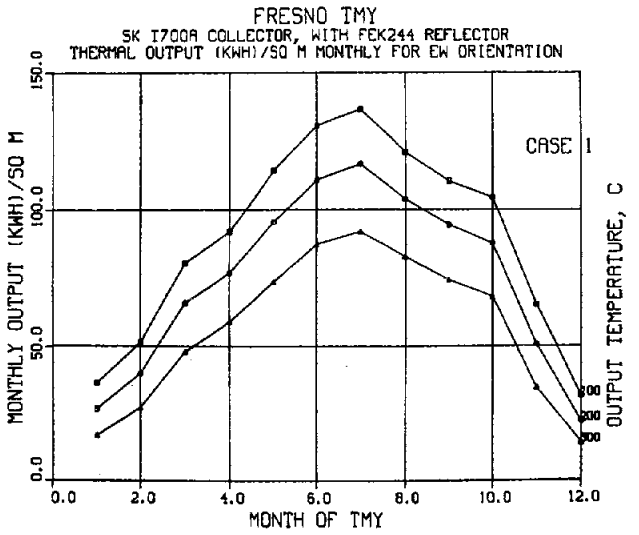

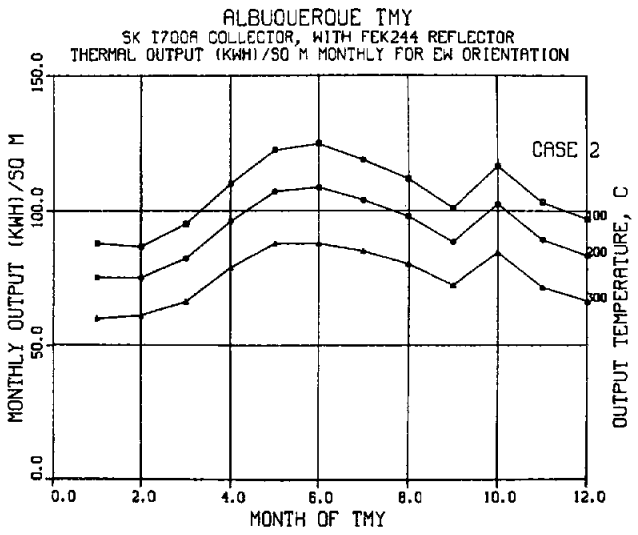

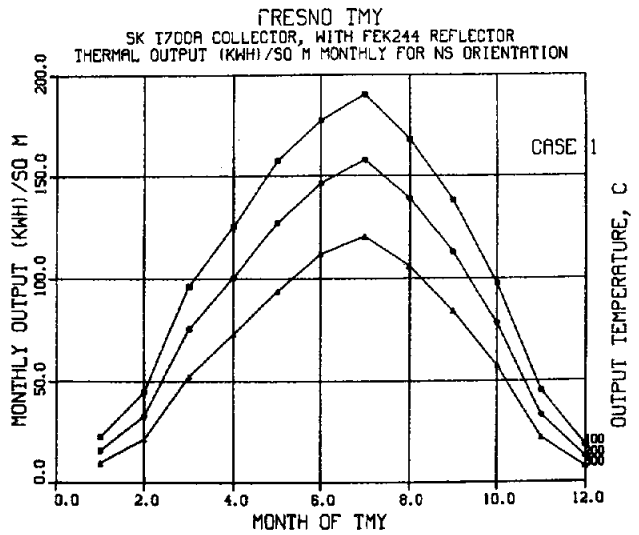

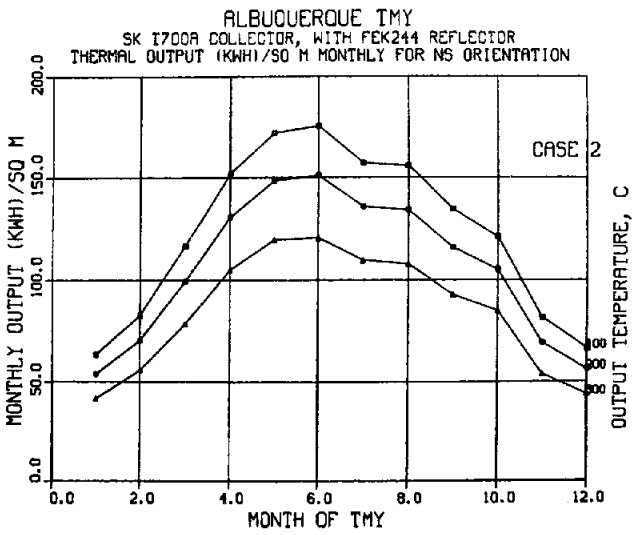

Figure D5. Annual Thermal Output for Fresno (CASE 1)

Figure D6. Annual Thermal Output for Albuquerque (CASE 2)

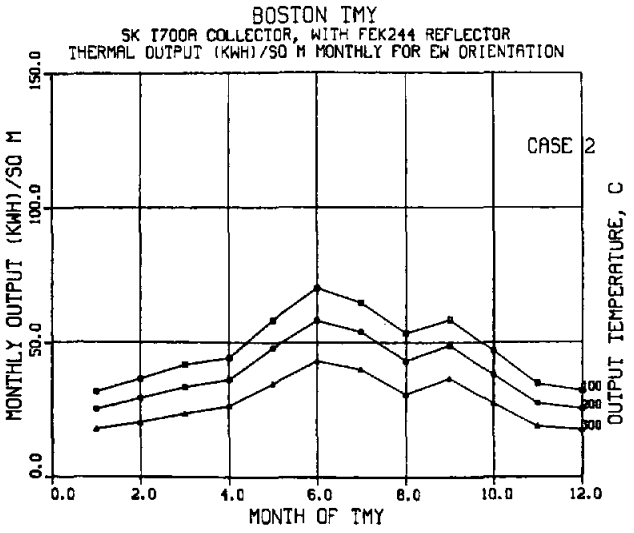

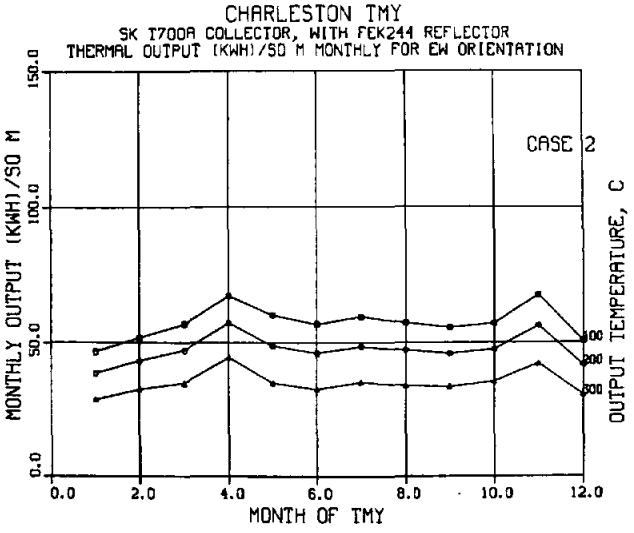

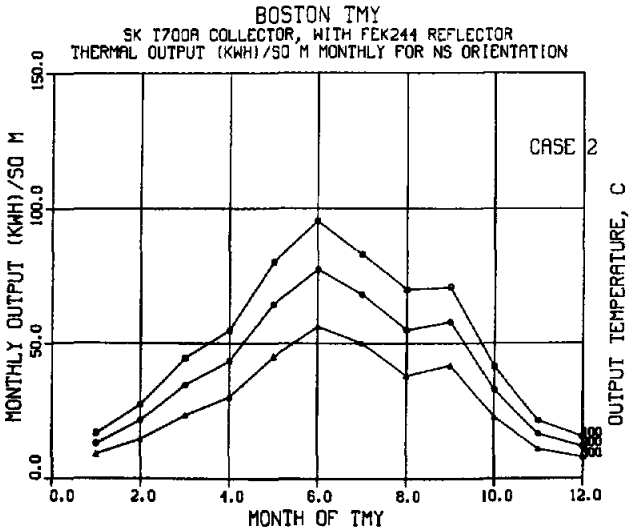

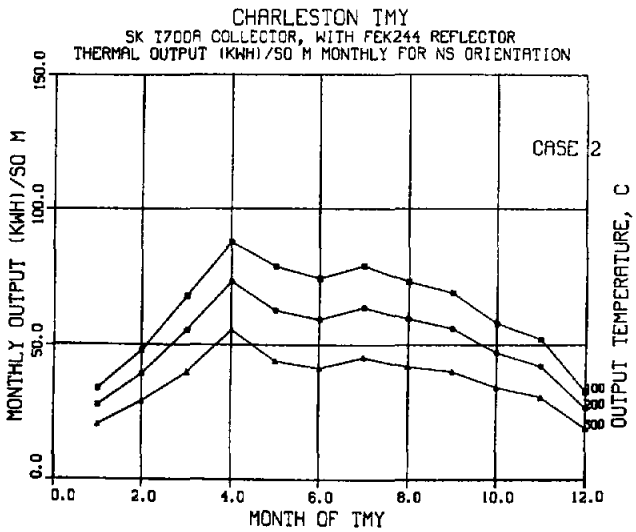

Figure D7. Annual Thermal Output for Boston (CASE 2)

Figure D8. Annual Thermal Output for Charleston (CASE 2)

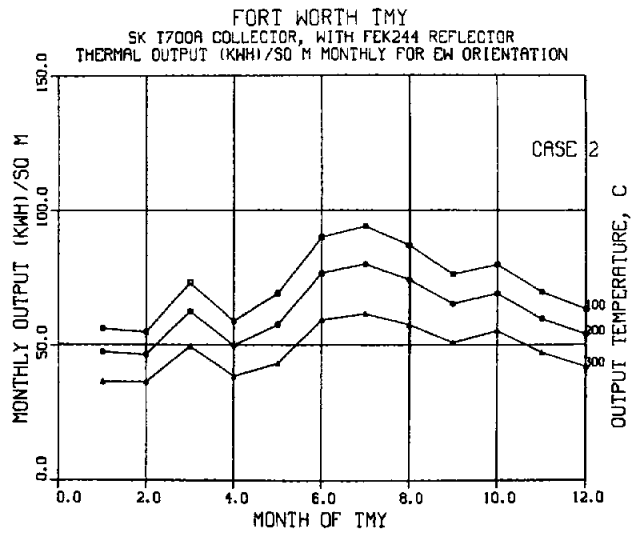

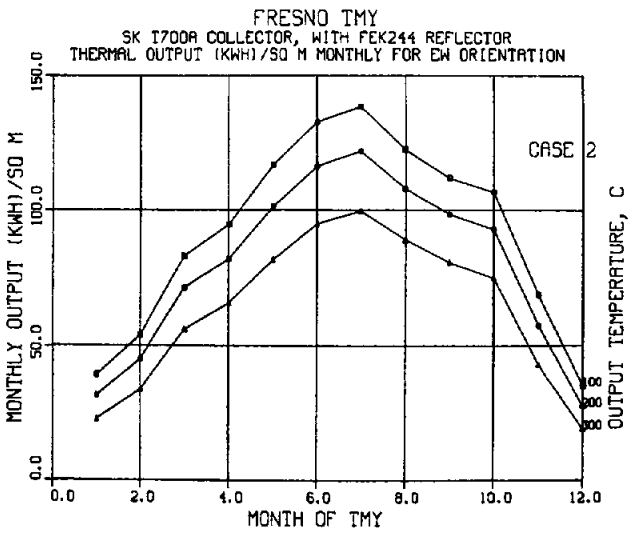

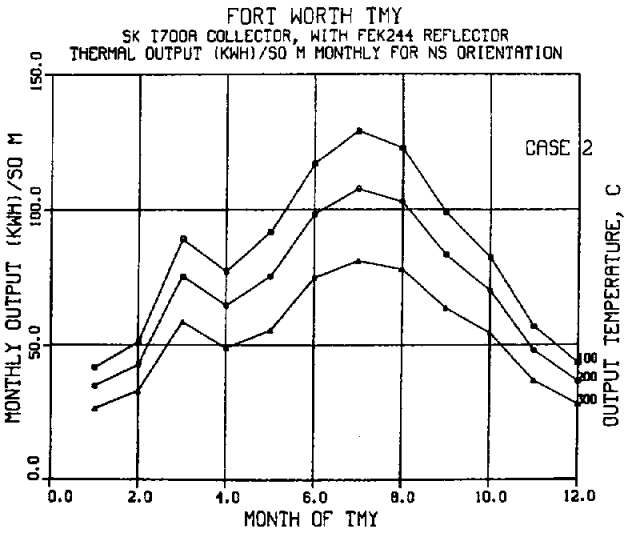

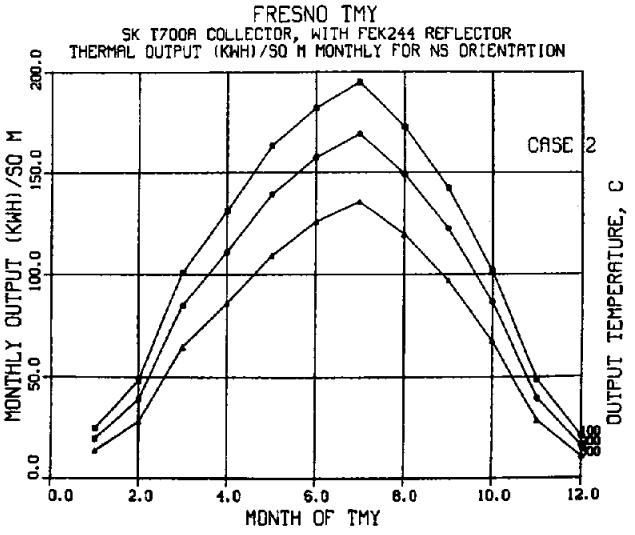

Figure D9. Annual Thermal Output for Fort Worth (CASE 2)

Figure D10. Annual Thermal Output for Fresno (CASE 2)

References

[1]*Solar Total Energy Program Plan,* SAND76-0167 (revised) (Albuquerque, NM: Sandia Laboratories, August 1976).

[2]*Thermal 66 Technical Data Sheet,* IC FP-64, (St. Louis, MO: Monsanto Industrial Chemicals Co., Inc.).

[3]*Technical Data Sheet, Q2-1162 Heat Transfer Liquid (Syltherm 800),* (Midland, Michigan: Dow Corning Corp).

[4]T. D. Harrison, *Midtemperature Solar Systems Test Facility Prediction for Thermal Performance Based on Test Data: Solar Kinetics T-700 Solar Collector With Glass Reflector Surface,* SAND80-1964/7 (Albuquerque, NM: Sandia National Laboratories, March 1981).

[5]T. D. Harrison, *Midtemperature Solar Systems Test Facility Predictions for Thermal Performance Based on Test Data: Solar Kinetics T-700 Solar Collector with FEK-244 Reflector Surface,* SAND80-1964/1, (Albuquerque, NM: Sandia National Laboratories, November 1980).

[6]T. D. Harrison, *Midtemperature Solar Systems Test Facility Program for Predicting Thermal Performance of Line-Focusing Concentrating Solar Collectors,* SAND80-1964 (Albuquerque, NM: Sandia National Laboratories, November 1980).

[7]MICROSTAT—A statistical analysis package for Northstar microcomputer, Ecosoft, Inc., P. O. Box 68602, Indianapolis, Indiana 46268.

[8]L. L. Lukens, *Experimental Parabolic Trough Collector Performance Characterization,* SAND 81-0313, (Albuquerque, NM: Sandia National Laboratories) May 1981.

DISTRIBUTION:

TIC-4500-R70 UC–62a (231)

AAI Corporation
PO Box 6787
Baltimore, MD 21204

Acurex Solar Corporation
485 Clyde Avenue
Mountain View, CA 94042
Attn: J. Vindum

Advanco Corporation
999 N. Sepulveda Boulevard
Suite 314
El Segundo, CA 90245

Alpha Solarco
1014 Vine Street, Suite 2230
Cincinnati, OH 45202

Anaconda Metal Hose Co.
689 South Main Street
Waterbury, CT 06720
Attn: W. Genshino

Applied Concepts Corp.
PO Box 2760
Reston, VA 22090
Attn: J. S. Hauger

Applied Solar Resources
490 East Pima
Phoenix, AZ 85004
Attn: W. H. Coady

Arizona Public Service Co.
Box 21666, MS 1795
Phoenix, AZ 85036
Attn: B. L. Broussard

BDM Corporation
1801 Randolf Street
Albuquerque, NM 87106
Attn: T. Reynolds

Battelle Memorial Institute
Pacific Northwest Laboratory
PO Box 999
Richland, WA 99352
Attn: K. Drumheller

Bechtel National, Inc.
PO Box 3965
50 Beale Street
San Franscisco, CA 94119
Attn: E. Y. Lam

Black and Veatch (2)
PO Box 8405
Kansas City, MO 64114
Attn: J. C. Grosskreutz
D. C. Gray

Bloomer-Fiske, Inc.
4000 S. Princeton
Chicago, IL 60609
Attn: C. Cain

Budd Company (The)
Fort Washington, PA 19034
Attn: W. W. Dickhart

Budd Company
Plastic R&D Center
356 Executive Drive
Troy, MI 48084
Attn: J. N. Epel

Burns & Roe (2)
185 Crossways Park Drive
Woodbury, NY 11797
Attn: R. J. Vondrasket
J. Wysocki

Burns & ROE, Inc.
800 Kinderkamack Road
Oradell, NJ 07649
Attn: G. Fontana

Burns & Roe (2)
185 Crossways Park Dr.
Woodbury, NY 11797
Attn: R. J. Vondrasket
J. Wysocki

Carrier Corp.
Energy Systems Division
Summit Landing
PO Box 4895
Syracuse, NY 13221
Attn: R. A. English

DISTRIBUTION (cont):

Corning Glass Company (2)
Corning, NY 14830
Attn: A. F. Shoemaker
W. Baldwin

Custom Engineering, Inc.
2805 South Tejon Street
Englewood, CO 80110

DSET
Black Canyon Stage
PO Box 185
Phoenix, AZ 85029
Attn: G. A. Zerlaut

Desert Research Insititute
Energy Systems Laboratory
1500 Buchanan Boulevard
Boulder City, NV 89005
Attn: J. O. Bradley

Donnelly Mirrors, Inc.
49 West Third Street
Holland, MI 494233
Attn: J. A. Kinster

Eaton Corporation
Industrial Drives Operations
Cleveland Division
3249 East 80 Street
Cleveland, OH 44104
Attn: R. Glatt

Electric Power Research Institute (2)
3412 Hillview Avenue
Palo Alto, CA 94303
Attn: J. Cummings
J. E. Bigger

Energetics
833 E. Arapahoe Street
Suite 202
Richardson, TX 85081
Attn: G. Bond

Energy Technology Engineering Center
PO Box 1449
Canoga Park, CA 91304
Attn: J. Roberts

E-Systems, Inc.
Energy Tech. Center
PO Box 226118
Dallas, TX 75266
Attn: R. R. Walters

Eurodrive, Inc.
2001 W. Main Street
Troy, OH 45373
Attn: S. D. Warner

Exxon Enterprises (3)
PO Box 592
Florham Park, NJ 07923
Attn: J. Hamilton
P. Joy
M. C. Noland

Florida Solar Energy Center (2)
300 State Road, Suite 401
Cape Canaveral, FL 32920
Attn: C. Beech
D. Block

Ford Motor Company
Glass Division, Technical Center
25500 West Outer Drive
Lincoln Park, MI 48246
Attn: V. L. Lindberg

Foster Wheeler Solar Develop. Center
12 Peach Tree Hill Road
Livingston, NJ 07039
Attn: A. C. Gangadharan

General Motors
Harrison Radiator Division
Lockport, NY 14094
Attn: L. Brock

Georgia Power Company (2)
270 Peachtree
PO Box 4545
Atlanta, GA 30302
Attn: J. Roberts
W. Davis

Glitsch, Inc.
PO Box 226227
Dallas, TX 75266
Attn: R. W. McClain

DISTRIBUTION (cont):

Haveg Industries, Inc.
1287 E. Imperial Highway
Santa Fe Spings, CA 90670
Attn: J. Flynt

Highland Plating
1128 N. Highland
Los Angeles, CA 90038
Attn: M. Faeth

Honeywell, Inc.
Energy Resources Center
2600 Ridgeway Parkway
Minneapolis, MN 55413
Attn: J. R. Williams

Insights West
900 Wilshire Boulevard
Los Angeles, CA 90017
Attn: J. H. Williams

Jacobs Engineering Co.
251 South Lake Avenue
Pasadena, CA 91101
Attn: H. Cruse

Jet Propulsion Laboratory (3)
4800 Oak Grove Drive
Pasadena, CA 91103
Attn: J. Becker
J. Lucas
V. C. Truscello

Lawrence Livermore Laboratory
University of California
PO Box 808
Livermore, CA 94500
Attn: W. C. Dickinson

Los Alamos National Laboratory
Los Alamos, NM 87545
Attn: C. D. Bankston

McDonnel-Douglas Astronautics (3)
5301 Bolsa Avenue
Huntington Beach, CA 92647
Attn: J. B. Blackmon
J. Rogan
D. Steinmeyer

Meridan Corporation (2)
5201 Leesburg Pike
Suite 400
Fall Church, VA 22041
Attn: J. White
J. Meglen

Morse Chain
Division of Borg-Warner Corporation
4650 Steele Street
Denver, CO 80211
Attn: F. Fukayama

New Mexico State University
Solar Energy Department
Las Cruces, NM 88001

Omnium G
1815 Orangethrope Park
Anaheim, CA 92801
Attn: S. P. Lazzara

Owens-Illinois
1020 N. Westwood
Toledo, OH 43614
Attn: Y. K. Pei

PPG Industries, Inc.
One Gateway Center
Pittsburg, PA 15222
Attn: C. R. Frownfelter

Parsons of California
3437 S. Airport Way
Stockton, CA 95206
Attn: D. R. Biddle

DISTRIBUTION (cont):

Schott America
11 East 26th Street
New York, NY 10010
Attn: J. Schrauth

Shelltech Associates
809 Tolman Drive
Stanford, CA 94305
Attn: C. R. Steele

Solar Energy Information Center
1536 Cole Boulevard
Gold, CO 80401
Attn: R. Ortiz

Solar Energy Research Institute (8)
1617 Cole Blvd
Golden, CO 80401
Attn: B. L. Butler
G. Gross
B. P. Gupta
J. Thornton
Library (4)

Solar Kinetics, Inc.
PO Box 47045
Dallas, TX 75247
Attn: G. Hutchison

Southwest Research Institute
PO. Box 28510
San Antonio, TX 78284
Attn: D. M. Deffenbaugh

Stanford Research Institute
Menlo Park, CA 94025
Attn: A. J. Slemmons

Stearns-Rogers
4500 Cherry Creek
Denver, CO 80217
Attn: W. R. Lang

W. B. Stine
1230 Grace Drive
Pasadena, CA 91105

Sun Gas Company
Suite 800, 2 N. Park E.
Dallas, TX 75231
Attn: R. C. Clark

Sundstrand Electric Power
4747 Harrison Avenue
Rockford, IL 61101
Attn: A. W. Adam

Sunpower Systems, Inc.
510 South 52 Street
Tempe, AZ 85281
Attn: W. Matlock

Suntec Systems, Inc.
2101 Wooddale Drive
St. Paul, MN 55110
Attn: J. Davison

Swedlow, Inc. (2)
12122 Western Avenue
Garden Grove, CA 92645
Attn: E. Nixon
J. M. Friedfeld

TRW, Inc.
Energy Systems Group of TRW, Inc.
One Space Park, Bldg. R4, Room 2074
Redondo Beach, CA 90278
Attn: J. M. Cherne

Texas Tech University
Dept. of Electrical Engineering
PO Box 4709
Lubbock, TX 79409
Attn: J. D. Reichert

3M-Decorative Products Division
209-2N 3M Center
St. Paul, MN 55101
Attn: B. Benson

3M-Product Development
Energy Control Products
207-1W 3M Center
St. Paul, MN 55101
Attn: J. R. Roche

DISTRIBUTION (cont):

Toltec Industries, Inc.
40th and East Main
Clear Lake, IA 50428
Attn: D. Chenault

US Department of Energy (3)
Albuquerque Operations Office
PO Box 5400
Albuquerque, NM 87185
Attn: G. N. Pappas
C. B. Quinn
J. Weisiger

US Department of Energy
Division of Energy Storage Systems
Washington, DC 20545
Attn: J. Gahimer

US Department of Energy (7)
Division of Solar Thermal Energy Systems
Washington, DC 20585
Attn: W. W. Auer
G. W. Braun
J. E. Greyerbiehl
M. U. Gutshtein
B. Hockheiser
J. F. Rannels
F. Wilkins

US Department of Energy (2)
San Franscisco Operations Office
1333 Broadway, Wells Fargo Bldg
Oakland, CA 94612
Attn: R. W. Hughey

University of New Mexico (2)
Department of Mechanical Engineering
Albuquerque, NM 87113
Attn: M. W. Wilden
W. A. Cross

Viking
3467 Ocean View Blvd
Glendale, CA 91208
Attn: G. Goranson

Winsmith
Division of UMC Industries, Inc.
Springville, NY 14141
Attn: R. Bhise

Wyle Laboratories
7800 Governor's Drive West
Huntsville, AL 35807
Attn: R. Losey

10 A. Narath
400 R. P. Stromberg (4)
1510 D. B. Hayes
1520 T. B. Lane
1810 R. G. Kepler
1820 R. E. Whan
1830 M. J. Davis
1833 J. L. Jellison
1840 N. J. Magnani
2540 K. L. Gillespie
3161 J. E. Mitchell
3600 R. W. Hunnicutt
3700 R. R. Russell
7530 W. E. Caldes
7550 F. W. Neilson
8110 R. C. Wayne
8343 C. F. Melius
8452 A. C. Skinrood
8453 W. R. Delameter
8453 W. G. Wilson
9221 R. M. Workhoven (3)
9700 E. H. Beckner
9720 D. G. Schueler
9720 W. P. Schimmel
9721 J. F. Banas
9722 V. E. Dudley
9722 J. V. Otts
9725 R. H. Braasch
9727 J. A. Leonard
8214 M. A. Pound
3141 L. J. Erickson (5)
3151 W. L. Garner (3)
for DOE/TIC (Unlimited Release)

☆U.S. GOVERNMENT PRINTING OFFICE: 1982-0-676-027/656